



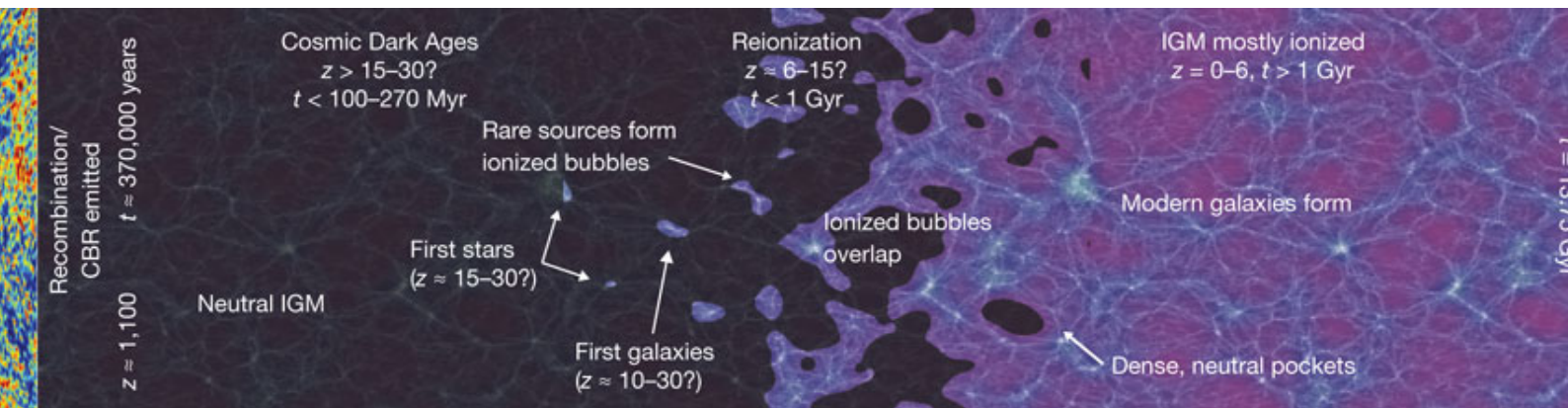
Bachelor of Science Thesis

September 12th, 2017

Cosmic Dawn in a Fuzzy Universe

Constraining the nature of Dark Matter
with 21 cm Cosmology

Author: OLOF NEBRIN



Supervisor: PROF. GARRETT MELLEMA

Stockholm University
Department of Astronomy

Contact info

Email:

olne8343@student.su.se

Tel:

+ 46 72-252 25 10

“Being asked to what end he had been born, he replied, “*To study sun and moon and heavens.*” — Diogenes Laërtius
on Anaxagoras’ view of life

Contents

Abstract	1
1. Introduction	3
2. Theoretical Background	5
2.1. The Λ CDM Model of the Universe	6
2.2. Structure & Galaxy Formation in the Λ CDM paradigm	8
2.2.1. Structure Formation	9
2.2.2. Galaxy Formation	12
2.3. Reionization, Cosmic Dawn & 21 cm Cosmology	17
2.3.1. When did reionization take place?	17
2.3.2. Can stars reionize the Universe by $z = 6$?	18
2.3.3. Cosmic Dawn	20
2.3.4. 21 cm Cosmology	22
2.4. Small-scale problems in Λ CDM	24
2.5. Fuzzy Dark Matter	24
2.5.1. Dynamics	24
2.5.2. Observational constraints	28
3. Methods	31
3.1. Model	31
3.2. Parameter selection & model scenarios	34
4. Results	39
4.1. Scenario Group A	40
4.1.1. Global 21 cm signal	40
4.1.2. 21 cm Power Spectrum	43
4.2. Scenario Group B	48
4.2.1. Global 21 cm signal	48
4.2.2. 21 cm Power Spectrum	50
4.3. Scenario Groups C & D	55
4.4. Summary of Numerical Predictions	62
5. Discussion & Conclusion	63
5.1. Discussion	63
5.1.1. Robustness of Results	63
5.1.2. Observational Probes	64
5.1.3. Future Work	66
5.2. Conclusion	66

Acknowledgments	69
A. Appendix	71
A.1. Structure & Galaxy formation in Λ CDM	71
A.1.1. Deriving the differential equation for δ	71
A.1.2. Approximate expressions for $\sigma(M)$ and the low-mass HMF	72
A.1.3. Ly- α cooling and the minimum mass of galaxies	74
A.2. Simple model of Cosmic Dawn	75
A.3. Jeans mass in FDM	77
Bibliography	79

Abstract

The cold dark matter (CDM) paradigm underlying the standard Λ CDM model of cosmology is successful on large scales but faces potential problems on small scales partly related to a seeming overproduction of dwarf galaxies. This could be alleviated in exotic dark matter models that suppresses small-scale structure formation. One such attractive model is known as **fuzzy dark matter** (FDM). FDM posits that dark matter is composed of ultra-light bosons with masses $m_{\text{FDM}} \sim 10^{-22}$ eV. With such light particle masses, quantum effects become important. More specifically, a pressure-like term appears in the equations of motion that counteracts gravitational collapse on small scales. Because small galaxies form first in CDM, it follows that the early history of galaxy formation predicted by FDM should be markedly different. One novel way to probe this effect would be to use the 21 cm line of hydrogen which acts as a sensitive probe of the epoch of reionization (EoR) and **Cosmic Dawn** — when the first galactic sources of X-rays started to reheat the intergalactic medium (IGM). In this thesis, the evolution of the 21 cm signal have been simulated for both CDM and FDM. These simulations indicate that the fluctuations in the 21 cm signal amenable to future observations are extremely weak ($\ll 1$ mK) — and probably unobservable — for FDM at high redshifts $z \sim 15 - 16$ compared to CDM (which tend to yield signals with amplitudes $\gg 1$ mK). This is mainly due to the delayed galaxy formation in FDM resulting in delayed Lyman- α coupling of the 21 cm spin temperature to the kinetic temperature of the IGM. **A robust prediction from all FDM scenarios explored in this thesis is that any detection of a signal at $z \sim 15 - 16$ would rule out interesting particle masses for FDM, and would be evidence for CDM-like structure formation.** Future work that properly models ionization fluctuations during the EoR could also yield strong predictions at lower redshifts.

1. Introduction

The modern understanding of galaxy formation revolves around dark matter — it is within the gravitationally dominating dark matter halos that galaxies like our own reside. There is therefore an interesting intersection between astrophysical cosmology and “fundamental” cosmology concerned with particle physics and gravitation. The fundamental nature of dark matter will have a great impact on when and how the first stars and galaxies formed in the Universe. This opens up the possibility of constraining fundamental dark matter physics from the observations of galaxy formation through cosmic history. The most suitable place for doing so is in the high-redshift Universe where the very first galaxies formed.

The standard model of cosmology is based on the idea that dark matter is “cold” (i.e. non-relativistic) at early times and composed of relatively massive particles so that quantum effects can be ignored.¹ This leads to a bottom-up picture of structure formation wherein small structures and galaxies form first. The predictions of this model on relatively large scales fit observations very well. So any deviations from this picture must modify the physics of dark matter on small scales, and therefore radically change how the very first galaxies formed. An exciting new way to probe this high-redshift regime is the use of the cosmological 21 cm line of hydrogen that sensitively depends on the state of the intergalactic medium, which at high redshifts is heavily influenced by radiation from the first galaxies. This thesis entertains the question of whether it is possible to rule out a specific competitor to the standard cold dark matter model — fuzzy dark matter — using 21 cm cosmology. In the next chapter, the physics underlying structure and galaxy formation, 21 cm cosmology, fuzzy dark matter as well as its motivation is reviewed in some detail.

¹By this, it is meant that the de Broglie wavelength for the dark matter particles is very small compared to scales relevant for galaxy formation.

2. Theoretical Background

“It must be acknowledged that all the sciences are so closely interconnected that it is much easier to learn them all together than to separate one from the other. If, therefore, someone seriously wishes to investigate the truth of things, he ought not to select one science in particular, for they are all interconnected and interdependent.”

— René Descartes, *Rules for the Direction of the Mind*

“Everyone is pleased: the relativists who feel they are being appreciated, who are suddenly experts in a field they hardly knew existed; the astrophysicists for having enlarged their domain, their empire, by the annexation of another subject, general relativity.”

— Thomas Gold in 1963 at the *First Texas Symposium on Relativistic Astrophysics* (as quoted in [Kra99], p. 333)

It is safe to say that cosmology is the broadest area of not just astrophysics, but physics as a whole. Its many sub-disciplines involves the application of general relativity, stellar physics, atomic and molecular physics, particle physics, radiative transfer and more. This is not so surprising given that the object of study is the entire Universe. In this thesis the connection between the Epoch of Cosmic Dawn, when the first stars formed and started to heat up the neutral hydrogen in the intergalactic medium (IGM), and the underlying theory of dark matter, has been studied. This involves the application of physics from many of the aforementioned fields, and so it is apt to review some of the essential background — from the Λ CDM model to 21 cm cosmology and dark matter physics — on which later results will build.

2.1. The Λ CDM Model of the Universe

Observations indicate that the Universe is expanding (became well known after [Hub29]), that it is homogeneous and isotropic on large scales (see e.g. discussion in [Pee93]), with negligible spatial curvature [Pla16a].¹ Assuming these properties, the dynamics of the Universe is described by the **Friedmann equation** for a flat Universe (for a derivation using GR see [Ken90], otherwise see e.g. [Lid03]),

$$H^2 \equiv \left(\frac{\dot{a}}{a}\right)^2 = H_0^2 \left(\Omega_{m,0}a^{-3} + \Omega_{\gamma,0}a^{-4} + \Omega_{\Lambda,0}\right). \quad (2.1)$$

Here a is the **scale factor** (and $\dot{a} \equiv da/dt$ is the time derivative of the scale factor) that scales all spatial distances, H_0 is the **Hubble constant** and Ω_i is the **density parameter** of content “i”. For a flat Universe, the density parameter could be thought of as the fraction of the total energy density of the Universe in a certain form. Observations indicate that non-relativistic matter makes up approximately 31 percent of the Universe’s energy content at the present (for some of the latest data on cosmological parameters, see [Pla16a]). Thus, $\Omega_{m,0} \simeq 0.31$. The scaling a^{-3} originates from the fact that the density of matter dilutes with the volume. Radiation and relativistic matter on the other hand dilutes as a^{-4} and makes up a negligible fraction $\Omega_{\gamma,0} \sim 9 \times 10^{-5}$. At the present it is dark energy that dominates; $\Omega_{\Lambda,0} \simeq 0.69$. Unlike the matter and radiation, the dark energy doesn’t seem to dilute as the Universe expands. Solutions to the Friedmann equation for one dominant component are summarized in Table I.

The total matter density can also be split into baryonic and dark matter, with the latter dominating ($\Omega_{DM,0} \simeq 0.26$ and $\Omega_{b,0} \simeq 0.05$). The great abundance of dark matter not only explains the rotation curves in galaxies, but also underlies our modern understanding of structure and galaxy formation [WR78, Pee82, BFPR84, Pee17]. The nature of dark matter is therefore of great importance, not only in particle physics but also in astrophysical cosmology. In the next section, the relationship between dark matter and structure and galaxy formation is explored in detail.

¹On the latter point, it’s interesting to point out that it has been argued that an exactly flat or negatively curved Universe of infinite extent might be unphysical. This would be because the spatial integration in the action, from which the equations of motion are derived, diverges [BT88].

Table I.
Major epochs in the Λ CDM model

THE DOMINATING COMPONENT	REDSHIFT REGIME	SCALE FACTOR BEHAVIOUR
Radiation [†]	$z \gtrsim \frac{\Omega_{m,0}}{\Omega_{rad,0}} - 1 \simeq 3400$	$a(t) \propto t^{1/2}$
Matter	$z \lesssim \frac{\Omega_{m,0}}{\Omega_{rad,0}} - 1 \simeq 3400$ $z \gtrsim \left(\frac{\Omega_{\Lambda,0}}{\Omega_{m,0}}\right)^{1/3} - 1 \simeq 0.31$	$a(t) \propto t^{2/3}$
Dark Energy	$z \lesssim \left(\frac{\Omega_{\Lambda,0}}{\Omega_{m,0}}\right)^{1/3} - 1 \simeq 0.31$	$a(t) \propto \exp(\sqrt{\Omega_{\Lambda,0}} H_0 t)$

[†]At extremely high redshifts (i.e. in the very early Universe) radiation was probably subdominant to a scalar field known as the inflaton, acting much like the dark energy does today. The ultimate origin of the density perturbations that later grew into galaxies can be traced to quantum fluctuations in this inflaton field.

2.2. Structure & Galaxy Formation in the Λ CDM paradigm



FIGURE 2.1. In the CDM model, puny dark matter halos, perhaps all the way down to $\sim M_{\oplus}$, would litter the interstellar medium, neither hosting stars nor emitting any visible light of their own [DMS05]. If we could see them, it might look something like this. Since small structures form first in the CDM model, these halos would be relics of epochs long gone.

Given the backdrop of a Universe that is uniform on large scales — described by the Λ CDM model of the previous section — where did galaxies come from? Some key results in the pursuit of the answer to this question will be reviewed here, and will be built upon later when considering fuzzy dark matter.

2.2.1. Structure Formation

The Friedmann equation describes the Universe as a whole, which is assumed to be homogeneous and isotropic on large scales. On smaller scales inhomogeneities develop that, given enough time², can be morphed into dark matter halos within which galaxies can form. The problem of structure formation largely revolves around the quantity δ — the **density perturbation** — defined through $\rho_m(\mathbf{x}, t) = \bar{\rho}_m(t)(1 + \delta(\mathbf{x}, t))$ where $\bar{\rho}_m(t)$ is the mean matter density of the Universe.³ The dark matter, as envisaged in the standard Λ CDM model, is pressureless while baryonic matter is not. But on mass scales $\gtrsim 10^5 M_\odot$ the baryonic effects of pressure are negligible and we can treat dark and baryonic matter as a single fluid [Pee93, BL01]. With only a pressureless fluid, gravity will be the only relevant force.

On sub-horizon scales and for weak gravitational fields, Newtonian gravity is sufficient to determine the evolution of δ . To start with, the equations governing the density field ρ_m will be the fluid equations in an expanding Universe (for an introduction to astrophysical fluid dynamics, see e.g. [RB07], while [Pee93] specifically considers fluids in an expanding background). Dropping the subscript in ρ_m for convenience, these are (e.g. [Pee93])

$$\begin{aligned} \frac{\partial \mathbf{v}}{\partial t} + \frac{1}{a} (\mathbf{v} \cdot \nabla) \mathbf{v} &= -\frac{\dot{a}}{a} \mathbf{v} - \frac{1}{a} \nabla \phi, \\ \frac{\partial \rho}{\partial t} + 3\frac{\dot{a}}{a}\rho + \frac{1}{a} \nabla \cdot (\rho \mathbf{v}) &= 0, \\ \nabla^2 \phi &= 4\pi G a^2 \bar{\rho} \delta. \end{aligned} \quad (2.2)$$

The first equation, known as the **Euler equation**, describes the evolution of the *peculiar* velocity field $\mathbf{v} = a\dot{\mathbf{x}}$ (the 'total' velocity, factoring in the expansion of space, is $\mathbf{u} = \mathbf{v} + \dot{a}\mathbf{x}$) under the influence of the gravitational potential ϕ . The second equation is the **continuity equation** and encapsulates the conservation of mass. And the third equation is the **Poisson equation** that governs the response of ϕ to a density perturbation δ . These three equations can be reduced to a single analytically tractable differential equation for δ if we assume that δ is a small perturbation ($\delta \ll 1$). The details are presented in Appendix 1 and the result is

$$\frac{\partial^2 \delta}{\partial t^2} + 2\frac{\dot{a}}{a} \frac{\partial \delta}{\partial t} = \frac{3}{2} \Omega_m \left(\frac{\dot{a}}{a} \right)^2 \delta. \quad (2.3)$$

First thing to note is that this partial differential equation has no spatial derivatives or any \mathbf{x} -dependence. This means that, all else being equal, density fluctuations will evolve similarly (as long as we are restricting ourselves to sub-horizon scales). The only other factor that comes into play is the cosmological epoch during which

²For some fluctuations, as we will see, there will never be enough time because their growth is inhibited when the Universe becomes vacuum dominated.

³From now on, \mathbf{x} will refer to the comoving spatial coordinates.

Table II.
Evolution of the density perturbation in Λ CDM

COSMOLOGICAL EPOCH	APPROXIMATIONS MADE	SOLUTIONS [†]
Radiation domination	$\dot{a}/a \simeq 1/2t$, $\Omega_m \simeq 0$	$\delta \propto \log(a)$
Matter domination	$\dot{a}/a \simeq 2/3t$, $\Omega_m \simeq 1$	$\delta \propto a$
Dark energy domination	$\dot{a}/a \simeq \sqrt{\Omega_{\Lambda,0}}H_0$, $\Omega_m \simeq 0$	$\delta = \text{const.}$

[†]Note that decaying solutions are not considered here.

δ evolves. Solutions to this equation for different cosmological epochs are summarized in Table II.

To understand why the Universe is uniform on large scales while increasingly non-uniform on small scales, it is appropriate to Fourier transform δ ,

$$\delta = \frac{1}{(2\pi)^3} \int d^3k \delta_k e^{-ik \cdot x}. \quad (2.4)$$

By inspection it is easy to see that δ_k will also satisfy Eq. 2.3.⁴ Next, the **power spectrum** $P(k)$ is defined through (e.g. [LF13])

$$\langle \delta_k \delta_{k'} \rangle = (2\pi)^3 \delta_D(\mathbf{k} - \mathbf{k}') P(k), \quad (2.5)$$

where $\delta_D(\mathbf{k} - \mathbf{k}')$ is the Dirac delta function and angular brackets denote an average over the entire statistical ensemble. The power spectrum could be thought of as a Fourier transformation of the **correlation function**, $\xi(x) \equiv \langle \delta(x') \delta(x' + x) \rangle$ [Pee93, LF13],

$$\xi(x) = \int \frac{d^3k}{(2\pi)^3} P(k) e^{ik \cdot x}. \quad (2.6)$$

Assuming isotropy, $\xi(x) = \xi(r)$ where $r = |x|$. A more important quantity for the purposes of this thesis is σ — the root-mean-square (RMS) density fluctuation within a sphere of comoving radius R that encloses a volume V and mass $M = 4\pi R^3 \bar{\rho}_0/3$ ($\bar{\rho}_0$ refers to the present mean density). It is basically the correlation function smoothed below a scale R (or equivalently, for $k \gtrsim 1/R$),

$$\sigma(M)^2 = \frac{1}{V^2} \int \frac{dk}{2\pi^2} k^2 P(k) |\tilde{W}(kR)|^2. \quad (2.7)$$

⁴This simply follows because time derivatives only act on $\delta(x, t)$ in the integrand,

$$\frac{\partial \delta_k}{\partial t} = \int d^3x \frac{\partial \delta}{\partial t} e^{ik \cdot x}.$$

Here $\tilde{W}(kR)$ is the Fourier transformation of the **window function** $W(r)$. Without getting bogged down in the details (for details, see [Pee93]), the basic qualitative point is that $|\tilde{W}(kR)|^2 \sim V^2$ for $kR \lesssim 1$ and $|\tilde{W}(kR)|^2 \sim 0$ else. If $\delta(\mathbf{x})$ is a Gaussian field (as inflation predicts [Pee93]) with zero mean, σ^2 can be understood to be the variance of the field. So a 4σ fluctuation is much more rare than a 1σ fluctuation. As for the present amplitude of σ , it is conventional to use observations to normalize σ on a scale $R = 8h^{-1}$ Mpc. Recent observations by Planck indicate that $\sigma_8 \equiv \sigma(R = 8h^{-1}$ Mpc) = 0.815 ± 0.009 [Pla16a]. When a $\nu\sigma(M)$ -fluctuation becomes of order 1 — or more specifically $\delta_{\text{crit}} \simeq 1.69$ in a matter-dominated Universe — the linear perturbation theory underlying Eq. 2.3 breaks down, and the fluctuation have decoupled from the expansion of the Universe and formed a halo of mass M and mean density $18\pi^2\bar{\rho}$ evaluated at that time (e.g. [TARW06, LF13]). It is within such halos that galaxies eventually can form (this is treated in more detail in the next subsection).

Knowing the power spectrum (or the correlation function) therefore makes it possible to specify $\sigma(M)$ and answer the question of when the first halos and galaxies formed. While Eq. 2.3 yields scale-invariant solutions, in practise the amplitude of density perturbations *do* depend on the scale of interest. There are two reasons for this:

- Quantum fluctuations in the inflaton field driving inflation generates a primordial power spectrum $P_{\text{prim}}(k) \propto k^{n_s}$ with a **spectral index** $n_s \simeq 1$ (e.g. [Pee93, Teg05]). Recent observational constraints yield $n_s = 0.968 \pm 0.006$ [Pla16a].
- Large-scale fluctuations evolve on super-horizon scales for longer than small-scale fluctuations — and super-horizon evolution of δ is *not* described by Eq. 2.3. On super-horizon scales, a relativistic treatment give $\delta \propto 1/\bar{\rho}_{\text{back}}a^2$ where $\bar{\rho}_{\text{back}}$ is the total background density [Pee93, Pad02]. During radiation domination $\bar{\rho}_{\text{back}} \simeq \bar{\rho}_\gamma \propto a^{-4}$ so that $\delta \propto a^2$. But during matter domination $\bar{\rho}_{\text{back}} \simeq \bar{\rho} \propto a^{-3}$ so that $\delta \propto a$ (same solution as for sub-horizon scales). It becomes clear that the horizon distance at matter-radiation equality, $R_H(z_{\text{eq}})$, is an important scale. At matter-radiation equality, the primordial power spectrum will have transformed into $P(k) \propto P_{\text{prim}}(k)T^2(k)$ where the **transfer function** $T(k)$ behaves roughly as follows [Pad06],

$$T(k) \propto \begin{cases} 1 & \text{for } k \ll 1/R_H(z_{\text{eq}}) \\ k^{-4}(\log k)^2 & \text{for } k \gg 1/R_H(z_{\text{eq}}) \end{cases}. \quad (2.8)$$

A remarkably accurate first-order approximation of $\sigma(M)$ for $M \lesssim 10^{14} M_\odot$ can be derived by using Eq. 2.8, making the approximation $n_s \simeq 1$ and using a sharp- k window function (where $\tilde{W}(x) = 1$ for $x < 1$ and zero else), and the growth factor $\delta \propto a$ from Table II. The result of the derivation in Appendix A.1 is,

$$\sigma(M) \simeq \sigma_8 \left\{ \frac{\mu - \log^3(8M/M_{\text{eq}})}{\mu - \log^3(8M_8/M_{\text{eq}})} \right\}^{1/2} a, \quad (2.9)$$

where $\mu \simeq 20$. A halo of mass M will therefore form out of a $\nu\sigma$ -fluctuation at redshift

$$1 + z_{\text{col}} \simeq \frac{\nu\sigma_8}{\delta_{\text{crit}}} \left\{ \frac{\mu - \log^3(8M/M_{\text{eq}})}{\mu - \log^3(8M_8/M_{\text{eq}})} \right\}^{1/2}. \quad (2.10)$$

The most important deduction from Eq. 2.10 is that in Λ CDM, low-mass halos form first — the very essence of **hierarchical structure formation**. For example, Eq. 2.10 predicts that a halo of mass $M \sim 10^8 M_\odot$ would form at $1 + z_{\text{col}} \sim 3\nu$, compared to $1 + z_{\text{col}} \sim \nu$ for a $10^{12} M_\odot$ halo.⁵

Beyond making possible the estimate of when dark matter halos form, knowing σ also allows estimating the halo mass distribution — the **halo mass function** (HMF). Assuming that δ is Gaussian, the HMF can be shown to be (e.g. [PS74, Pee93, LF13])

$$\frac{\partial n}{\partial M} = \sqrt{\frac{2}{\pi}} \frac{\bar{\rho}_0}{M^2} \frac{\delta_{\text{crit}}}{\sigma(M)} \left| \frac{\partial \log \sigma}{\partial \log M} \right| e^{-\delta_{\text{crit}}^2/2\sigma(M)^2}, \quad (2.11)$$

where $(\partial n / \partial M) dM$ is understood to be the number of halos in the mass interval $[M, M + dM]$ per unit comoving volume. Using Eq. 2.9, it can then be shown (see Appendix A.1 for a derivation) that the number density of small halos should scale as

$$\frac{\partial n}{\partial M} \propto M^{-\gamma}, \quad \gamma \simeq 2 + \frac{5}{2} \frac{1}{\log(8M/M_{\text{eq}})}. \quad (2.12)$$

In the vast range mass range $1 M_\oplus \lesssim M \lesssim 10^9 M_\odot$ the exponent is $\gamma \simeq 1.9$. It is clear that Λ CDM predicts a large population of small halos. This follows as long as the power spectrum used in deriving this result is valid. For Λ CDM, this is indeed the expectation. Simulations indicate that the Milky Way could be teeming with tiny halos with masses as small as that of the Earth (i.e. $\sim M_\oplus$) [DMS05].

2.2.2. Galaxy Formation

Once a halo has collapsed and virialized, what determines the fate of the baryons? Will they be incorporated into galaxies or will the halos be devoid of any starlight? A prerequisite for the gas to collapse, fragment and form stars is that the gas

⁵To evaluate Eq. 2.10, the following expressions were used:

$$M_{\text{eq}} \simeq 2.4 \times 10^{17} \left(\frac{\Omega_{\text{m},0} h^2}{0.14} \right)^{-1/2} \left(\frac{1 + z_{\text{eq}}}{3400} \right)^{-3/2} M_\odot,$$

$$M_8 \simeq 2.7 \times 10^{14} \left(\frac{\Omega_{\text{m},0} h^2}{0.14} \right) \left(\frac{h}{0.68} \right)^{-3} M_\odot.$$

can lose its pressure support more rapidly than it can collapse. Thus, galaxies “happen” when $t_{\text{cool}} \lesssim t_{\text{ff}}$ (see e.g. [Sil77, WR78, BFPR84, TR98, Pad02]). There are a number of different cooling processes. Before the baryons can cool, they will have a temperature close to the **virial temperature**, defined through (e.g. [LF13])

$$T_{\text{vir}} = \frac{\mu m_p v_c^2}{2k_B}, \quad (2.13)$$

where μ is the mean molecular weight of the baryonic gas ($\mu = 0.59$ for a primordial mix of H and He) and $v_c = (GM/R_{\text{vir}})^{1/2}$ is the circular velocity within the halo. The virial radius could in turn be found from $R_{\text{vir}} = (3M/4\pi\rho_{\text{vir}})^{1/3}$ where the virial density (i.e. the density of a collapsed halo) is — as noted in the last section — $\sim 18\pi^2\bar{\rho}$ evaluated at the collapse redshift. As a rule of thumb, *the lower the halo mass the lower the virial temperature*. Thus, the minimum halo mass in the Universe is determined by the most efficient process of cooling at relatively low temperatures. If only hydrogen and helium are present, this cooling process is Ly- α cooling, which is efficient near $T_{\text{vir}} \sim 10^4$ K. However, in the picture of galaxy formation painted in the Λ CDM model, molecular hydrogen probably allowed cooling at even lower virial temperatures, yielding **minihalos** with masses as small as $\sim 10^6 M_\odot$ populated by the first metal-poor stars (called Population III stars, or Pop III for short) [TSR⁺97, ABN02].

The first stars forming in these minihalos were probably very massive and emitted copious amounts of Lyman-Werner photons with enough energy to dissociate the molecular hydrogen that made the formation of stars in minihalos possible in the first place [LF13]. Thus, the lower mass limit to galaxies is subsequently set by Ly- α cooling [GJKB08]. Halos hosting gas that can cool via Ly- α emission and other atomic cooling processes are called **atomic cooling halos**. Below the physics constraining the masses of galaxies is outlined first using an order-of-magnitude estimate and next employing a more sophisticated program.

2.2.2.1. Back-of-the-envelope estimate of the mass of the first proper galaxies in Λ CDM

Ly- α cooling occurs when electrons collisionally excite hydrogen atoms to the $n = 2$ state, followed by (in a low density medium) spontaneous de-excitation accompanied by the emission of a Lyman- α photon. In Appendix A.1 it is shown that for a hydrogen gas that is collisionally ionized, with $\sigma(M)$ approximated as a power law ($\sigma(M) = \sigma_0(M/M_0)^{-\eta}a$), the condition $t_{\text{cool}} < t_{\text{ff}}$ is met for a $\nu\sigma$ -halo with mass $\gtrsim M_{\text{Ly}\alpha,\text{min}}$ where,

$$M_{\text{Ly}\alpha,\text{min}} \sim M_0^{\frac{3\eta}{2(3\eta/2-1)}} \left(\frac{\alpha^2 \beta c^2 \delta_{\text{crit}}}{2G\mu \log(\alpha^{-2}) \nu \sigma_0} \right)^{\frac{3}{2(1-3\eta/2)}} \left(18\pi^2 \bar{\rho}_0 \right)^{\frac{1}{2(3\eta/2-1)}}. \quad (2.14)$$

Here $\alpha \simeq 1/137$ is the fine-structure constant and $\beta \equiv m_e/m_p$. The dependence on α and β reflects the dependence on the underlying atomic physics of Ly- α cooling.

The exponent $\eta = -\partial \log \sigma / \partial \log M$ can be estimated from Eq. 2.9 to be

$$\eta \simeq \frac{3}{2} \frac{\log^2(8M_0/M_{\text{eq}})}{\mu - \log^3(8M_0/M_{\text{eq}})}. \quad (2.15)$$

Anticipating a relatively small halo mass, we can set $M_0 \sim 3 \times 10^8 M_\odot$ which yields $\eta \simeq 0.081$ and $\sigma_0 \simeq 5.8 (\sigma_8/0.81)$. Using this and $\mu = 0.59$ gives us

$$M_{\text{Ly}\alpha, \text{min}} \sim \frac{8.0 \times 10^8}{\nu^{1.71}} \left(\frac{\sigma_8}{0.81} \right)^{-1.71} \left(\frac{\Omega_{m,0} h^2}{0.14} \right)^{-0.57} M_\odot. \quad (2.16)$$

So for a rare 4σ -halo, efficient cooling occurs above $\sim 7.5 \times 10^7 M_\odot$. We see that the mass of the first galaxies forming from atomic cooling reflects both rigid atomic physics as well as cosmological initial conditions⁶ and the nature of dark matter (through the dependence on the power spectrum). The derivation of Eq. 2.16 hinges fundamentally upon the Λ CDM paradigm through the assumption of a CDM power spectrum and the scale-invariant growth solution $\delta \propto a$ during matter-domination. If dark matter is more exotic than imagined in Λ CDM and breaks scale invariant growth, then the lower limit to galactic masses would be consequently altered.

⁶The scaling with σ_8 could be swapped for Q , the primordial amplitude of density perturbations as they enter the horizon. According to [TARW06], it has a value of $Q \sim 2 \times 10^{-5}$. Note furthermore that the exponent η itself depends on cosmological parameters through its dependence on M_{eq} , but the dependence is weaker.

2.2.2.2. More sophisticated estimates of the range of galactic masses in Λ CDM

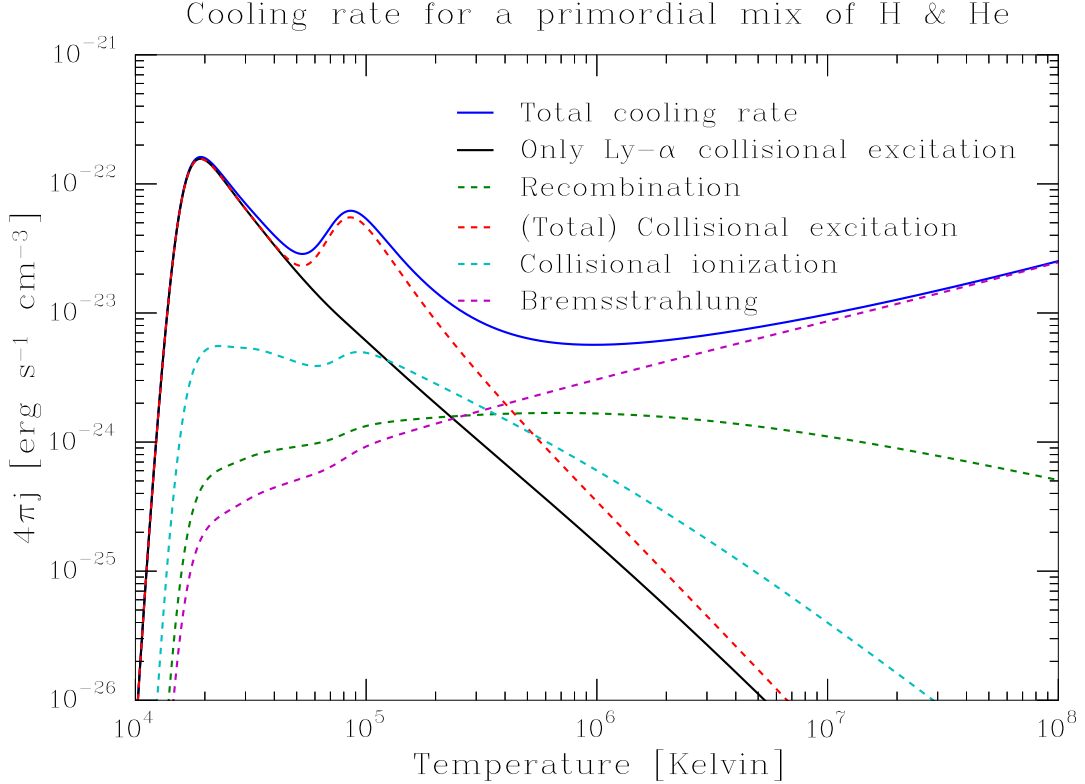


FIGURE 2.2. A plot of the cooling rate of a primordial mix of hydrogen and helium. This plot can be compared to Figure 1 in [KWH96]. Above $\sim 5 \times 10^4$ K, Ly- α cooling stops being the dominant cooling process.

Having laid out the underlying astrophysics and cosmological initial conditions that determine the nature of the first galaxies so as to give some intuition, we can now move on to more sophisticated estimates. There are other cooling processes beyond Ly- α cooling, which tend to dominate at higher temperatures. These additional cooling processes include collisional ionization, recombination and bremsstrahlung. For a primordial mix of hydrogen and helium, the rate of cooling due to these processes are listed in Table 1 in [KWH96]. A plot of the resulting cooling rate(s) is shown in Figure 2.2.

With the realization that cooling is crucial to understand the masses of galaxies in the Universe, it became conventional to make 'cooling diagrams' (see e.g. [BFPR84, Pea98, Pad02, TARW06]). In a cooling diagram, the baryonic number density is plotted against temperature. Only in the special regions in this diagram where $t_{\text{cool}} \lesssim t_{\text{ff}}$ do we expect galaxies to form. To find the range of galactic masses predicted by the underlying theory of structure formation, we plot the baryonic number density of a $\nu\sigma$ -halo against its virial temperature and find where it intersects the efficient cooling region. The result of this exercise is plotted, using the cooling rate in Figure 2.2, in Figure 2.3.

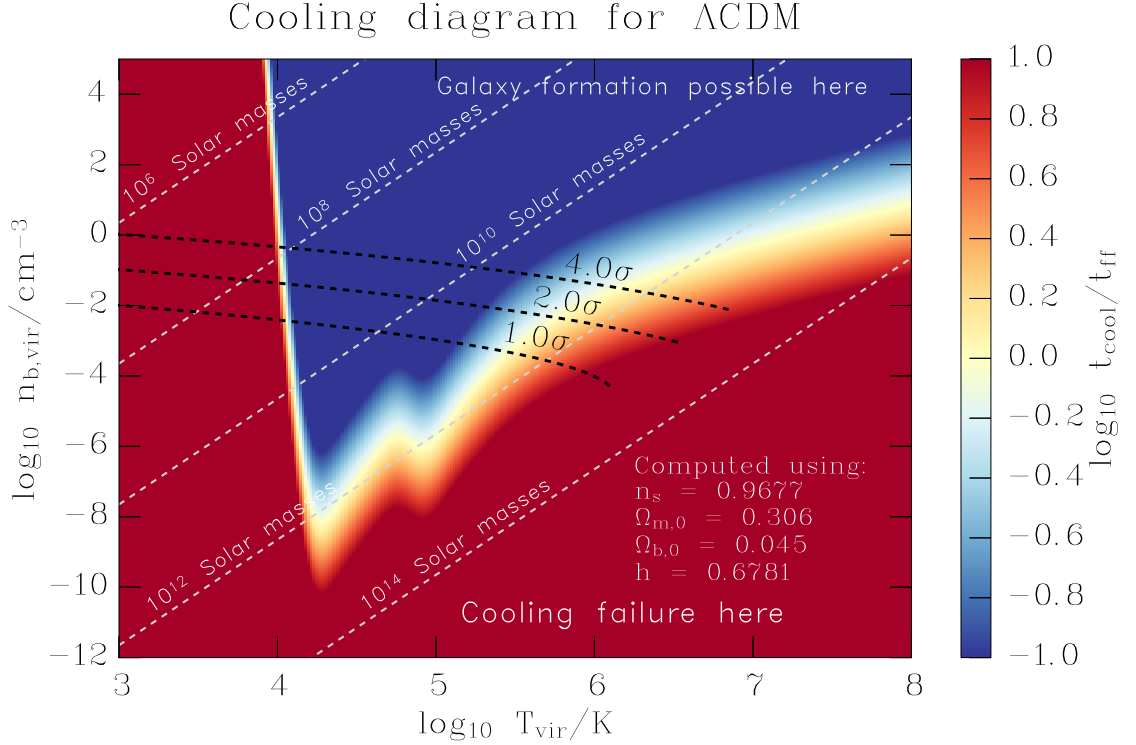


FIGURE 2.3. A cooling diagram plotting the baryonic virial number density of a newly formed halo versus its virial temperature. Only in the blue region, where $t_{\text{cool}}/t_{\text{ff}} < 1$, can galaxies form. The cooling time-scale is calculated using the cooling rate for a primordial mix of hydrogen and helium, as listed in Table I of [KWH96]. The range of galactic masses predicted by Λ CDM can be understood from seeing where halos are predicted to lie on this diagram. The black lines show $n_{b,\text{vir}}$ as a function of T_{vir} , as predicted by Λ CDM, for 1, 2 and 4σ fluctuations. Note that the program underlying this plot did not use Eq. 2.9 for $\sigma(M)$, but rather employs a more accurate numerical calculation using the transfer equation in Eq. 29 of [EH98].

As can be seen in the figure, the the range of galactic masses picked out in Λ CDM ranges from a little under $10^8 M_\odot$ (for a 4σ -halo) to $\sim 10^{12} M_\odot$. Note that the former limit agrees very well with the order-of-magnitude estimate in 2.16. As the metallicity of the Universe increases, cooling at higher temperatures becomes more efficient, yielding a slightly higher upper limit. This relatively simple combination of atomic physics and cosmological initial conditions therefore yields a remarkably good explanation of the observed galactic masses in the Universe. Cooling diagrams are useful to assess galaxy formation in different dark matter scenarios. Later in this chapter, a cooling diagram will be presented for fuzzy dark matter.

2.3. Reionization, Cosmic Dawn & 21 cm Cosmology

The **Epoch of Reionization** (EoR) was the period in the early Universe when the neutral intergalactic medium (IGM) became ionized. How and when this took place are questions of great importance to cosmology. Another related radical change in the state of matter — and the focus of this thesis — came during **Cosmic Dawn**, during which the first sources of light started to heat up the previously adiabatically cooling IGM. Studying the heating history of the IGM therefore tells us something about the first stars and galaxies. A new exciting avenue of research lies just ahead of us. New and upcoming radio telescopes will be able to study the 21 cm signal of hydrogen, unleashing a wealth of new information about the EoR and Cosmic Dawn. In this section the aforementioned concepts regarding the EoR and Cosmic Dawn will be explored in some detail.

2.3.1. When did reionization take place?

After recombination at $z \sim 10^3$, the Universe was almost perfectly neutral. A residual **ionization fraction** $x \equiv n_e / (n_e + n_{\text{HI}}) = n_{\text{HII}} / n_{\text{H}} \sim 3 \times 10^{-4}$ remained at $z \sim 200$ (see e.g. Figure 2.5 in [LF13]). It is around this redshift when the IGM temperature T_K starts to decouple from the CMB temperature. This is because the residual ionization fraction is too small to make heating through Compton scattering efficient in making $T_K \sim T_\gamma$ (where T_γ is the CMB temperature). With no efficient heating at redshifts $z \lesssim 200$, the IGM temperature drops adiabatically like $T_K \propto a^{-2} = (1+z)^2$. The ionization fraction stayed roughly constant until the first galaxies started to form, from which copious amounts of ionizing radiation were being emitted. This ionizing radiation eventually reionized the Universe, yielding $x \sim 1$. When did this occur?

One way to probe it is through the **Gunn-Peterson optical depth** τ_{GP} . This is the optical depth to Ly- α photons as they traverse the Universe. Photons emitted with $\lambda < \lambda_{\text{Ly}\alpha}$ would eventually redshift into resonance $\lambda \simeq \lambda_{\text{Ly}\alpha}$ and be absorbed. Since only neutral hydrogen can absorb Ly- α photons, τ_{GP} becomes a measure of the neutral fraction $x_{\text{HI}} \equiv 1 - x$. It can be shown that the Gunn-Peterson optical depth is roughly [Mad00, LF13],

$$\tau_{\text{GP}} \sim 2 \times 10^4 x_{\text{HI}} (1 + \delta) \left(\frac{h}{0.7} \right) \left(\frac{\Omega_{\text{b},0}}{0.05} \right) \left(\frac{\Omega_{\text{m},0}}{0.3} \right)^{-1/2} (1 + z)^{3/2}. \quad (2.17)$$

If the Universe was approximately neutral, so that $x_{\text{HI}} \sim 1$, we would get such a large optical depth that the Universe should be completely opaque to Ly- α radiation. But Eq. 2.17 is *not* valid for photons emitted with $\lambda > \lambda_{\text{Ly}\alpha}$. In this case there would be no redshifting into resonance, resulting in $\tau_{\text{GP}} = 0$. In 1965, Gunn and Peterson [GP65] used observational data presented the same year of a quasar at $z_q \sim 2$ to argue that the IGM must be nearly perfectly ionized from the apparent *absence* of absorption at wavelengths $\lambda < \lambda_{\text{Ly}\alpha} (1 + z_q)$. If the Universe is ionized, we expect to see a **Lyman- α forest** — the only absorption features coming from a 'forest' of HI clouds between us and the quasar.

Table III.

Number of ionizing photons per baryon, ζ		
	POP II STARS	POP III STARS
$\mathcal{N}_{\gamma,*}$	$3 - 4 \times 10^3$	$3 - 4 \times 10^4$
f_*	~ 0.1	~ 0.1
f_{esc}	~ 0.1	~ 0.1
ζ	$\sim 30 - 40$	$\sim 300 - 400$

References: [LF13, KC14, Mel17]

Since then, observations of numerous quasars have indicated that there is significant absorption in the IGM itself — a **Gunn-Peterson trough** — at $z \sim 6$ (e.g. [FSS⁺03]). From Eq. 2.17 we see that this indicates that the IGM must have been significantly more neutral at that time compared with the present. However, note that because τ_{GP} is so large, the Universe can be almost completely ionized and still yield $\tau_{\text{GP}} \gg 1$ [ME03]. Thus the phase transition from a predominantly neutral Universe to an almost completely ionized one — the EoR — must have taken place at some redshift $z > 6$. Another way to assess when the EoR took place is to compute the optical depth due to Thomson scattering (photon scattering off electrons). This optical depth is directly related to the ionization fraction of the Universe (x instead of x_{HI}) — since you need free electrons around — and is also much smaller than τ_{GP} . Recent constraints on the Thomson optical depth from Planck indicate that a significant fraction of the Universe was ionized by roughly $z \sim 8$ [Pla16b]. Any model of structure and galaxy formation consistent with observations should therefore be able to reionize the Universe by $z \sim 6 - 8$.

2.3.2. Can stars reionize the Universe by $z = 6$?

A very simple order-of-magnitude estimate can be made for when a model of structure formation predicts that reionization should have been finished. If the number of ionizing photons produced *per baryon in a galaxy* is ζ , then ζf_{col} — where f_{col} is the fraction of baryons in galaxies (the **collapse fraction**) — is the number of ionizing photons produced *per baryon* in the Universe as a whole. If this number exceeds some number of order unity, then there are more than one ionizing photon per neutral hydrogen atom, which thus permits the reionization of the Universe. The factor ζ can be split into several factors,

$$\zeta = \mathcal{N}_{\gamma,*} f_* f_{\text{esc}},$$

where $\mathcal{N}_{\gamma,*}$ is the number of ionizing photons produced *per stellar baryon*, f_* is the fraction of the baryons in galaxies incorporated into stars (the **star formation efficiency**) and f_{esc} is the fraction of ionizing photons that manage to escape the galaxy into the IGM (the **escape fraction**). All of these factors have considerable uncertainty. Rough estimates are listed in Table III. The collapse fraction can be calculated by integrating the HMF,

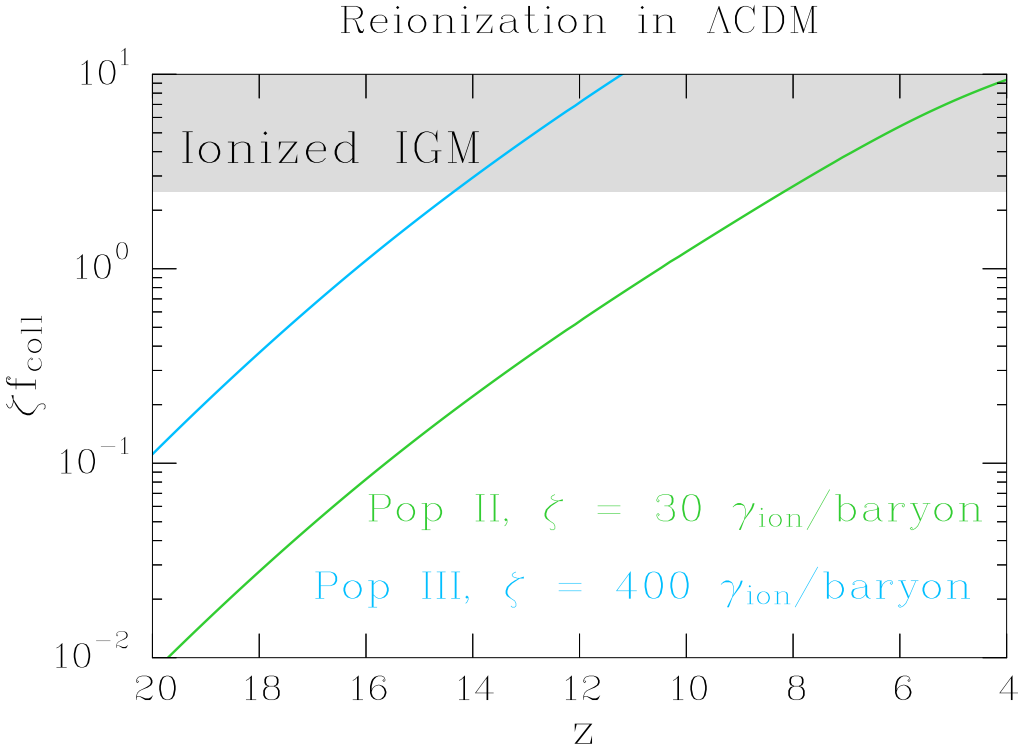


FIGURE 2.4. A plot of ζf_{coll} to assess whether the Universe can be reionized sufficiently rapidly to fall in line with observational constraints. As can be seen, in Λ CDM both Pop II stars and Pop III stars can reionize the IGM before $z = 6$. The calculation used $n_s = 0.9677$, $\Omega_{\text{m},0} = 0.306$ and $h = 0.6781$. The grey area, where the Universe is reionized, starts at $1 + n_{\text{rec}} = 2.5$.

$$f_{\text{coll}} = \frac{1}{\bar{\rho}_0} \int_{M_{\text{min}}}^{\infty} dM M \frac{\partial n}{\partial M}. \quad (2.18)$$

Here M_{min} corresponds to the minimum (redshift-dependent) halo mass which allows efficient cooling. As discussed earlier (and which can be seen clearly in Figure 2.2 and Figure 2.3), Ly- α cooling is only efficient above $T_{\text{vir}} \sim 10^4$ K.⁷ In Figure 2.4 $\zeta f_{\text{coll}} (T_{\text{vir}} > 10^4$ K) is plotted using the HMF in Eq. 2.11 but with a numerical calculation of $\sigma(M)$. The Universe will be reionized when $\zeta f_{\text{coll}} \simeq 1 + n_{\text{rec}}$ where n_{rec} takes into account the fact that recombination will demand an additional n_{rec} number of photons per baryon to fully ionize the IGM. Typical values are $n_{\text{rec}} \sim 1 - 2$ [Mel17]. From Figure 2.4 it is clear that Λ CDM can be reionized before $z = 6$ even with Pop II stars.

⁷To write M_{min} in terms of T_{vir} , the following formula, which can be derived from the definition of T_{vir} , can be used,

$$M_{\text{min}} = 2^{3/2} \left(\frac{3}{4\pi} \right)^{1/2} \left(\frac{k_B T_{\text{vir}}}{G \mu m_p} \right)^{3/2} \bar{\rho}_0^{-1/2} (1+z)^{-3/2}.$$

2.3.3. Cosmic Dawn

Even before the Universe had been significantly reionized, the formation of the first radiating objects had an important influence on their surroundings. The Universe had exited the Dark Ages and entered the period known as **Cosmic Dawn** (e.g. [RDIM17]). This had dramatic effects on the otherwise ever-cooling IGM. At redshifts $z \lesssim 200$ the IGM cooled adiabatically as $T_K \propto a^{-2}$, whereas the CMB cools as $T_\gamma \propto a^{-1}$. But at the present, photo-ionization have led to $T_K \sim 10^4$ K $\gg T_\gamma$. What was the nature of this transition? The gradual heating of the IGM must have been driven by the first sources of radiation within virialized halos. The radiation emanating from these sources should preferably be quite energetic, because the photoionization cross section of hydrogen (in its ground state) scales like $\sigma_{\nu, \text{ion}} \propto \nu^{-3}$ [Shu91].⁸

Since the cross section decreases with photon energy, this means that if the IGM is to be successfully heated far away from a source, the photons should be fairly energetic. Because of this, the effects of X-ray (e.g. [MMR97, Fur06, PF07, LF13, MFS13, RDIM17]), and even gamma-ray [LED⁺17], heating of the IGM has been explored in the literature. X-ray binaries — binary stars where a small object (e.g. a black hole) accretes mass from a larger companion star, heating the material up and making it radiate X-rays [RB07] — are particularly promising candidates (e.g. [RDIM17]). Regardless of the details, we can model the frequency integrated (comoving) X-ray emissivity as being proportional to the star formation rate [MFS13]. If a fraction $f_{X,h}$ of the X-ray energy is injected into the neutral fraction of the IGM, then to first approximation, the heating rate is,

$$\epsilon_X \sim f_{X,h} N_X h\nu_0 f_* n_{b,0} \frac{df_{\text{coll}}}{dt}. \quad (2.19)$$

Here N_X is the number of X-ray photons per *stellar* baryon, $h\nu_0$ is some reference energy and $f_* n_{b,0} df_{\text{coll}}/dt$ is the rate at which baryons are incorporated into stars. The heating rate can be related to the temperature change in the IGM due to X-ray heating, \dot{T}_K^X , via $\epsilon_X \sim (3/2) n_{b,0} k_B \dot{T}_K^X$. Thus,

$$\dot{T}_K^X \sim \frac{2}{3} f_{X,h} \frac{N_X}{k_B} h\nu_0 f_* \frac{df_{\text{coll}}}{dt}. \quad (2.20)$$

Integrating this over time then yields

$$\Delta T_K^X(z) \sim \frac{2}{3} f_{X,h} \frac{N_X}{k_B} h\nu_0 f_* f_{\text{coll}}(z). \quad (2.21)$$

⁸I've ignored a frequency dependent gaunt factor $g(\nu)$ which is of order unity [Shu91]. It makes the photoionization cross section vary as $\nu^{-7/2}$ for $h\nu \gg 13.6$ eV (see e.g. [Shu91, Pad00, SN10]), but the qualitative point remains.

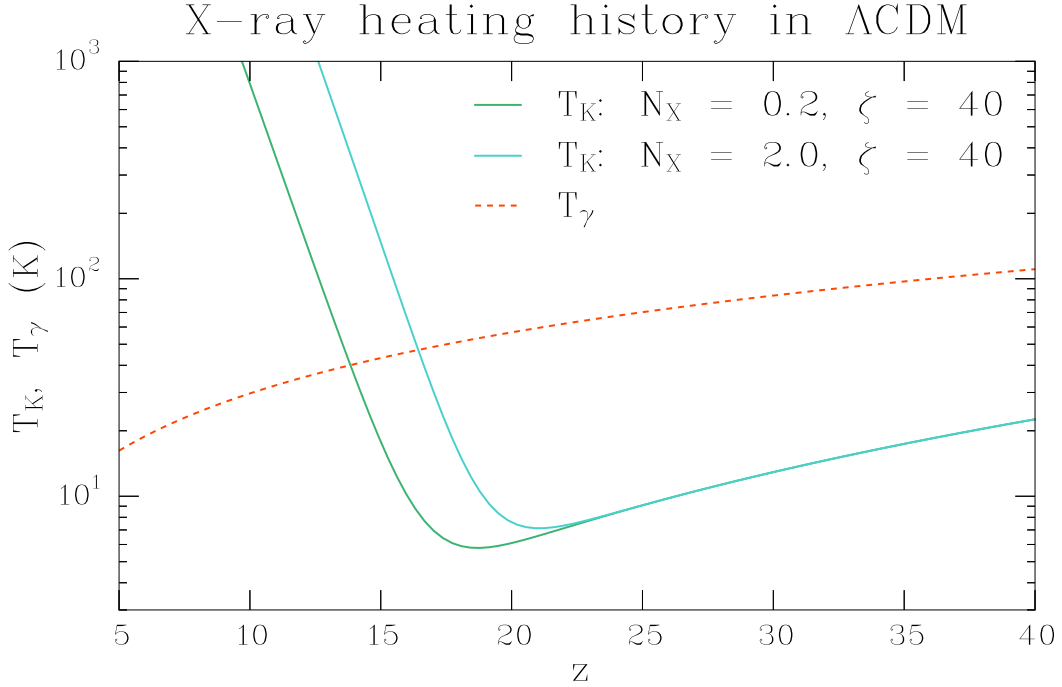


FIGURE 2.5. The Λ CDM heating history of the IGM as predicted by Eq. A.25 with the Pop II parameters in Table II. Because a number of crude approximations have been used, this heating history should be taken with a grain of salt. But interestingly enough it happens to be very similar to the more sophisticated model in [Fur06] (see Figure 1 in that paper).

Using $f_{X,h} = 0.2$ (valid for ionization fractions $\sim 10^{-3}$ [Fur06]), $N_X = 0.2$ [MFS13, RDIM17], $h\nu_0 = 1$ keV [PF07, MFS13]⁹, and $f_\star = 0.1$, it follows that

$$\begin{aligned} \Delta T_K^X &\sim 10^3 \left(\frac{N_X}{0.2} \right) \left(\frac{f_{X,h}}{0.2} \right) \left(\frac{f_\star}{0.1} \right) \left(\frac{h\nu_0}{1 \text{ keV}} \right) \left(\frac{f_{\text{coll}}}{4 \times 10^{-2}} \right) \text{ K} \\ &= 10^3 f_X \left(\frac{f_{X,h}}{0.2} \right) \left(\frac{f_\star}{0.1} \right) \left(\frac{h\nu_0}{1 \text{ keV}} \right) \left(\frac{f_{\text{coll}}}{4 \times 10^{-2}} \right) \text{ K}. \end{aligned} \quad (2.22)$$

Here I have evaluated f_{coll} at $z \sim 10$ and defined the **X-ray efficiency** $f_X \equiv (N_X/0.2)$. This estimate is similar to the one given by [Fur06], and is quite close to what is seen in simulations (see e.g. Figure 1 in the same paper). Note the intimate relation between how much the IGM is heated and the nature of dark matter, from which f_{coll} derives. In Appendix A.2 a slightly more sophisticated (but still a very simple) model of the heating history of the IGM is derived that takes adiabatic cooling into account. The resulting heating history is plotted in Figure 2.5.

⁹[MFS13] uses $h\nu_0 = 0.3$ keV, but they have a factor α — the spectral energy index — in front of the $\epsilon_{X,\nu}$, so that they get a factor $\alpha/(\alpha - 1) = 3$ (for $\alpha = 1.5$) in front of Eq. 2.19. Choosing $h\nu_0 \simeq 1$ keV thus compensates for this.

2.3.4. 21 cm Cosmology

One exciting way to study the heating history and reionization of the Universe is by observing the 21 cm line of hydrogen. The 21 cm line arises from the hyperfine splitting of the hydrogen ground state due to spin-spin coupling between the electron and proton. The energy difference between the triplet (parallel spins) and singlet (total spin of zero) states is a mere $\Delta E_{21\text{cm}} = 5.88 \times 10^{-6}$ eV, corresponding to a frequency of $\nu_{21\text{cm}} = 1420$ MHz [Gri04]. The Einstein A-coefficient for the transition between these states is $A_{10} = 2.85 \times 10^{-15}$ s⁻¹ [LF13]. It is customary to *define* a **spin temperature** T_S that determines the relative population of the triplet n_1 and singlet n_0 population via a Boltzmann-type distribution (e.g. [PL08, Loe10, LF13]),

$$\frac{n_1}{n_0} \equiv 3e^{-T_\star/T_S} \simeq 3 \left(1 - \frac{T_\star}{T_S}\right), \quad (2.23)$$

where the factor of 3 comes from the ratio of statistical weights, g_1/g_0 , and $T_\star \equiv \Delta E_{21\text{cm}}/k_B = 62.8$ mK. The last step is justified because $T_\star \ll T_S$ for all practical purposes. Photons travelling through the IGM can be absorbed and excite the electron from the singlet state. The net absorption can be shown to yield an optical depth of (e.g. [LF13]),

$$\begin{aligned} \tau_{21\text{cm}} &\simeq \frac{3A_{10}}{32\pi} \frac{hc^3}{\nu_{21\text{cm}}^2} \frac{x_{\text{HI}}\bar{n}_H(1+\delta_{\text{HI}})}{k_B T_S H(z)} \\ &\simeq 7.9 \times 10^{-3} (1 + \delta_{\text{HI}}) \left(\frac{\Omega_{b,0}h^2}{0.021}\right) \left(\frac{\Omega_{m,0}h^2}{0.14}\right)^{-1/2} (1+z)^{3/2} \frac{x_{\text{HI}}}{T_S}. \end{aligned} \quad (2.24)$$

The last step is derived by considering only relatively high redshifts where the Universe is matter dominated. Because $\tau_{21\text{cm}} \ll \tau_{\text{GP}}$ this makes 21 cm a much more attractive way of studying the early stages of reionization and the heating of the IGM. The study of the heating history of the IGM is possible because the spin temperature couples with the IGM temperature as will be seen shortly. At redshift z the 21 cm line will be redshifted to $21(1+z)$ cm, which is always in the radio regime of the spectrum. Because the Planck spectrum of the CMB peaks in the microwave region, we can relate the CMB black body spectrum B_ν to T_γ using the Rayleigh-Jeans limit $B_\nu = 2\nu^2 k_B T_\gamma / c^2$. Similarly, we can *define* the 21 cm **brightness temperature** T_b via its intensity $I_\nu \equiv 2\nu^2 k_B T_b / c^2$.¹⁰

Using this, the radiative transfer equation can be solved for the 21 cm brightness temperature. Since we are interested in the contrast between the 21 cm and CMB radiation, we define the *differential* 21 cm brightness temperature $\delta T_b \equiv T_b - T_\gamma$.

¹⁰In general, the brightness temperature is defined via $I_\nu = B_\nu (T_b)$, but we're only focusing on a regime of the spectrum where the Rayleigh-Jeans limit is an excellent approximation.

The result is [LF13],

$$\begin{aligned}\delta T_b &\simeq \frac{T_s - T_\gamma}{1+z} \tau_{21\text{cm}} \\ &\simeq 7.9 x_{\text{HI}} (1 + \delta_{\text{HI}}) \left(\frac{\Omega_{b,0} h^2}{0.021} \right) \left(\frac{\Omega_{m,0} h^2}{0.14} \right)^{-1/2} (1+z)^{1/2} \left(1 - \frac{T_\gamma}{T_s} \right) \text{ mK.}\end{aligned}\quad (2.25)$$

The spin temperature is determined by an equilibrium between[LF13]

- Absorption of CMB photons,
- Collisional excitation and de-excitation from H-H, H-e and H-p collisions and,
- UV photon scattering excitation and de-excitation.

In analogy with the spin temperature, we can define a **color temperature** T_C via $P_{01} \simeq 3P_{10} (1 - T_\star/T_C)$ where P_{10} and P_{01} are the UV scattering de-excitation and excitation rates respectively (in s^{-1}). After some tedious algebra, this allows us to write the spin temperature as (e.g. [FOB06, PF07, PL08, LF13]),

$$T_s^{-1} \simeq \frac{T_\gamma^{-1} + x_C T_K^{-1} + x_\alpha T_C^{-1}}{1 + x_C + x_\alpha}, \quad (2.26)$$

$$x_C \equiv \frac{C_{10} T_\star}{A_{10} T_\gamma}, \quad (2.27)$$

$$x_\alpha \equiv \frac{P_{10} T_\star}{A_{10} T_\gamma}, \quad (2.28)$$

where C_{10} is the collisional de-excitation rate. The **Wouthuysen-Field effect coupling**, or **Ly- α coupling**, x_α is related, through the UV scattering de-excitation rate P_{10} , to the Ly- α background flux in the Universe, J_α (J_ν in $\text{cm}^{-2} \text{ Hz}^{-1} \text{ ster}^{-1} \text{ s}^{-1}$ evaluated at $\nu_{\text{Ly}\alpha}$). Absorption of a Ly- α photon excites the electron to the $n = 2$ state, from which it can then spontaneously de-excite to either the singlet or triplet $n = 1$ state. This will change the hyperfine population, and therefore also T_s . And this is captured in Eq. 2.26. This effect is called the **Wouthuysen-Field effect** after Siegfried A. Wouthuysen [Wou52] and George B. Field [Fie59] who discovered it. The Ly- α coupling can be written in terms of J_α as [Fur06, PF07, PL12, LF13]

$$x_\alpha = S_\alpha \frac{J_\alpha}{J_\nu^c}. \quad (2.29)$$

Where $J_\nu^c = 1.165 \times 10^{-10} \left(\frac{1+z}{20} \right) \text{ cm}^{-2} \text{ Hz}^{-1} \text{ ster}^{-1} \text{ s}^{-1}$ and $S_\alpha \sim 1$ is a correction factor (a more accurate fit can be found in [PL12, LF13]). As for the **collisional coupling** x_C , it can be expanded as[PL12]

$$x_C = \frac{T_\star}{A_{10} T_\gamma} \left\{ \kappa_{10}^{\text{H-H}} (T_K) n_{\text{HI}} + \kappa_{10}^{\text{H-e}} (T_K) n_e + \kappa_{10}^{\text{H-p}} (T_K) n_p \right\}. \quad (2.30)$$

Fits to the rate coefficients $\kappa_{10}^{\text{H-H}}$ and $\kappa_{10}^{\text{H-P}}$ can be found in [PL12], whereas $\kappa_{10}^{\text{H-P}}$ is relatively small (and as a first approximation can be ignored) in the relevant temperature range (see pp. 413-414 in [LF13]). Given the linear dependence on three different collision rates, the collisional coupling could be split into three terms: $x_C^{\text{H-H}}$, $x_C^{\text{H-e}}$ and $x_C^{\text{H-P}}$. At relatively low redshifts of interest for studying Cosmic Dawn and EoR, x_α dominates over x_C .

2.4. Small-scale problems in Λ CDM

While Λ CDM provides a very successful model on large scales, potential problems are encountered on small scales. As shown in Eq. 2.12, the predicted HMF scales as $\partial n / \partial M \propto M^{-1.9}$ for small halo masses. This result in the prediction of an abundance of small halos populating the Universe, some of which should end up in the Local Group. However, there is a discrepancy between this prediction and the number of satellite galaxies observed around the Milky Way. This discrepancy is known as the **Missing Satellite Problem**. This could indicate new dark matter physics that yield a cut-off in the power spectrum (so that on small scales $\sigma \simeq$ constant, yielding $\partial n / \partial M \propto |\partial \log n / \partial \log M| \simeq 0$), but it could also be explained by baryonic feedback from supernovae that ejects the gas from which stars form, thus quenching star formation in dwarf galaxies [DS86]. Then there would be few dwarf galaxies observed even though the number of halos would line up with the prediction of Λ CDM. A more serious related problem is known as the **Too-Big-To-Fail Problem**. This is the seeming prediction by Λ CDM that the most massive satellite galaxies should be even more massive and dense than the ones observed around the Milky Way. This is unexpected because supernovae feedback should not lead them to fail to produce stars, and so they should be readily visible to observers. Furthermore, they are too dense. This latter points bring us to the final problem known as the **Cusp/Core Problem**. The dark matter density profiles in CDM halos are expected to be cuspy and diverge like $\rho \sim r^{-1}$ towards the center [NFW96]. Observations instead seem to favour cored density profiles. Whether this simply indicates that simulations of Λ CDM do not incorporate strong enough baryonic feedback or hints at new dark matter physics (or perhaps both) is an open question. It at least motivates a serious look at dark matter models that deviate from CDM on small scales. For more details on small-scale problems in Λ CDM, see e.g. the reviews in [WBG⁺15, PD17] and the interesting papers in [ZMM⁺16, PS16, TGSP⁺17].

2.5. Fuzzy Dark Matter

2.5.1. Dynamics

One way to try to solve the aforementioned potential small-scale problems in Λ CDM is to reconsider the very nature of dark matter. Any plausible solution of that type should preferably rely on as few free parameters as possible. One especially

attractive solution to the small-scale problems in Λ CDM goes under many names. The most common are **fuzzy dark matter** (FDM) [HBG00, HOTW17], **ultra-light axions** (ULA) [CAMD17], **wave dark matter** (ψ DM) [SCB14] and **scalar field dark matter** (SFDM) [TRM17]. These names can be used interchangeably. The *only* free parameter that goes into FDM is the particle mass, m_{FDM} . The dark matter is assumed to be a scalar field ϕ (the quanta of which are spin-0 particles), governed by the action [HOTW17, Gri08, Pea98, Pee93],¹¹¹²

$$\mathcal{S} = \int d^4x \sqrt{-g} \left\{ \frac{1}{2} \nabla^\mu \phi \nabla_\mu \phi - \frac{1}{2} \left(\frac{m_{\text{FDM}} c}{\hbar} \right)^2 \phi^2 \right\}, \quad (2.31)$$

with an exceedingly light particle mass $m_{\text{FDM}} \sim 10^{-22}$ eV (much smaller than, e.g., the electron mass: $m_e \simeq 5 \times 10^5$ eV). The astrophysical motivation for considering such a small particle mass is that the FDM “particles” will have de Broglie wavelengths [HOTW17]

$$\frac{\lambda}{2\pi} = \frac{\hbar}{m_{\text{FDM}} v} \simeq 1.92 \left(\frac{m_{\text{FDM}}}{10^{-22} \text{ eV}} \right)^{-1} \left(\frac{v}{10^2 \text{ km s}^{-1}} \right)^{-1} \text{ kpc}. \quad (2.32)$$

In other words, FDM behaves wave-like on scales comparable to the cores observed in galaxies. This will also have a significant impact on structure formation. But why would a particle this light ever be considered in particle physics?¹³ On the face of it, such a light particle might seem artificial. But Nature favours symmetry (indeed, the forces of Nature could even be derived from symmetries [Pea98, Gri08, Sch15]), and the action in Eq. 2.31 is invariant under a global continuous shift symmetry

¹¹The **action** is a quantity that, when extremized ($\delta\mathcal{S} = 0$), yields the equations of motion. Both Newton’s equations of motion as well as field equations (e.g. Einstein’s field equations or the Dirac equation) can be derived from actions. If the action is only a time integral, then the integrand is known as the **Lagrangian** L of the system. If the integral is also over volume, then the integrand is known as the Lagrangian density, \mathcal{L} (often just shortened to “Lagrangian”). Writing down the action or Lagrangian of a system is often the starting point in fundamental physics because it is easier to see the symmetries involved. For example, if the Lagrangian has no explicit time dependence it can be shown that there is a quantity, the Hamiltonian, which is conserved. For an introduction to the use of the action in Newtonian mechanics, see [LL69, Pad00], for the use in general relativity see [Pee93, Pad00], and for the use in particle physics see [Gri08, Sch15].

¹²Some basic concepts of general relativity are used here. First, the **metric tensor** — describing the geometry of spacetime — $g_{\mu\nu}$. It can be defined via the line element, $ds^2 = g_{\mu\nu} dx^\mu dx^\nu$. The Einstein summation convention is used where repeated indices are summed over, so that what is implied is $ds^2 = \sum_{\mu,\nu} g_{\mu\nu} dx^\mu dx^\nu$. The indices range from 0 to 3, where $x^0 \equiv ct$ and the rest are the spatial coordinates. The line element of the flat Minkowski spacetime of special relativity can be recovered with $g_{\mu\nu} = \eta_{\mu\nu} \equiv \text{diag}(1, -1, -1, -1)$. And the more relevant FLRW line element describing a flat expanding Universe can be derived from the metric tensor $g_{\mu\nu} = \text{diag}(1, -a^2, -a^2, -a^2)$. Furthermore, $g \equiv \det g_{\mu\nu}$ and the ∇ ’s are covariant derivatives. For a good introductions to general relativity, see [Ken90, Pee93, Pad00].

¹³I would like to note that cosmologists have considered scalar field models of dark energy — called *quintessence* — since the 80’s (see the discussion and references in [Pee93, PR03]). These models require particle masses $m \sim 10^{-33}$ eV to explain the observed accelerated expansion of the Universe. So theorists investigating FDM are not considering hitherto unfathomable particle masses.

$\phi \rightarrow \phi + \mathcal{C}$ for some constant \mathcal{C} if $m_{\text{FDM}} = 0$. This coupled with the argument that quantum gravity only makes such symmetries approximate would yield a tiny but non-zero particle mass plausible [HOTW17]. What equations govern the dynamics of FDM? We can derive the equations of motion of the FDM scalar field by varying the action above with respect to the field itself. We get¹⁴

$$\begin{aligned}\delta\mathcal{S} &= \int d^4x \sqrt{-g} \left\{ \nabla^\mu \phi \nabla_\mu \delta\phi - \left(\frac{m_{\text{FDM}} c}{\hbar} \right)^2 \phi \delta\phi \right\} \\ &= - \int d^4x \sqrt{-g} \left\{ \nabla_\mu \nabla^\mu \phi + \left(\frac{m_{\text{FDM}} c}{\hbar} \right)^2 \phi \right\} \delta\phi.\end{aligned}\quad (2.33)$$

So if $\delta\mathcal{S} = 0$ we arrive at the **Klein-Gordon equation** (named in part after Oskar Klein, 1894-1977, who worked at what has now become Stockholm University),

$$\left\{ \nabla_\mu \nabla^\mu + \left(\frac{m_{\text{FDM}} c}{\hbar} \right)^2 \right\} \phi = 0. \quad (2.34)$$

Because the particles considered are bosons, they can — even with their extremely small masses — form a Bose-Einstein condensate where almost all particles occupy the ground state [WC09]. Thus, even though the particles are extremely light, the distribution of energies can still make most of them non-relativistic. This justifies a non-relativistic approximation to Eq. 2.34. It can be shown that, in the non-relativistic limit, the FDM field will behave like a fluid with a modified Euler equation (e.g. [HOTW17]),

$$\frac{\partial \mathbf{v}}{\partial t} + \frac{1}{a} (\mathbf{v} \cdot \nabla) \mathbf{v} = -\frac{\dot{a}}{a} \mathbf{v} - \frac{1}{a} \nabla \phi + \frac{\hbar^2}{2a^3 m_{\text{FDM}}^2} \nabla \left(\frac{\nabla^2 \sqrt{\rho}}{\sqrt{\rho}} \right). \quad (2.35)$$

By comparison with Eq. 2.2, we see a pressure term¹⁵ $(\hbar^2/2a^3 m_{\text{FDM}}^2) \nabla \left(\nabla^2 \sqrt{\rho} / \sqrt{\rho} \right)$. As long as the particle mass is not too large, this pressure will prohibit gravitational collapse on small scales. In the Appendix it is shown that FDM density perturbations can not grow on scales below the **FDM Jeans mass** $M_{\text{FDM,J}}$ (or, equivalently, above the **FDM Jeans wavenumber** $k_{\text{FDM,J}}$),

$$M_{\text{FDM,J}}(z) \simeq 1.0 \times 10^8 m_{\text{FDM},22}^{-3/2} \left(\frac{\Omega_{\text{m},0} h^2}{0.14} \right)^{1/4} \left(\frac{1+z}{13} \right)^{3/4} M_\odot, \quad (2.36)$$

$$k_{\text{FDM,J}}(z) \simeq 36 m_{\text{FDM},22}^{1/2} \left(\frac{\Omega_{\text{m},0} h^2}{0.14} \right)^{1/4} \left(\frac{1+z}{13} \right)^{-1/4} \text{Mpc}^{-1},$$

where I have defined $m_{\text{FDM},22} \equiv m_{\text{FDM}}/10^{-22}$ eV. The effect of the Jeans mass on the power spectrum can be understood easily. Since (sub-horizon) density

¹⁴In the second step I use $\nabla_\mu (\delta\phi \nabla^\mu \phi) = \nabla^\mu \phi \nabla_\mu \delta\phi + \delta\phi \nabla_\mu \nabla^\mu \phi$ (just the product rule). And the left hand side vanishes when integrated over using the divergence theorem since $\delta\phi = 0$ on this boundary.

¹⁵A pressure term on the right-hand side of the Euler equation generally looks like $-\nabla p/\rho$ (e.g. [RB07]).

perturbations start to grow significantly first at matter-radiation equality, it follows that structure formation will be either delayed or prohibited below $M_{\text{FDM,J}}(z_{\text{eq}}) \simeq 6.5 \times 10^9 M_\odot$. This was first confirmed in [HBG00] who found the FDM power spectrum could be written as $P_{\text{FDM}}(k) = P_{\text{CDM}}(k) T_F^2(k)$ where P_{CDM} is the power spectrum predicted by CDM (as discussed earlier in this chapter) and

$$T_F(k) \simeq \frac{\cos x^3}{1+x^8}, \quad (2.37)$$

$$x \simeq 1.61 m_{\text{FDM,22}}^{1/18} \frac{k}{k_{\text{FDM,J}}(z_{\text{eq}})}.$$

The FDM power spectrum drops to $\frac{1}{2}P_{\text{CDM}}(k)$ at $k_{1/2} \simeq \frac{1}{2}k_{\text{FDM,J}}(z_{\text{eq}}) m_{\text{FDM,22}}^{-1/18}$, and the corresponding mass scale is $\sim 8M_{\text{FDM,J}}(z_{\text{eq}})$. At the time of this writing, there are no published results of N-body simulations that includes the pressure term in Eq. 2.35 *and* baryonic physics. However, one article doing this is in preparation according to [MVR⁺17]. Instead, there have been dark matter-only simulations that incorporates the pressure-like effect of FDM (e.g. [WC09, SCB14]), or CDM simulations (with or without baryonic physics) initialized using an FDM power spectrum (e.g. [SCBH16, IVH⁺17]).

In Figure 2.6 a cooling diagram for AFDM is plotted, which clearly shows that the halos in which the first galaxies form have masses $\sim 10^{10} M_\odot$ (since the density of the gas in a halo is proportional to the background density when the halo formed). This is just what is expected from the earlier argument concerning the FDM Jeans mass at matter-radiation equality. *It is therefore plausible that very luminous Pop III stars form in abundance in these relatively massive galaxies and play an important role during the EoR and Cosmic Dawn.*

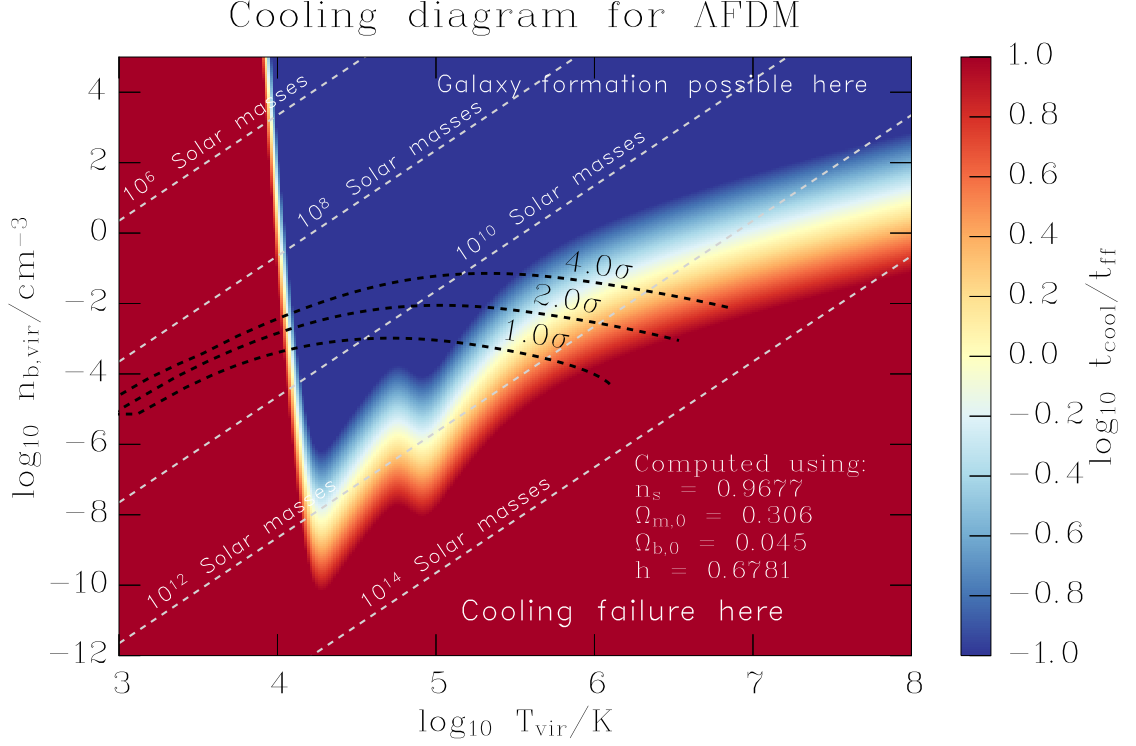


FIGURE 2.6. Cooling diagram for AFDM, with $m_{\text{FDM},22} = 1$. Eq. 2.37 was used to compute the FDM power spectrum. Scale-dependent growth in FDM was incorporated using the fitting function in [DBN17]. This cooling diagram can be compared with the cooling diagram for Λ CDM in Figure 2.3.

That the number of halos below $\sim 10^{10} M_\odot$ in FDM should be much smaller than in CDM can also be understood from the HMF in Eq. 2.11. For a cutoff to the power spectrum near $\sim 10^{10} M_\odot$ (as predicted by Eq. 2.37 for $m_{\text{FDM},22} = 1$), it follows that $\sigma(M \ll 10^{10} M_\odot) \simeq \text{constant}$. Thus, $\partial n / \partial M \propto \partial \log \sigma / \partial \log M \simeq 0$ for $M \ll 10^{10} M_\odot$. Furthermore, and more relevant for galaxy formation, Figure 2.6 indicates that barely no *galaxies* (and not just halos) inside halos of mass $\sim 10^9 M_\odot$ form even at late times due to cooling failure.

2.5.2. Observational constraints

A few important observational constraints on m_{FDM} exist at the moment. Delayed structure and galaxy formation will impact when reionization takes place. According to [SCBH16], $m_{\text{FDM},22} \geq 1.2$ is consistent with Planck data as well as the high-redshift luminosity function. Recently, it has been argued, through the use of N-body simulations, that the Lyman- α forest puts a more severe constraint: $m_{\text{FDM},22} \gtrsim 10$ [IVH⁺17, KMS⁺17]. However, these N-body simulations simply made use of CDM dynamics with an FDM power spectrum, thus ignoring the pressure term in Eq. 2.35. Because of this and other intrinsic astrophysical

uncertainties, it has, even more recently, been argued that the Lyman- α forest cannot exclude $m_{\text{FDM},22} \sim 1$ [ZKL⁺17]. Simulations that do not neglect the FDM pressure term will therefore be needed to assess Lyman- α constraints.

Other observational constraints, *not* connected to structure formation, comes from the sizes of the density cores observed in galaxies. The core radius expected in a halo that forms at redshift z can be estimated from Eq. 2.32 using $v \simeq (GM/R_{\text{vir}})^{1/2}$, which gives us

$$\begin{aligned} R_{\text{core}} &\simeq \left(18\pi^2\right)^{-1/6} \left(\frac{3}{4\pi}\right)^{1/6} \frac{\hbar M^{-1/3}}{Gm_{\text{FDM}}} (1+z)^{-1/2}, \\ &\simeq 0.77 m_{\text{FDM},22}^{-1} \left(\frac{M}{10^{10} M_\odot}\right)^{-1/3} (1+z)^{-1/2} \text{ kpc}. \end{aligned} \quad (2.38)$$

This expression — both in terms of scaling and the numerical value itself — agrees almost perfectly with the expression derived more rigorously in [SLW⁺14], which reproduces the results in [SCB14] fairly well. Comparison of the predicted FDM core radius with observational data of dwarf spheroidal galaxies yields $m_{\text{FDM},22} \gtrsim 1.18$ or $m_{\text{FDM},22} \gtrsim 1.79$ depending on the data used [CSC17].

In summary, $m_{\text{FDM},22} \sim 1$ seems to be consistent with constraints from both structure formation and the density profiles of dwarf galaxies. This means that FDM may avoid the so-called *Catch-22* problem that seems to plague **warm dark matter** (WDM), which is another popular attempt at solving the small-scale problems in Λ CDM [MPA⁺12]. WDM posits that dark matter are made of light fermions ($m_{\text{WDM}} \sim 1$ keV) with non-negligible thermal motion that suppresses density fluctuations on small scales. WDM can also give rise to density cores. The Catch-22 problem arises from the realization that a particle mass small enough to give rise to kiloparsec-sized density cores in dwarf galaxies is too small to produce the very dwarf galaxies these cores are supposed to reside in. FDM avoids this problem, as Eq. 2.38 shows that $R_{\text{core}} \sim 1$ kpc even for $M > M_{\text{FDM,J}}(z_{\text{eq}})$.

An unexplored area that could put constraints on $m_{\text{FDM},22}$ comes from 21 cm cosmology. At this point, studies trying to constrain $m_{\text{FDM},22}$ using the 21 cm signal have focused on relatively low redshifts and neglected the evolution of the spin temperature [KMIS14, SMD⁺16].¹⁶ The evolution of the spin temperature can not be neglected during Cosmic Dawn and the EoR. Delayed structure formation will delay Cosmic Dawn, which should manifest itself in the 21 cm signal and might be probed with upcoming observations. Whether it is possible to differentiate FDM from CDM at Cosmic Dawn using the 21 cm signal is explored in this thesis.

¹⁶[SMD⁺16] produced the relatively weak constraint $m_{\text{FDM},22} > 0.26$.

3. Methods

3.1. Model

To study the 21 cm signal from Cosmic Dawn in both CDM and FDM a semi-analytical model by Pritchard and Furlanetto (PF) [PF07] was employed. Being semi-analytical and not an N-body simulation, the PF model is, relatively speaking, not very computationally expensive. This makes exploration of the parameter space less time consuming and could highlight potentially interesting results that can then be explored in more detailed N-body simulations. The PF model takes a matter power spectrum and compute a collapse fraction. Given the collapse fraction, and choosing values for the parameters ζ and f_x discussed in the last chapter, the 21 cm signal can be derived.

While the PF model is not an N-body simulation, it still permits calculations of fluctuations in the 21 cm signal from the inhomogeneous heating of the IGM. This is convenient because fluctuations in the 21 cm signal are, at the moment, observationally more interesting than the global mean 21 cm signal. The basic reason for this is that the global signal is dwarfed by galactic sky noise: $T_{\text{sky}} \simeq 180 (\nu/180 \text{ MHz})^{-2.6} \text{ K} \gg |\delta T_b|$ [FOB06, PL08]. Focusing on fluctuations in the 21 cm signal gets around this issue.¹ But to be clear, the PF model computes both the global 21 cm signal as well as fluctuations in it.

The fluctuations in the brightness temperature can to first order be expanded linearly as [PF07, LF13],

$$\delta_{T_b} = \beta \delta_b + \beta_x \delta_x + \beta_\alpha \delta_\alpha + \beta_T \delta_T - \delta_{\partial v}, \quad (3.1)$$

where δ_b is the baryon density fluctuation, δ_x is the fluctuation in the neutral fraction, δ_α the fluctuation in x_α , δ_T the fluctuation in the kinetic temperature T_K and $\delta_{\partial v}$ the fluctuation in the line-of-sight peculiar velocity gradient. The β coefficients in this expansion can be computed in terms of the couplings (where

¹This can be understood from the fact that $T_{\text{sky}}(\nu)$ is a known, quite smooth, function of frequency and direction, whereas δT_b is not smooth because a frequency (and so redshift) or angular increment corresponds to a spatial increment that can yield significant fluctuations in the signal. Only the average 21 cm signal over the whole sky is smooth like $T_{\text{sky}}(\nu)$.

$x_{\text{tot}} \equiv x_\alpha + x_C$), collision rates and the temperatures:

$$\begin{aligned}\beta &= 1 + \frac{x_C}{x_{\text{tot}}(1+x_{\text{tot}})}, \\ \beta_x &= 1 + \frac{x_C^{\text{H-H}} - x_C^{\text{H-e}}}{x_{\text{tot}}(1+x_{\text{tot}})}, \\ \beta_\alpha &= \frac{x_\alpha}{x_{\text{tot}}(1+x_{\text{tot}})}, \\ \beta_T &= \frac{T_\gamma}{T_K - T_\gamma} + \frac{1}{x_{\text{tot}}(1+x_{\text{tot}})} \left(x_C^{\text{H-e}} \frac{d \log \kappa_{10}^{\text{H-e}}}{d \log T_K} + x_C^{\text{H-H}} \frac{d \log \kappa_{10}^{\text{H-H}}}{d \log T_K} \right).\end{aligned}\tag{3.2}$$

Fourier transforming $\delta_{T_b}(\mathbf{x})$ then makes it possible to derive the 21 cm power spectrum $P_{21\text{cm}}$ (e.g. [LF13]),

$$\langle \delta_{T_b, \mathbf{k}} \delta_{T_b, \mathbf{k}'} \rangle = (2\pi)^3 \delta_D(\mathbf{k} - \mathbf{k}') P_{21\text{cm}}(\mathbf{k}).\tag{3.3}$$

In these expressions for the β coefficients, the approximations $T_C \simeq T_K$ and $\kappa_{10}^{\text{H-e}}, \kappa_{10}^{\text{H-H}} \gg \kappa_{10}^{\text{H-p}}$ [LF13] have been used. Furthermore, the PF model assumes that the baryon density fluctuations traces the dark matter density fluctuations, so that $\delta_b \simeq \delta_{\text{DM}}$. In CDM, this approximation is certainly valid for wavenumbers $k > k_{J,b}$ (the baryon Jeans wavenumber) and in FDM for wavenumbers $k > k_{J,\text{FDM}}$ (the FDM Jeans wavenumber).² Recent (see the introduction as well as results in [PYK⁺17]) as well as upcoming (e.g. discussion in [PL08, LF13]) 21 cm observations will be limited to probing scales $k \lesssim 1 \text{ Mpc}^{-1}$, and with a special focus towards scales $k \sim 0.1 \text{ Mpc}^{-1}$. This is significantly larger than the baryonic Jeans scale. As for the FDM Jeans scale, the criterion $1 \text{ Mpc}^{-1} \lesssim k_{J,\text{FDM}}$ yields a constraint on the particle mass,

$$m_{\text{FDM},22} \gtrsim 7.7 \times 10^{-4} \left(\frac{\Omega_{\text{m},0} h^2}{0.14} \right)^{-1/2} \left(\frac{1+z}{13} \right)^{1/2}.\tag{3.4}$$

Since we are interested in masses and redshifts of order $m_{\text{FDM},22} \sim 1$ and $z \sim 10$ respectively, we do not need to worry about a breakdown in the assumption that $\delta_b \simeq \delta_{\text{DM}}$. Furthermore, because the ratio between the FDM and CDM power spectra drops to 1/2 first at $k \simeq \frac{1}{2} k_{J,\text{FDM}} (z_{\text{eq}}) m_{\text{FDM},22}^{1/18} = 4.5 m_{\text{FDM},22}^{4/9} \text{ Mpc}^{-1} > 1 \text{ Mpc}^{-1}$ [HBG00] it follows that $\delta_{\text{DM}} \simeq \delta_{\text{CDM}}$ on scales of interest ($k \lesssim 1 \text{ Mpc}^{-1}$). Consequently, the contribution of the $\beta \delta_b$ term to the 21 cm brightness temperature power spectrum can be determined from the standard CDM power spectrum — even for FDM.

²The latter is true because for scales $k_{J,\text{FDM}} < k < k_{J,b}$ there is nothing that stops the amplitude of the baryonic perturbation from growing, even though the FDM cannot do so.

The major difference between the CDM and FDM 21 cm power spectra will mainly come from differences in the terms $\beta_x \delta_x$, $\beta_\alpha \delta_\alpha$ and $\beta_T \delta_T$. All of these terms ultimately depends on f_{coll} through their dependence on T_K , the ionization fraction and x_α . A suitable model of f_{coll} — especially for FDM — is clearly needed. At first, an attempt was made to derive f_{coll} primarily from first principle. Using the FDM power spectrum in [HBG00] and the redshift-independent model for δ_{crit} in [DBN17], a Python program was written to derive the halo mass function (which can be integrated to find f_{coll}). However, a comparison with the halo mass function derived by the same method in [DBN17] revealed a less-than-satisfactory match for unknown reasons.

Because of this, a simple fit to the halo mass function from [SCBH16] was used instead. These authors used the FDM power spectrum in [HBG00] and ran N-body simulations of FDM and CDM. Their simulations did not include the pressure-like effect of FDM, and are therefore just simulating CDM dynamics with an FDM power spectrum. But, as they note, this is not problematic given their focus on deriving a halo mass function for masses $\gtrsim 10^9 M_\odot$ and redshifts $z \geq 4$. This mass scale exceeds the FDM Jeans mass for redshifts $1 + z \lesssim 270 (\Omega_{m,0} h^2 / 0.14)^{-1/3} m_{\text{FDM},22}^2$, which is well above the relevant redshift range for Cosmic Dawn. Thus, the pressure-like term of FDM can be neglected on these scales and the FDM halo mass function can be fit as a deviation from the CDM halo mass function. The fit derived from the N-body simulations in [SCBH16] is

$$\frac{\partial n}{\partial \log M} |_{\text{FDM}} = \frac{\partial n}{\partial \log M} |_{\text{CDM}} \left\{ 1 + \left(\frac{M}{M_0} \right)^{-1.1} \right\}^{-2.2}, \quad (3.5)$$

$$M_0 = 1.6 \times 10^{10} m_{\text{FDM},22}^{-4/3} M_\odot.$$

There is a clear physical interpretation of this result: Namely that the halo mass function in FDM starts to deviate substantially from CDM for masses $M \lesssim M_{\text{FDM},1/2} \propto m_{\text{FDM},22}^{-4/3}$ where $M_{\text{FDM},1/2}$ is the mass scale where $P_{\text{FDM}}/P_{\text{CDM}} = 1/2$. The fit 3.5 will overestimate the number of low-mass halos ($M \lesssim 10^9 M_\odot$) in FDM compared to [DBN17], and because of this, also overestimate f_{coll} . However, it still predicts orders of magnitude fewer low-mass halos than CDM with a dividing line near $\sim 10^{10} m_{\text{FDM},22}^{-4/3} M_\odot$ — the two most important features of FDM. And because of the overestimate of f_{coll} , *any significant deviation from CDM discovered in this work is likely to be exacerbated with better modelling of the FDM halo mass function.*

Ionization is treated in a two-phase fashion in the PF model. First we have x_i , which is roughly the fraction of volume occupied by HII regions. Reionization is therefore complete when $x_i = 1$. Secondly, the quantity x_e denotes the ionization fraction in the largely neutral regions outside of HII bubbles. A drawback of the PF model is the modelling of ionization fluctuations close to reionization. When $x_i \gtrsim 0.1$ (or more conservatively, $x_i \gtrsim 0.05$), a significant fraction of the IGM is occupied by HII bubbles, which should leave a mark in the 21 cm power spectrum

due to the spatial inhomogeneity. However, the contribution of these ionization fluctuations are not incorporated into the PF model, which is why the authors of the model focused on the power spectrum at redshifts where $x_i \lesssim 0.1$ [PF07]. This limitation must be taken into account when interpreting the results in this thesis.

3.2. Parameter selection & model scenarios

To investigate whether 21 cm observations can differentiate CDM from FDM a suitable set of interesting and plausible parameters must be chosen. Three main criteria for parameter selection are:

1. For FDM, the particle mass must be interesting in the sense that it can explain the small-scale problems that motivated FDM in the first place.
2. Astrophysical parameters, like ζ (more importantly the parameters that go into it) and f_X , must be physically plausible and consistent with observations.
3. The Universe should be reionized by $z \sim 6 - 8$.

To satisfy the first criterion, $m_{\text{FDM},22} = 1, 2, 3$ was chosen for investigation. These particle masses are similar to the ones considered in [SCBH16] (who ran N-body simulations for $m_{\text{FDM},22} = 0.8, 1.6., 3.2$) and is roughly suitable for generating the sizable density cores observed in dwarf galaxies, and is consistent with constraints related to structure formation, as discussed in the previous chapter.

In trying to satisfy the second and third criteria one is inevitably faced with the considerable uncertainty in astrophysical parameters at high redshifts. With this in mind, four different groups of scenarios were chosen to explore the parameter space: A, B, C and D. The parameters for the scenario groups A and B were chosen to isolate the effects of f_* and f_X on the 21 cm signal. Beyond these and other parameters previously discussed, there are also three parameters that goes into computing the Ly- α intensity J_α (which x_α is proportional to, as seen in Eq. 2.29). These parameters are $\mathcal{N}_{\alpha,*}$, $\mathcal{N}_{\text{LyL},*}$ and α_s . $\mathcal{N}_{\alpha,*}$ and $\mathcal{N}_{\text{LyL},*}$ are the number of photons per stellar baryon emitted in the frequency intervals $[\nu_{\text{Ly}\alpha}, \nu_{\text{Ly}\beta}]$ and $[\nu_{\text{Ly}\alpha}, \nu_{\text{LyL}}]$ respectively, where ν_{LyL} is the Lyman limit frequency. The parameter α_s comes in through the assumption that the emissivity in the interval $[\nu_{\text{Ly}\alpha}, \nu_{\text{Ly}\beta}]$ scales as ν^{α_s-1} [BL05].

For scenario groups A and B, $\mathcal{N}_{\alpha,*}$, $\mathcal{N}_{\text{LyL},*}$ and α_s are taken to be constant regardless of $m_{\text{FDM},22}$. The numerical values chosen were $\mathcal{N}_{\alpha,*} = 6520$, $\mathcal{N}_{\text{LyL},*} = 9690$ and $\alpha_s = 0.14$, characteristic of Pop II stars [BL05]. This is not entirely realistic for a mixed population of Pop II and Pop III stars, but it serves the purpose of isolating the effects of more important parameters like f_* and f_X .

Variations in $\mathcal{N}_{\alpha,*}$, $\mathcal{N}_{\text{LyL},*}$ and α_s are considered in the more realistic scenario groups C and D. The following procedure for estimating these parameters was used:

- $\mathcal{N}_{\alpha,*}$ and $\mathcal{N}_{\text{LyL},*}$ depends on whether the emitting stars are Pop II or Pop III. If the fraction of stars that are Pop II is f_{II} and the fraction that are Pop III is $1 - f_{\text{II}}$, then we have

$$\mathcal{N}_{\alpha,*} = f_{\text{II}} \mathcal{N}_{\alpha,\text{II}*} + (1 - f_{\text{II}}) \mathcal{N}_{\alpha,\text{III}*}, \quad (3.6)$$

$$\mathcal{N}_{\text{LyL},*} = f_{\text{II}} \mathcal{N}_{\text{LyL},\text{II}*} + (1 - f_{\text{II}}) \mathcal{N}_{\text{LyL},\text{III}*}, \quad (3.7)$$

where $\mathcal{N}_{\alpha,\text{II}*} \simeq 6520$, $\mathcal{N}_{\text{LyL},\text{II}*} \simeq 9690$, $\mathcal{N}_{\alpha,\text{III}*} \simeq 2670$ and $\mathcal{N}_{\text{LyL},\text{III}*} \simeq 4800$ [BL05].

- Next, f_{II} can be determined from $\mathcal{N}_{\gamma,*}$ through a similar relation for the ionizing photons,

$$\mathcal{N}_{\gamma,*} = f_{\text{II}} \mathcal{N}_{\gamma,\text{II}*} + (1 - f_{\text{II}}) \mathcal{N}_{\gamma,\text{III}*}. \quad (3.8)$$

From Table III we have $\mathcal{N}_{\gamma,\text{II}*} \simeq 4 \times 10^3$ and $\mathcal{N}_{\gamma,\text{III}*} \simeq 4 \times 10^4$. Solving for f_{II} yields

$$f_{\text{II}} = \frac{\mathcal{N}_{\gamma,*} - \mathcal{N}_{\gamma,\text{III}*}}{\mathcal{N}_{\gamma,\text{II}*} - \mathcal{N}_{\gamma,\text{III}*}}. \quad (3.9)$$

- Using this expression for f_{II} in Eq. 3.6 then let us compute $\mathcal{N}_{\alpha,*}$ given a value for $\mathcal{N}_{\gamma,*}$. This way of finding $\mathcal{N}_{\alpha,*}$ is accurate. Determining α_s on the other hand is more complicated. A simple averaging was used to estimate α_s ,

$$\alpha_s - 1 \simeq \frac{(\alpha_{s,\text{II}} - 1) f_{\text{II}} \mathcal{N}_{\alpha,\text{II}*} + (\alpha_{s,\text{III}} - 1) (1 - f_{\text{II}}) \mathcal{N}_{\alpha,\text{III}*}}{f_{\text{II}} \mathcal{N}_{\alpha,\text{II}*} + (1 - f_{\text{II}}) \mathcal{N}_{\alpha,\text{III}*}} \quad (3.10)$$

where $\alpha_{s,\text{II}} = 0.14$ and $\alpha_{s,\text{III}} = 1.29$ [BL05].

The rest of the parameters were chosen as follows,

- Scenario groups A and C contains fiducial parameters that are the most conservative. At first, approximate values for ζ in FDM were derived to satisfy the third criterion.³ After this, values for $\mathcal{N}_{\gamma,*}$ were picked in accordance with the second criterion, assuming $f_* = 0.1$ and $f_{\text{esc}} = 0.3$.⁴ For CDM, the Pop II parameters listed in Table II were used. An X-ray efficiency $f_X = 1.0$ was adopted for both CDM and FDM, in effect assuming that the X-ray efficiency at high redshifts equals the present one.

³Recall from the previous chapter that the Universe is reionized when $\zeta f_{\text{coll}} \simeq 1 + n_{\text{rec}}$. Thus, $\zeta \simeq (1 + n_{\text{rec}})/f_{\text{coll}}(z_{\text{reion}})$. In the calculations here, a value of $n_{\text{rec}} = 1.5$ was chosen and $z_{\text{reion}} = 6$ (in accordance with the third criteria).

⁴Using the derived values of ζ and starting with the assumption that $f_* = f_{\text{esc}} = 0.1$, values for $\mathcal{N}_{\gamma,*}$ were derived. Because $\mathcal{N}_{\gamma,*}$ exceeded the Pop III value (see Table II) for $m_{\text{FDM},22} = 1$ — violating the second criterion — this was then corrected for by decreasing $\mathcal{N}_{\gamma,*}$ and increasing f_{esc} by a factor of three for all FDM scenarios. f_* and f_{esc} are degenerate with respect to the reionization history, but f_{esc} is less constrained.

- Scenario groups B and D contains more extreme parameter choices than groups A and C. In particular, the star formation and X-ray efficiencies are boosted to $f_{\star} = 0.3$ (but kept at $f_{\star} = 0.1$ for CDM to not make reionization occur too early) and $f_X = 100$ respectively. These parameter choices effectively try to minimize any observational differences between CDM and FDM while still using observationally viable (albeit fairly extreme) parameters.

Table IV on the next page summarizes the parameters selected for each scenario. The cosmological parameters adopted were $\Omega_m = 0.3060$, $\Omega_b = 0.0490$, $h = 0.6781$, $\sigma_8 = 0.8150$ and $n_s = 0.9677$, consistent with Planck [Pla16a]. Data is collected from $z = 24.5$ to $z = 6.0$ at redshift intervals $\Delta z = 0.5$.

Table IV.
Model scenarios

Scenario group	Dark matter model	$\mathcal{N}_{\gamma,*}$	f_*	f_{esc}	ζ^{\dagger}	f_X	$\mathcal{N}_{\text{LyL},*}$	$\mathcal{N}_{\alpha,*}$	α_s
A	CDM	4.0×10^3	0.10	0.10	40	1	9690	6520	0.140
A	$m_{\text{FDM},22} = 1$	2.5×10^4	0.10	0.30	750	1	9690	6520	0.140
A	$m_{\text{FDM},22} = 2$	7.0×10^3	0.10	0.30	210	1	9690	6520	0.140
A	$m_{\text{FDM},22} = 3$	4.0×10^3	0.10	0.30	120	1	9690	6520	0.140
B	CDM	4.0×10^3	0.10	0.10	40	100	9690	6520	0.140
B	$m_{\text{FDM},22} = 1$	2.5×10^4	0.30	0.30	2250	100	9690	6520	0.140
B	$m_{\text{FDM},22} = 2$	7.0×10^3	0.30	0.30	630	100	9690	6520	0.140
B	$m_{\text{FDM},22} = 3$	4.0×10^3	0.30	0.30	360	100	9690	6520	0.140
C	CDM	4.0×10^3	0.10	0.10	40	1	9690	6520	0.140
C	$m_{\text{FDM},22} = 1$	2.5×10^4	0.10	0.30	750	1	6838	4274	0.559
C	$m_{\text{FDM},22} = 2$	7.0×10^3	0.10	0.30	210	1	9283	6199	0.181
C	$m_{\text{FDM},22} = 3$	4.0×10^3	0.10	0.30	120	1	9690	6520	0.140
D	CDM	4.0×10^3	0.10	0.10	40	100	9690	6520	0.140
D	$m_{\text{FDM},22} = 1$	2.5×10^4	0.30	0.30	2250	100	6838	4274	0.559
D	$m_{\text{FDM},22} = 2$	7.0×10^3	0.30	0.30	630	100	9283	6199	0.181
D	$m_{\text{FDM},22} = 3$	4.0×10^3	0.30	0.30	360	100	9690	6520	0.140

${}^{\dagger}\zeta \equiv \mathcal{N}_{\gamma,*} f_* f_{\text{esc}}.$

4. Results

In this chapter the results of the simulations are presented. First, scenario groups A and B are investigated in detail and in a fairly individual manner. This is to build up some intuition for how the 21 cm signal evolves as the most important parameters are varied. These are:

- The FDM particle mass $m_{\text{FDM},22}$, which impacts structure formation through f_{coll} .
- The star formation efficiency f_{\star} which, along with f_{coll} , is among the most important factors that governs the Lyman- α coupling x_{α} .
- The X-ray heating efficiency f_X that, along with f_{coll} , controls the evolution of the IGM temperature T_K and thus the spin temperature T_S .

Once the results of scenario group A and B have been reviewed, and some intuition built up, the slightly more realistic scenario groups C and D are considered. These scenarios also gauge, when compared to A and B, the importance of α_s , $\mathcal{N}_{\alpha,\star}$ and $\mathcal{N}_{\text{LyL},\star}$. However, the variations in these parameters are not expected to yield large deviations from A and B, so the intuition built up from reviewing scenario group A and B need not be repeated. The main focus will be on whether the overall picture is consistent with scenario groups A and B so that the results obtained are fairly robust. Any deviations from A and B will be commented upon.

4.1. Scenario Group A

4.1.1. Global 21 cm signal

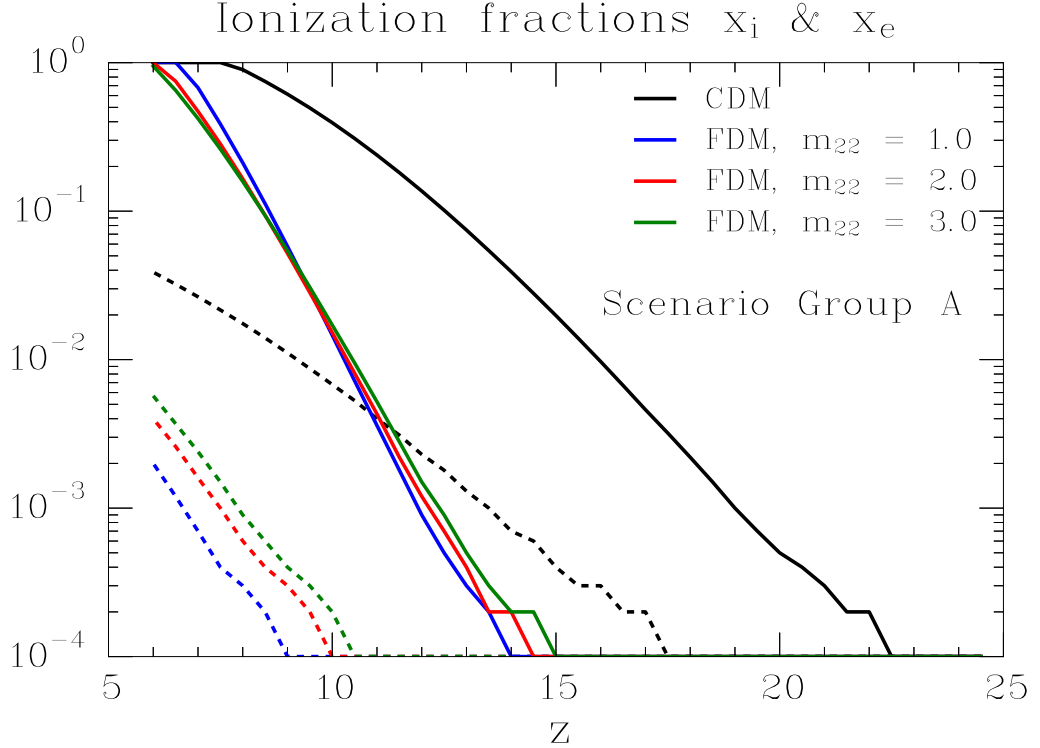


FIGURE 4.1. The computed ionization fractions x_i (solid) and x_e (dashed) for scenario group A.

Before delving into the more observationally illuminating 21 cm power spectrum, it is appropriate to compare the different evolution of global mean quantities. In Figure 4.1 the ionization fractions for Scenario Group A are plotted. As can be seen in the figure, in the FDM scenarios reionization ($x_i \sim 1$) takes place at $z \sim 6$, while reionization takes place at $z \simeq 7.5$. This confirms that the chosen parameters for scenario group A satisfy all criteria outlined in Chapter 3. The ionization fraction outside HII regions, x_e , increases with time due to the X-rays that are able to penetrate deep into the IGM.

Next, the kinetic temperature, the spin temperature (given by 2.26) and the CMB temperature are all plotted in Figure 4.2. The first notable observation is that Cosmic Dawn (loosely defined to be when $T_K \geq T_\gamma$) is significantly delayed in FDM relative to CDM. This is expected because roughly, as expressed in Eq. 2.22, $T_K \propto f_{\text{coll}}$. Since f_{coll} decreases as $m_{\text{FDM},22}$ decreases, this explains the delayed IGM heating as well as the predicted colder IGM before reionization (after reionization, all of the IGM is photoheated to $\sim 10^4$ K).

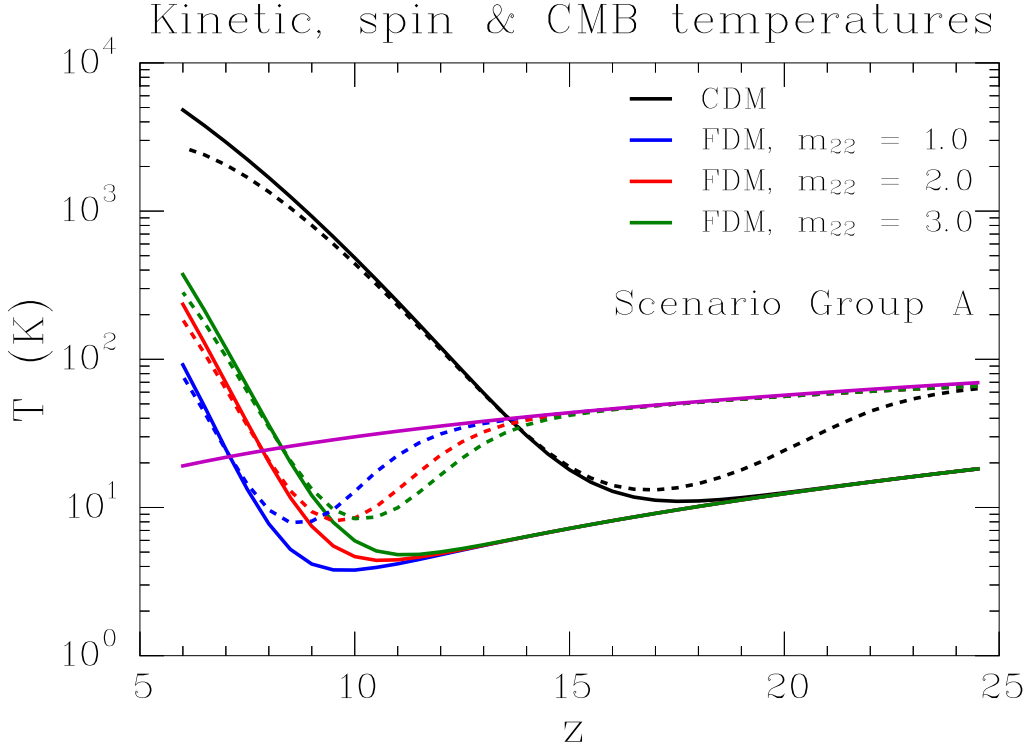


FIGURE 4.2. The kinetic (all the solid lines except the magenta-colored) and spin (dashed) temperatures for scenario group A. The CMB temperature is also plotted (solid magenta) for comparison.

The second notable observation is the delayed coupling of the spin temperature to the kinetic temperature. For CDM, significant $T_S - T_K$ coupling occurs at $z \sim 16$ compared to $z \sim 8 - 9$ for FDM. For the relatively low redshifts plotted here, the collisional coupling x_C is negligible compared to the Wouthuysen-Field effect coupling x_α . The latter, similarly to T_K , scales approximately linearly with f_{coll} : $x_\alpha \propto (1+z)^{-1} J_\alpha \propto (1+z) f_\star f_{\text{coll}}$ (see e.g. Eq. 18 in [FOB06]). The delayed coupling of the spin temperature to the kinetic temperature is therefore mainly due to the smaller collapse fraction in FDM relative to CDM. All else being equal (i.e. keeping f_\star constant), decreasing $m_{\text{FDM},22}$ will decrease the redshift at which $T_S \sim T_K$.

Having outlined the evolution of both the ionization fraction and the spin temperature, it is now possible to understand the evolution of the global 21 cm brightness temperature, δT_b .

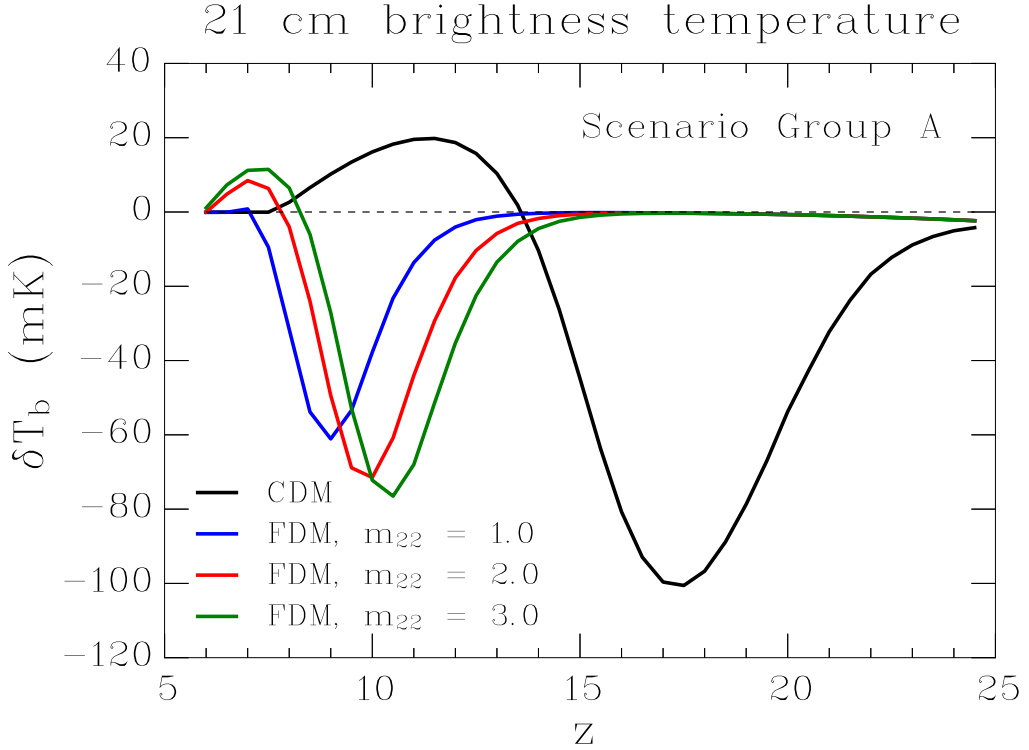


FIGURE 4.3. The global 21 cm brightness temperature for scenario group A.

The simulated evolution of δT_b for scenario group A is plotted in Figure 4.3. Recall that (Eq. 2.25, using $x_{\text{HI}} \simeq 1 - x_i$ and $\delta_{\text{HI}} = 0$ for the globally averaged signal)

$$\delta T_b \propto (1 - x_i)(1 + z)^{1/2} \left(1 - \frac{T_\gamma}{T_S}\right) \quad (4.1)$$

This means that δT_b should go to zero when reionization is finished, which is indeed observed in the figure: $\delta T_b = 0$ at $z \simeq 7.5$ for the CDM scenario, whereas the same happens first at $z \sim 6$ for the three FDM scenarios. Perhaps the most clear distinction between CDM and FDM is the redshift when $|\delta T_b|$ is maximized — at $z_{\text{max}}^{\text{CDM}} \sim 17$ for CDM and $z_{\text{max}}^{\text{FDM}} \sim 9-10$ for FDM. For all scenarios, this occurs shortly after T_S decouples from T_γ . During this period, $T_S \sim T_K < T_\gamma$, which yields an absorption signal ($\delta T_b < 0$). At this point, $1 - x_i \simeq 1$ and $T_\gamma/T_S \sim 3$ for all scenarios, so that the different magnitudes of δT_b should mainly derive from the redshift factor $(1 + z)^{1/2}$, yielding

$$|\delta T_b|_{\text{max}}^{\text{FDM}} \simeq \left(\frac{1 + z_{\text{max}}^{\text{FDM}}}{1 + z_{\text{max}}^{\text{CDM}}} \right)^{1/2} |\delta T_b|_{\text{max}}^{\text{CDM}} \simeq 0.76 \left(\frac{1 + z_{\text{max}}^{\text{FDM}}}{10.5} \right)^{1/2} |\delta T_b|_{\text{max}}^{\text{CDM}}. \quad (4.2)$$

For $|\delta T_b|_{\text{max}}^{\text{CDM}} \simeq 100$ mK we get $|\delta T_b|_{\text{max}}^{\text{FDM}} \simeq 76$ mK, not too far off from what is seen in Figure 4.3. As for the positive maximum in δT_b , this is also mainly controlled by the redshift scaling $\sim (1 + z)^{1/2}$.

4.1.2. 21 cm Power Spectrum

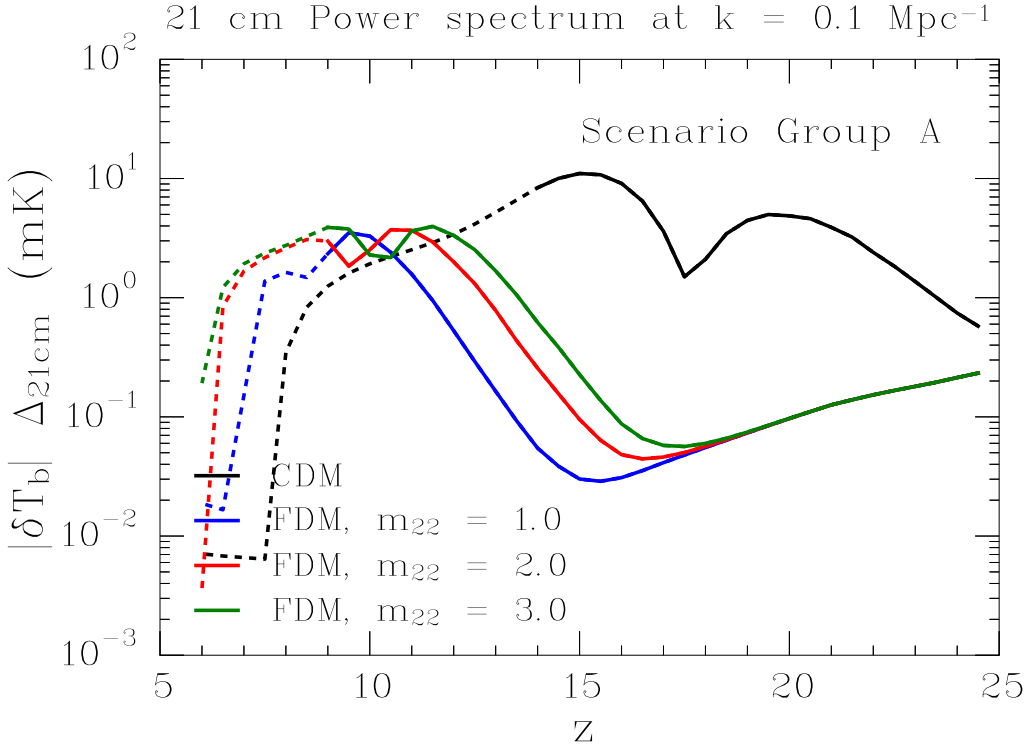


FIGURE 4.4. The predicted dimensionless 21 cm power spectrum (scaled by $|\delta T_b|$) at $k = 0.1 \text{ Mpc}^{-1}$ for scenario group A. The model for the power spectrum breaks down near reionization when x_i becomes large. Using Figure 4.1, the lines are dashed when $x_i \gtrsim 0.05$, roughly marking the redshift below which the results cannot be trusted.

With the global evolution of the 21 cm signal outlined, the fluctuations in the signal can be analyzed. The quantity of interest is $|\delta T_b| \Delta_{21\text{cm}}(k)$ where $|\delta T_b|$ is the magnitude of the global 21 cm signal and $\Delta_{21\text{cm}}(k)$ is the dimensionless 21 cm power spectrum, defined through $\Delta_{21\text{cm}}(k) \equiv (P_{21\text{cm}}(k) k^3 / 2\pi^2)^{1/2}$. In Figure 4.4, $|\delta T_b| \Delta_{21\text{cm}}(k)$ is plotted for $k = 0.1 \text{ Mpc}^{-1}$. The lines become dashed when $x_i \gtrsim 0.05$, beyond which the model breaks down.

For all scenarios except $m_{\text{FDM},22} = 1$ we see at least one bump in $|\delta T_b| \Delta_{21\text{cm}}$. For the CDM scenario we see two clear bumps:

- The first bump, peaked at $z \sim 19$, originates from fluctuations in the Lyman- α coupling x_α , i.e. the term $\beta_\alpha \delta_\alpha$ in Eq. 3.1. When the first galaxies hosting Lyman- α sources form, this will lead to an inhomogeneous distribution of x_α , and thus spatial fluctuations in the 21 cm signal. This peak in the 21 cm power spectrum then diminish as more galaxies form and effectively smooths the spatial distribution of x_α .

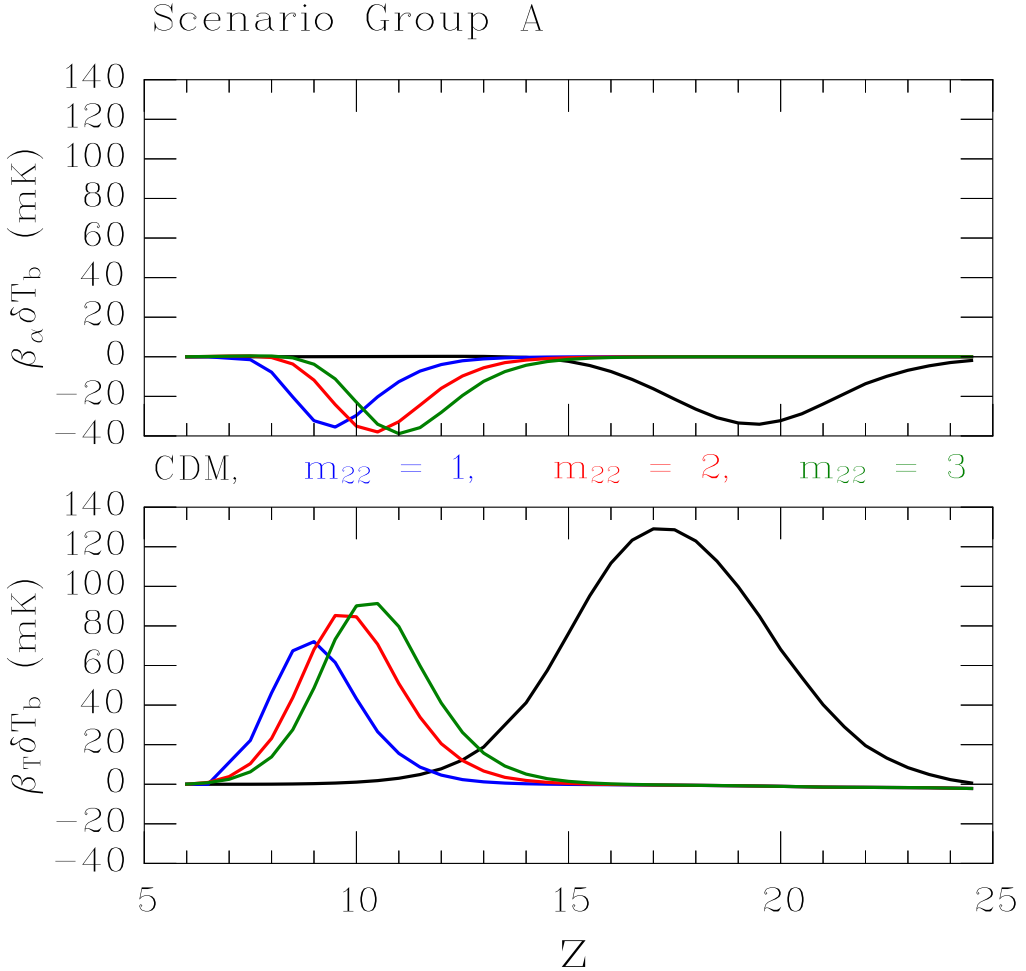


FIGURE 4.5. Comparison between the Lyman- α contribution (proportional to $\beta_\alpha \delta T_b$) and the X-ray heating contribution (proportional to $\beta_T \delta T_b$) to the 21 cm power spectrum for scenario group A.

- The second bump, peaked at $z \sim 15$, can be traced to the first stages of X-ray heating during Cosmic Dawn. More specifically, after x_α has risen sufficiently we will have $T_S \sim T_K$. Furthermore, the IGM temperature will become spatially inhomogeneous (i.e. increasing δ_T) due to the inhomogeneous distribution of X-ray sources (which reside in galaxies). These two effects will make the term $\beta_T \delta_T$ in Eq. 3.1 dominant. The X-ray bump will then diminish as more galaxies form and result in a more smooth kinetic temperature distribution.

A third bump in the 21 cm power spectrum is also expected at lower redshifts as HII bubbles starts to envelop the IGM during the EoR [PL08]. However, as discussed in the last chapter, the PF model breaks down for $x_i \gtrsim 0.05$ leading to no such feature in Figure 4.4. For the FDM scenarios the suppressed structure formation leads to a significant delay in the Lyman- α and X-ray heating bumps. The Lyman- α peak in the 21 cm power spectrum occurs near $z \sim 10 - 11$ with the X-ray heating peak following shortly after.

4.1 Scenario Group A

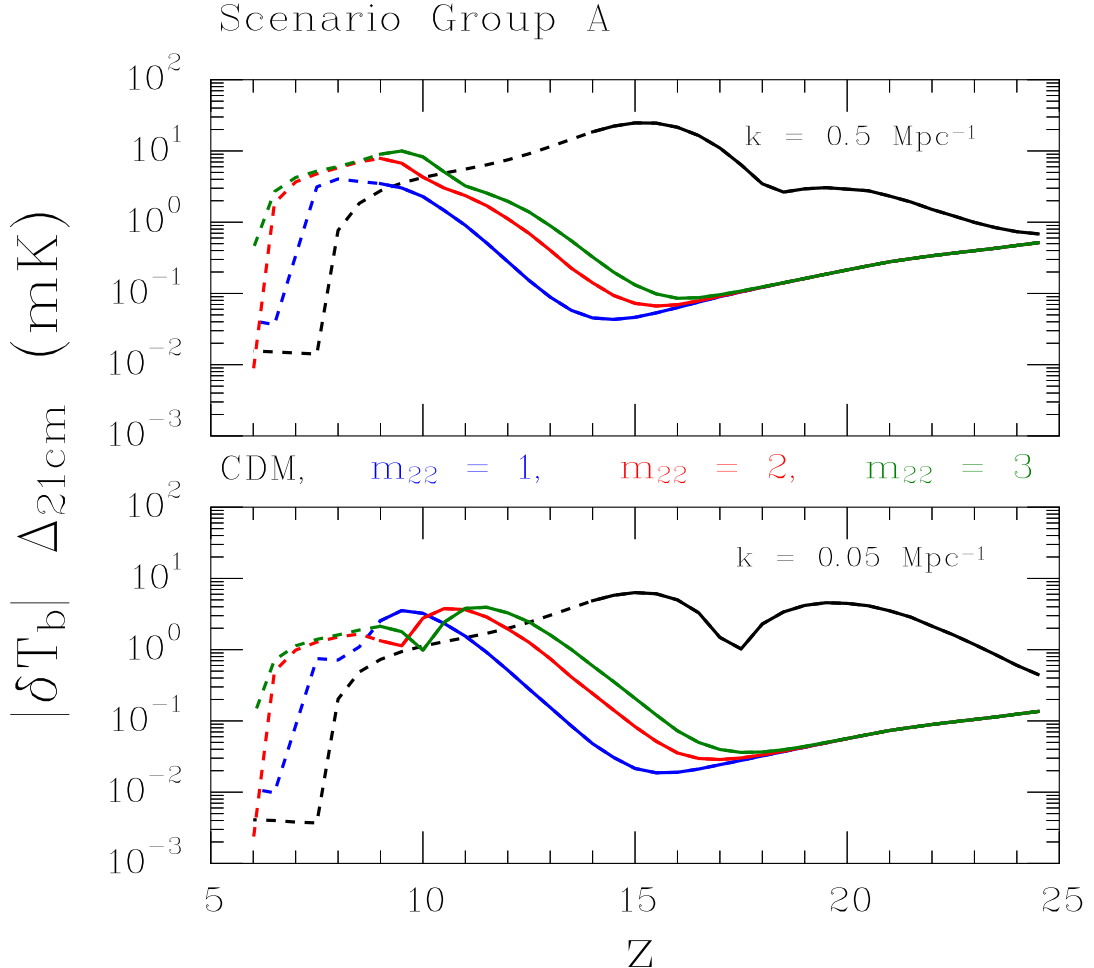


FIGURE 4.6. The predicted dimensionless 21 cm power spectrum (scaled by $|\delta T_b|$) at $k = 0.05 \text{ Mpc}^{-1}$ and $k = 0.5 \text{ Mpc}^{-1}$ for scenario group A. As in Figure 4.4, the lines are dashed when $x_i \gtrsim 0.05$.

Each contribution to fluctuations in the 21 cm signal is of the form $\beta_i \delta_i$ (see Eq. 3.1) and because δ_i traces the density fluctuations, the relative contribution to the total fluctuation is mainly controlled by β_i . Thus, by comparing $\beta_\alpha \delta T_b$ and $\beta_T \delta T_b$ it is possible to understand the origin of the Lyman- α and X-ray peaks in the 21 cm power spectrum [PF07]. Such a comparison is shown in Figure 4.5. By visual inspection, it is seen that, for CDM, when $\beta_\alpha \delta T_b$ is added to $\beta_T \delta T_b$, we expect two peaks in the 21 cm power spectrum somewhere in the range $15 \lesssim z \lesssim 20$. For FDM, we see that the peaks should be somewhere around $z \sim 10$. This fits well with what is seen in Figure 4.4. It is noteworthy that the appearance of the 21 cm power spectrum can be understood in terms of the *global mean* quantities on which β_α , β_T and δT_b depends.

For $14 \lesssim z \lesssim 21$, where the PF model is applicable for all dark matter scenarios, FDM predicts fluctuations in the 21 cm signal that are at least an order of magnitude smaller than what CDM predicts. Furthermore, the absolute magnitude of the fluctuations predicted by FDM in scenario group A are $< 1 \text{ mK}$ in this redshift interval (even dipping below 0.1 mK near $z \sim 16$ for all particle masses).

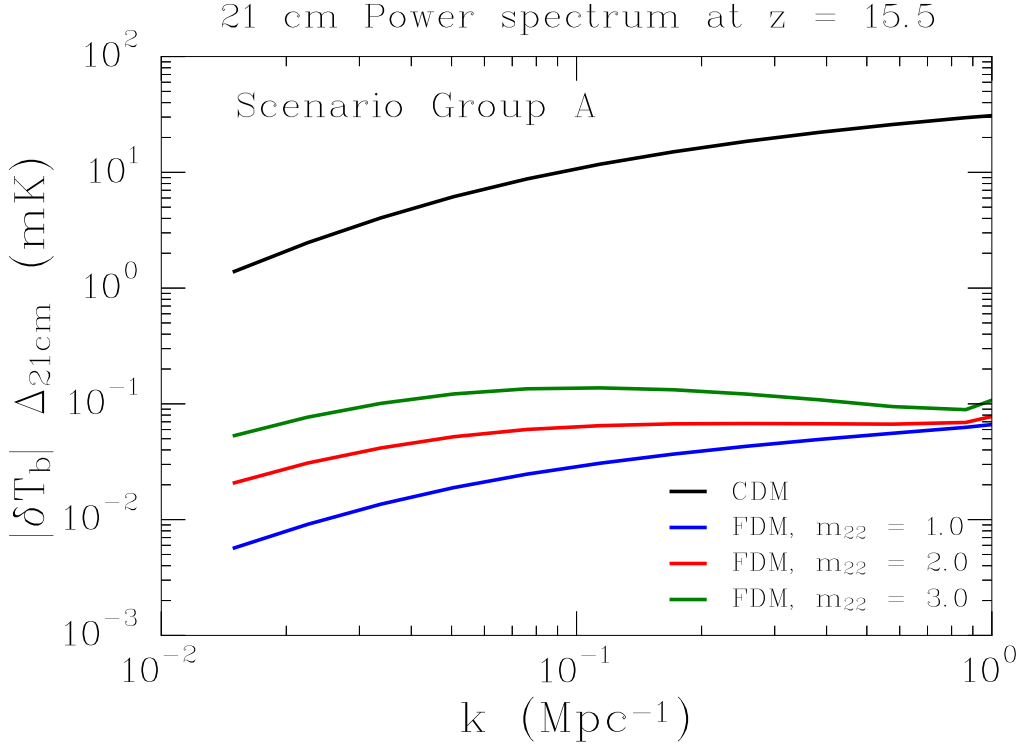


FIGURE 4.7. The predicted dimensionless 21 cm power spectrum as a function of k at $z = 15.5$ for scenario group A.

In Figure 4.6 it is seen that the 21 cm power spectrum on larger ($k = 0.05 \text{ Mpc}^{-1}$) and smaller ($k = 0.5 \text{ Mpc}^{-1}$) scales evolves in a qualitatively similar fashion as for $k = 0.1 \text{ Mpc}^{-1}$. The fluctuations on larger scales are smaller in magnitude than on small scales, as expected since all types of fluctuations traces the fluctuations in the density field. Like for $k = 0.1 \text{ Mpc}^{-1}$, the fluctuations in the 21 cm signal predicted by FDM are appreciably smaller than predicted by CDM for $14 \lesssim z \lesssim 21$, with the effect being most significant for $k = 0.5 \text{ Mpc}^{-1}$ among these three scales. The simulation also tracks the 21 cm power spectrum at fixed redshifts as a function of k . The resulting scale dependence at $z = 15.5$ is shown in Figure 4.7. As a summary and a benchmark for future reference, scenario group A predicts

$$|\delta T_b| \Delta_{21\text{cm}}(k = 0.5 \text{ Mpc}^{-1}) \Big|_{z=15.5}^A \simeq \begin{cases} 25 \text{ mK} & \text{for CDM} \\ 0.053 \text{ mK} & \text{for } m_{\text{FDM},22} = 1 \\ 0.067 \text{ mK} & \text{for } m_{\text{FDM},22} = 2 \\ 0.099 \text{ mK} & \text{for } m_{\text{FDM},22} = 3 \end{cases}, \quad (4.3)$$

$$|\delta T_b| \Delta_{21\text{cm}}(k = 0.1 \text{ Mpc}^{-1}) \Big|_{z=15.5}^A \simeq \begin{cases} 11 \text{ mK} & \text{for CDM} \\ 0.029 \text{ mK} & \text{for } m_{\text{FDM},22} = 1 \\ 0.064 \text{ mK} & \text{for } m_{\text{FDM},22} = 2 \\ 0.14 \text{ mK} & \text{for } m_{\text{FDM},22} = 3 \end{cases}, \quad (4.4)$$

4.1 Scenario Group A

$$|\delta T_b| \Delta_{21\text{cm}} (k = 0.05 \text{ Mpc}^{-1}) \Big|_{z=15.5}^{\text{A}} \simeq \begin{cases} 6.1 \text{ mK} & \text{for CDM} \\ 0.019 \text{ mK} & \text{for } m_{\text{FDM},22} = 1 \\ 0.052 \text{ mK} & \text{for } m_{\text{FDM},22} = 2 \\ 0.12 \text{ mK} & \text{for } m_{\text{FDM},22} = 3 \end{cases}. \quad (4.5)$$

The contrast between the predicted values from CDM and FDM will be useful when considering the possibility of distinguishing the two dark matter scenarios with 21 cm observations.

4.2. Scenario Group B

4.2.1. Global 21 cm signal

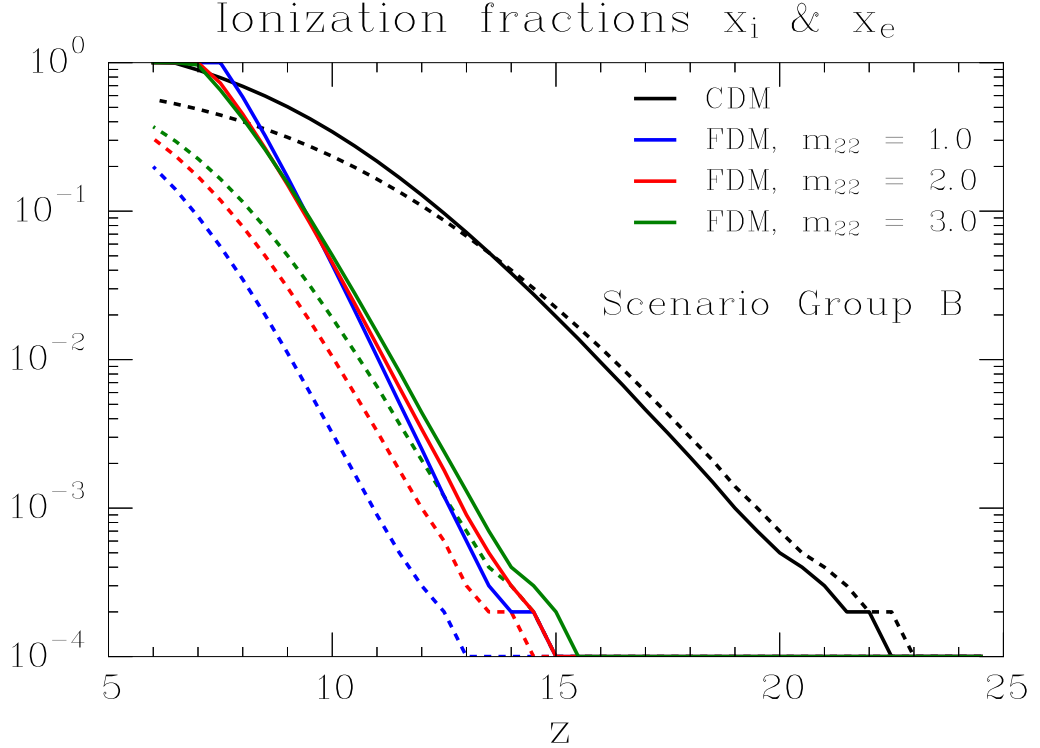


FIGURE 4.8. The computed ionization fractions x_i (solid) and x_e (dashed) for scenario group B.

For scenario group B, the increased star formation efficiency for FDM ($f_\star = 0.3$ compared to $f_\star = 0.1$ for scenario group A) should result in a more rapid reionization of the Universe. This is indeed observed in Figure 4.8. Reionization is completed for all FDM scenarios by $z \sim 7$, fairly close to what is seen for CDM. The ionization fraction of the largely neutral regions outside HII bubbles, x_e , is larger for scenario group B than scenario group A by roughly an order of magnitude during the EoR. This can be understood to be due to the increased X-ray heating efficiency $f_X = 100$ — a hundredfold increase from scenario group A [PL08].

The greatly increased value of f_X should also lead to a much more rapid heating of the IGM. Figure 4.9 shows this to be the case, with T_K starting to rise near $z \sim 13 - 15$ for the FDM scenarios compared to $z \sim 9 - 11$ for scenario group A. For CDM, the initial stages of heating occurs at $z \sim 23$ compared to $z \sim 18$ in scenario group A.

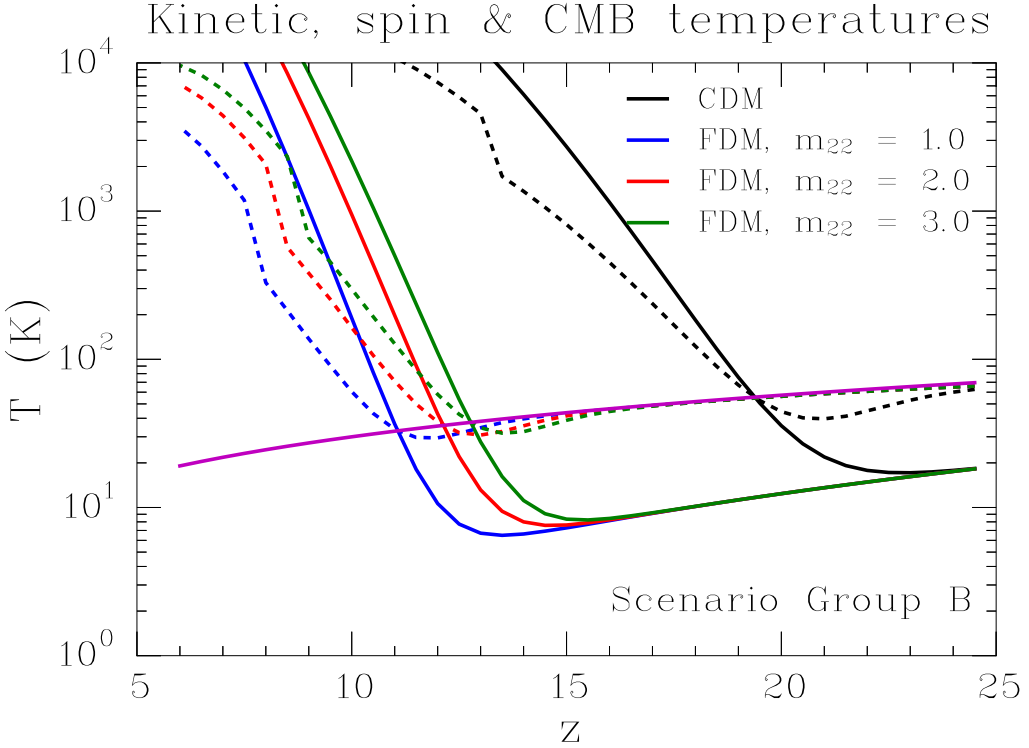


FIGURE 4.9. The kinetic (all the solid lines except the magenta-colored) and spin (dashed) temperatures for scenario group B. The CMB temperature is also plotted (solid magenta) for comparison.

The evolution of the spin temperature is also markedly different from in scenario group A. It is seen that the dip in the spin temperature is relatively small. As explained in [MFS13], this is mainly due to early X-ray heating. To see this, consider the expression for the spin temperature with $x_\alpha \gg x_C$ and $T_C \simeq T_K$. Eq. 2.26 then yields

$$\frac{T_\gamma}{T_S} \simeq \frac{1 + x_\alpha \frac{T_\gamma}{T_K}}{1 + x_\alpha}. \quad (4.6)$$

Now imagine two scenarios wherein x_α is kept constant (i.e. no variation in f_* and $\mathcal{N}_{*,\alpha}$), but not f_X . Then we have

$$\frac{(T_\gamma/T_S)_{\text{High } f_X}}{(T_\gamma/T_S)_{\text{Low } f_X}} \simeq \frac{1 + x_\alpha \frac{T_\gamma}{T_K} |_{\text{High } f_X}}{1 + x_\alpha \frac{T_\gamma}{T_K} |_{\text{Low } f_X}}. \quad (4.7)$$

Furthermore, a greater X-ray efficiency leads to a greater heating of the IGM. Thus, $\frac{T_\gamma}{T_K} |_{\text{High } f_X} < \frac{T_\gamma}{T_K} |_{\text{Low } f_X}$, evaluated at the same redshift. Therefore,

$$\frac{(T_\gamma/T_S)_{\text{High } f_X}}{(T_\gamma/T_S)_{\text{Low } f_X}} < 1. \quad (4.8)$$

Thus, all else being equal, increasing the X-ray efficiency will decrease the ratio T_γ/T_S .

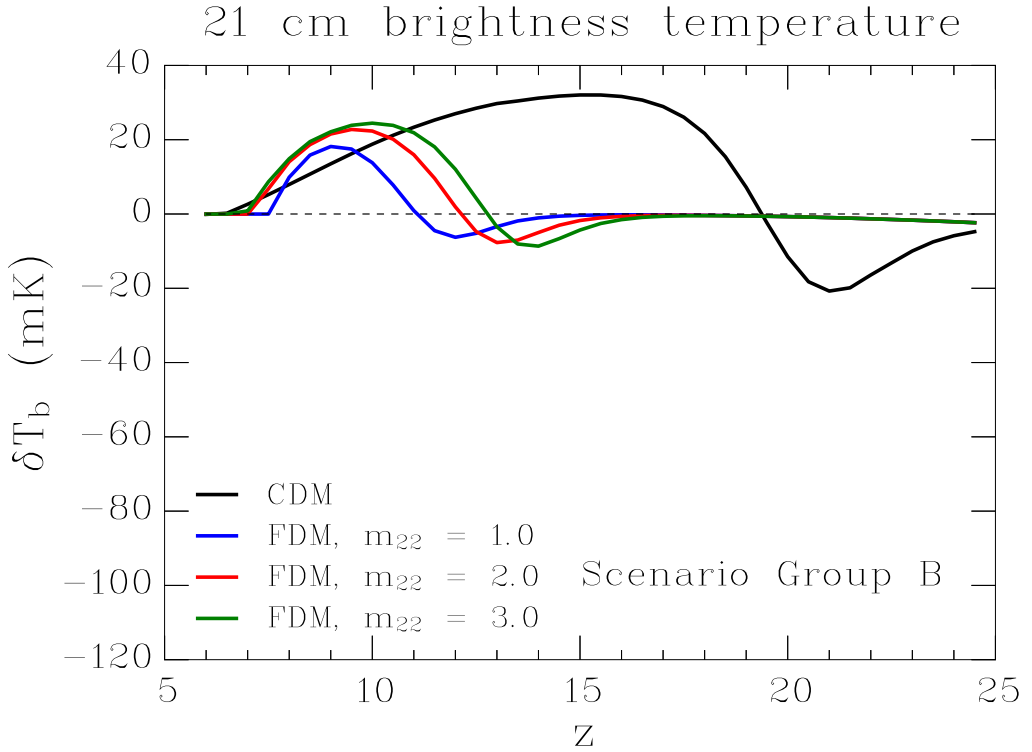


FIGURE 4.10. The global 21 cm brightness temperature for scenario group B.

That this explains the observation — when comparing Figure 4.9 and Figure 4.2 — that $(T_\gamma/T_S)_{f_X=100} < (T_\gamma/T_S)_{f_X=1}$, even with the variation in x_α (through f_\star), is reasonable because f_X has been varied by a factor of 100 whereas f_\star has only been varied by a factor of 3 between scenario groups A and B.

An important corollary of Eq. 4.8 is that the global 21 cm signal $\delta T_b \propto (1 - T_\gamma/T_S)$ will have a smaller dip for scenario group B than in scenario group A because of the increased X-ray efficiency (this point has been noted by [MFS13]). This is borne out in the simulation, as seen in Figure 4.10. In the figure it is also seen that the simulation predicts $|\delta T_b|_{\max}^{\text{CDM}} \simeq 32 \text{ mK}$, $|\delta T_b|_{\max}^{\text{FDM}} \simeq 24 \text{ mK}$ — both significantly weaker global signals than predicted in scenario group A, be they peaks or dips. As in scenario group A, it is seen that the CDM predicts a larger peak for δT_b , again mainly due to the redshift scaling $\delta T_b \propto (1+z)^{1/2}$, since for all scenarios we have $T_\gamma/T_S \ll 1$ near the peaks. The ionization fraction is also significant for FDM near their peaks in the signal, thus further diminishing the amplitude of the signal.

4.2.2. 21 cm Power Spectrum

Fluctuations in the 21 cm signal for scenario group B are expected to be shifted towards higher redshifts due to the early onset of X-ray heating and Lyman- α coupling. This is indeed seen in Figure 4.11. The Lyman- α and X-ray heating bumps have been pushed back to $z \gtrsim 20$ for CDM.

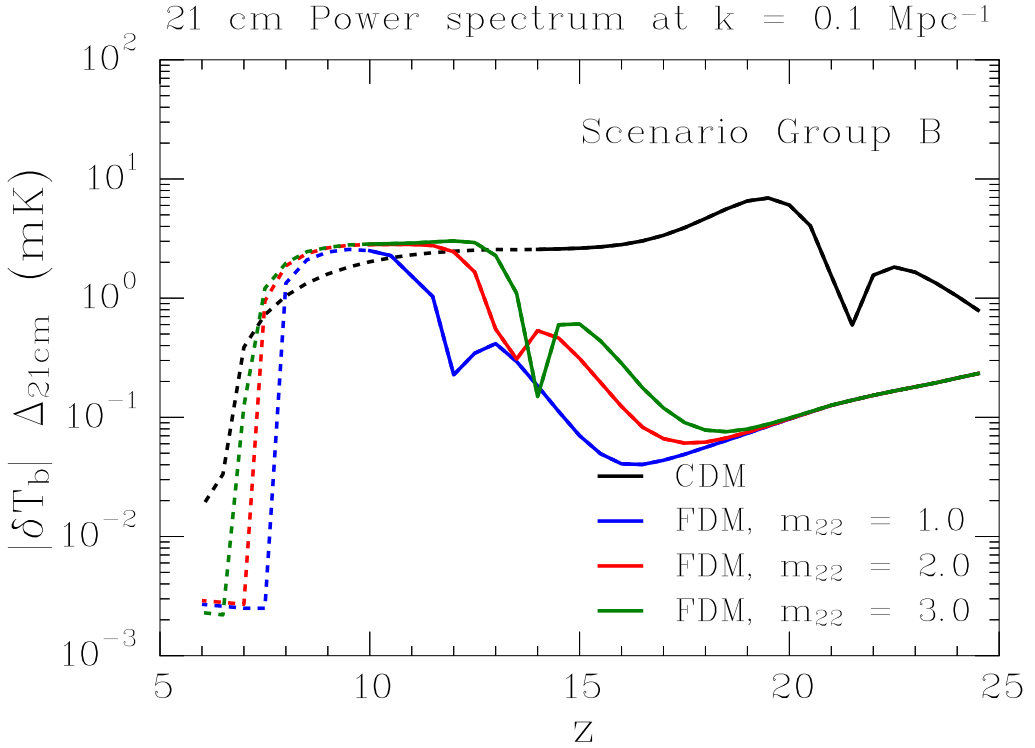


FIGURE 4.11. The predicted dimensionless 21 cm power spectrum (scaled by $|\delta T_b|$) at $k = 0.1 \text{ Mpc}^{-1}$ for scenario group B. The lines are dashed for $x_i \gtrsim 0.05$.

For FDM the peaks are situated at $10 \lesssim z \lesssim 15$ with amplitudes below $\sim 3 \text{ mK}$. At $z \simeq 15$ specifically, the FDM power spectrum has an amplitude of $\lesssim 0.6 \text{ mK}$ compared to almost 3 mK for CDM. The overall picture of suppressed fluctuations in the 21 cm signal at high redshifts is similar to what was found for scenario group A. The hundredfold increase in f_X and the threefold increase in f_\star seems to have little impact on this point. This can be understood to simply be because FDM produces barely no galaxies at high redshifts compared to CDM. With exceedingly few X-ray and Lyman- α emitting galaxies in FDM at $z \gtrsim 15$, increasing f_X and f_\star will not make much of a qualitative difference.

As for the different appearance of the power spectrum — especially the X-ray heating and Lyman- α bumps — compared to scenario group A, this can be understood from the evolution of $\beta_T \delta T_b$ and $\beta_\alpha \delta T_b$. This is plotted in Figure 4.12. For CDM, by inspection we see that the addition of $\beta_T \delta T_b$ and $\beta_\alpha \delta T_b$ should produce two bumps in the power spectrum around $z \sim 21$. This is indeed observed in Figure 4.11. The same exercise give rise to the expectation of bumps in the 21 cm spectrum somewhere in the range $11 \lesssim z \lesssim 15$ for FDM, which is also observed to be the case in the same figure. It is also noteworthy that, mainly due to weaker global 21 cm signal δT_b , the amplitudes of $\beta_T \delta T_b$ and $\beta_\alpha \delta T_b$ are much smaller than for scenario group A. This explains why the fluctuations in the 21 cm fluctuations are typically smaller in scenario group B than in scenario group A — at least for $k = 0.1 \text{ Mpc}^{-1}$.

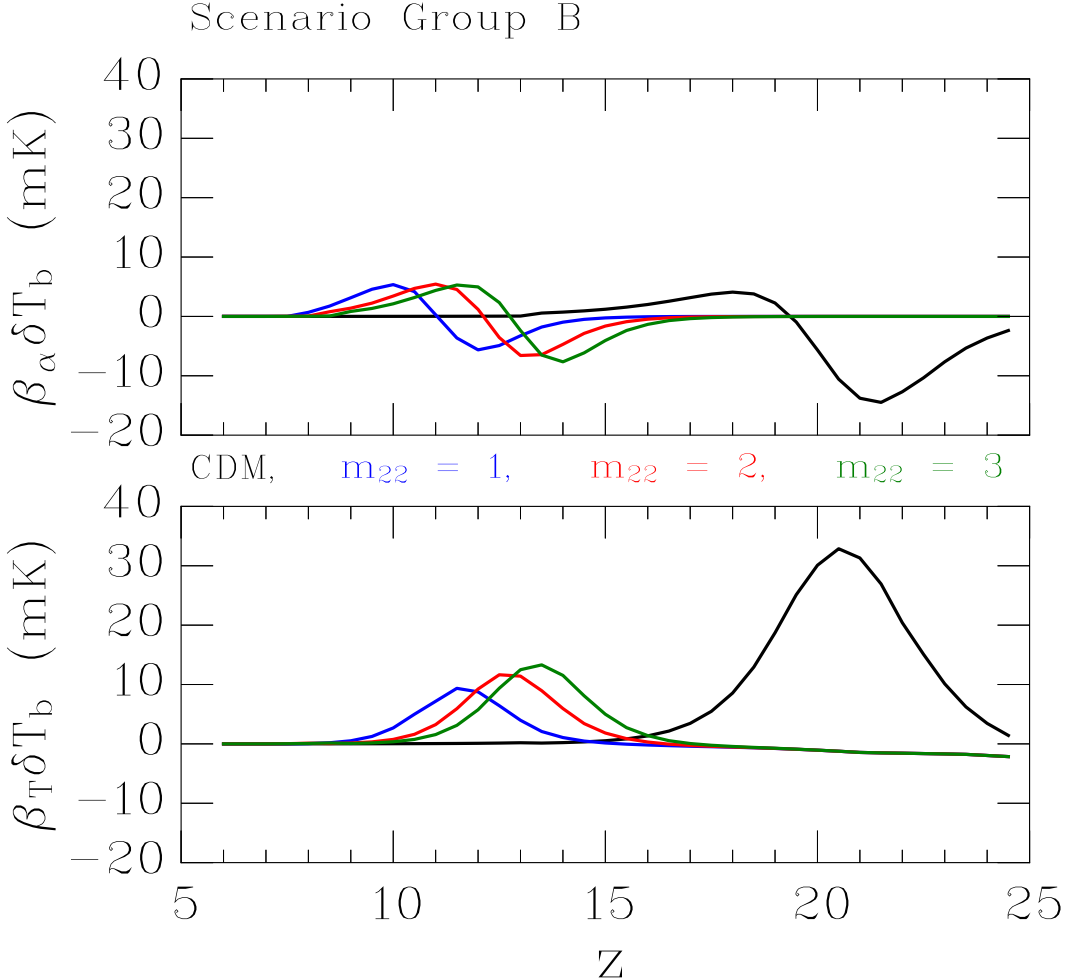


FIGURE 4.12. Comparison between the Lyman- α contribution (proportional to $\beta_\alpha \delta T_b$) and the X-ray heating contribution (proportional to $\beta_T \delta T_b$) to the 21 cm power spectrum for scenario group B. Note the y -scale, which extends to only 40 mK compared to 140 mK for scenario group A (Figure 4.5).

The evolution of the 21 cm power spectrum on different scales ($k = 0.05 \text{ Mpc}^{-1}$ and $k = 0.5 \text{ Mpc}^{-1}$) is shown in Figure 4.13 on the next page. As with scenario group A, the maximum of the 21 cm power spectrum is larger on small scales ($k = 0.5 \text{ Mpc}^{-1}$) than on intermediate and large scales ($k = 0.1 \text{ Mpc}^{-1}$ and $k = 0.05 \text{ Mpc}^{-1}$ respectively). However, at $z = 15.5$ where there are no bumps, the circumstances are reversed for two of the dark matter scenarios. This can be seen more clearly in Figure 4.14 wherein the 21 cm power spectrum is plotted against k at $z = 15.5$. Numerically, scenario group B predicts

$$|\delta T_b| \Delta_{21\text{cm}}(k = 0.5 \text{ Mpc}^{-1}) \Big|_{z=15.5}^B \simeq \begin{cases} 5.6 \text{ mK} & \text{for CDM} \\ 0.059 \text{ mK} & \text{for } m_{\text{FDM},22} = 1 \\ 0.10 \text{ mK} & \text{for } m_{\text{FDM},22} = 2 \\ 0.12 \text{ mK} & \text{for } m_{\text{FDM},22} = 3 \end{cases}, \quad (4.9)$$

4.2 Scenario Group B

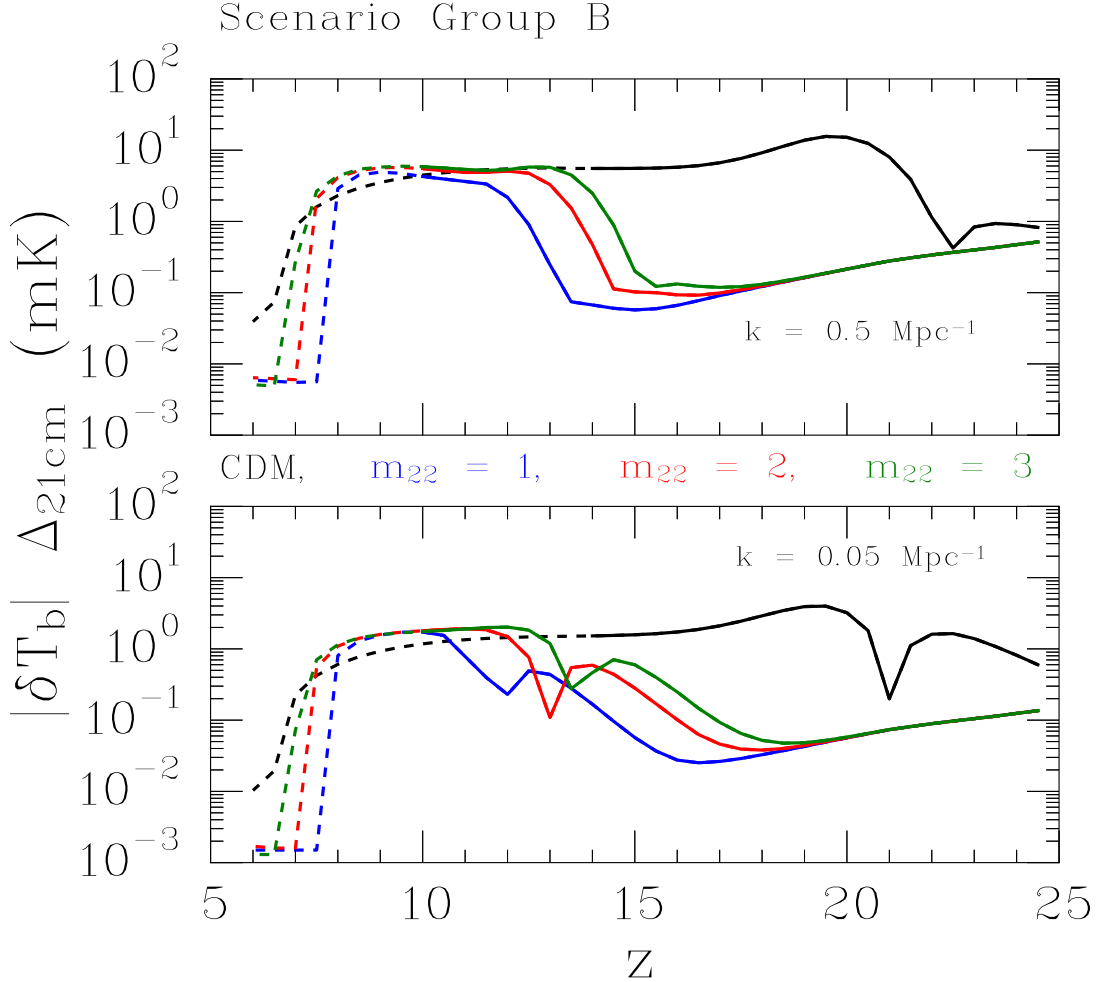


FIGURE 4.13. The predicted dimensionless 21 cm power spectrum (scaled by $|\delta T_b|$) at $k = 0.05 \text{ Mpc}^{-1}$ and $k = 0.05 \text{ Mpc}^{-1}$ for scenario group B. As in Figure 4.11, the lines are dashed when $x_i \gtrsim 0.05$.

$$|\delta T_b| \Delta_{21\text{cm}}(k = 0.1 \text{ Mpc}^{-1}) \Big|_{z=15.5}^B \simeq \begin{cases} 2.7 \text{ mK} & \text{for CDM} \\ 0.050 \text{ mK} & \text{for } m_{\text{FDM},22} = 1 \\ 0.20 \text{ mK} & \text{for } m_{\text{FDM},22} = 2 \\ 0.44 \text{ mK} & \text{for } m_{\text{FDM},22} = 3 \end{cases}, \quad (4.10)$$

$$|\delta T_b| \Delta_{21\text{cm}}(k = 0.05 \text{ Mpc}^{-1}) \Big|_{z=15.5}^B \simeq \begin{cases} 1.6 \text{ mK} & \text{for CDM} \\ 0.037 \text{ mK} & \text{for } m_{\text{FDM},22} = 1 \\ 0.17 \text{ mK} & \text{for } m_{\text{FDM},22} = 2 \\ 0.40 \text{ mK} & \text{for } m_{\text{FDM},22} = 3 \end{cases}. \quad (4.11)$$

Comparing the predicted fluctuations in the 21 cm signal at $z = 15.5$ with the predicted fluctuations in scenario group A at the same redshift (Eqs. 4.3, 4.4 and 4.5) yields a qualitatively consistent picture.

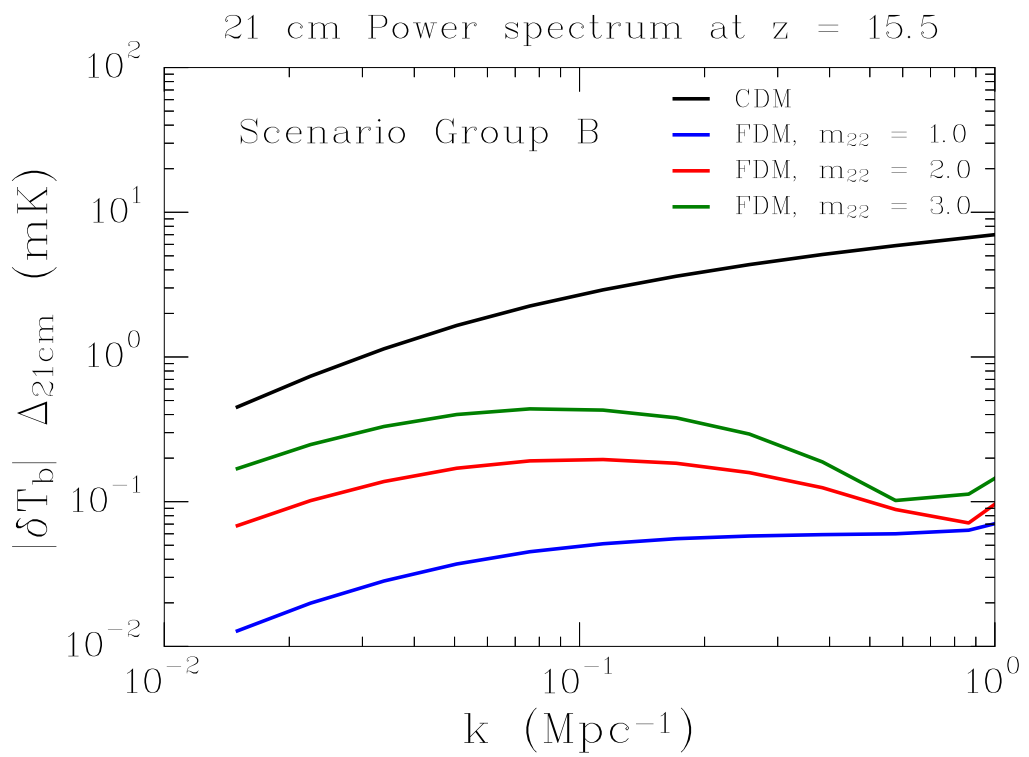


FIGURE 4.14. The predicted dimensionless 21 cm power spectrum as a function of k at $z = 15.5$ for scenario group B.

4.3. Scenario Groups C & D

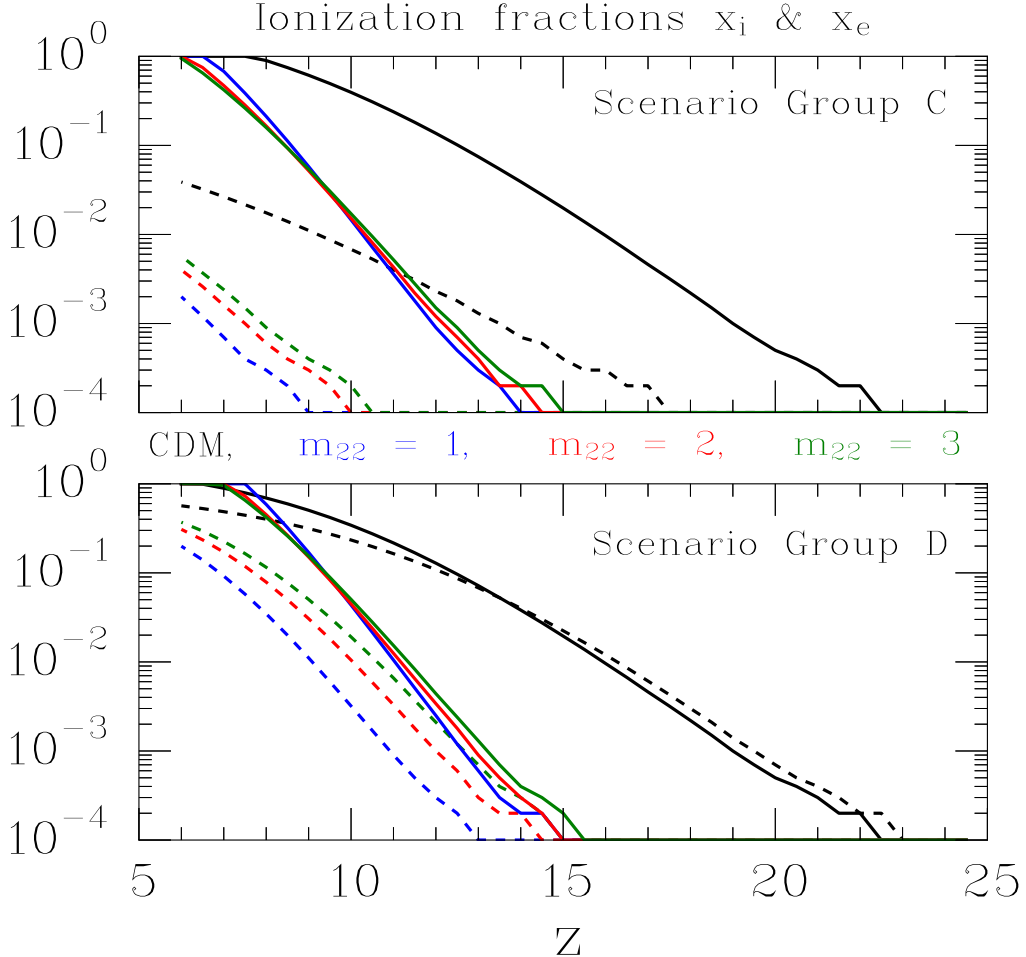


FIGURE 4.15. The computed ionization fractions x_i (solid) and x_e (dashed) for scenario groups C and D.

Having investigated scenario groups A and B, the main factors governing the evolution of the 21 cm signal in CDM and FDM have been explored in some detail. Now we consider scenario groups C and D wherein more realistic values for $\mathcal{N}_{\alpha,*}$, $\mathcal{N}_{LyL,*}$ and α_s are expected to yield second order corrections to the 21 cm signal in scenario groups A and B.

First off, the reionization history of the Universe is not expected to be different from groups A and B since it is governed by the unchanged parameters $\mathcal{N}_{\gamma,*}$, f_{esc} and f_* as well as the collapse fraction f_{coll} . In Figure 4.15 the ionization fractions are plotted for scenario groups C and D. A comparison with the evolution predicted in scenario groups A (Figure 4.1) and B (Figure 4.8) reveals no difference, as expected.

Next, in Figure 4.16 the evolution of the kinetic, the spin and the global brightness temperatures are plotted.

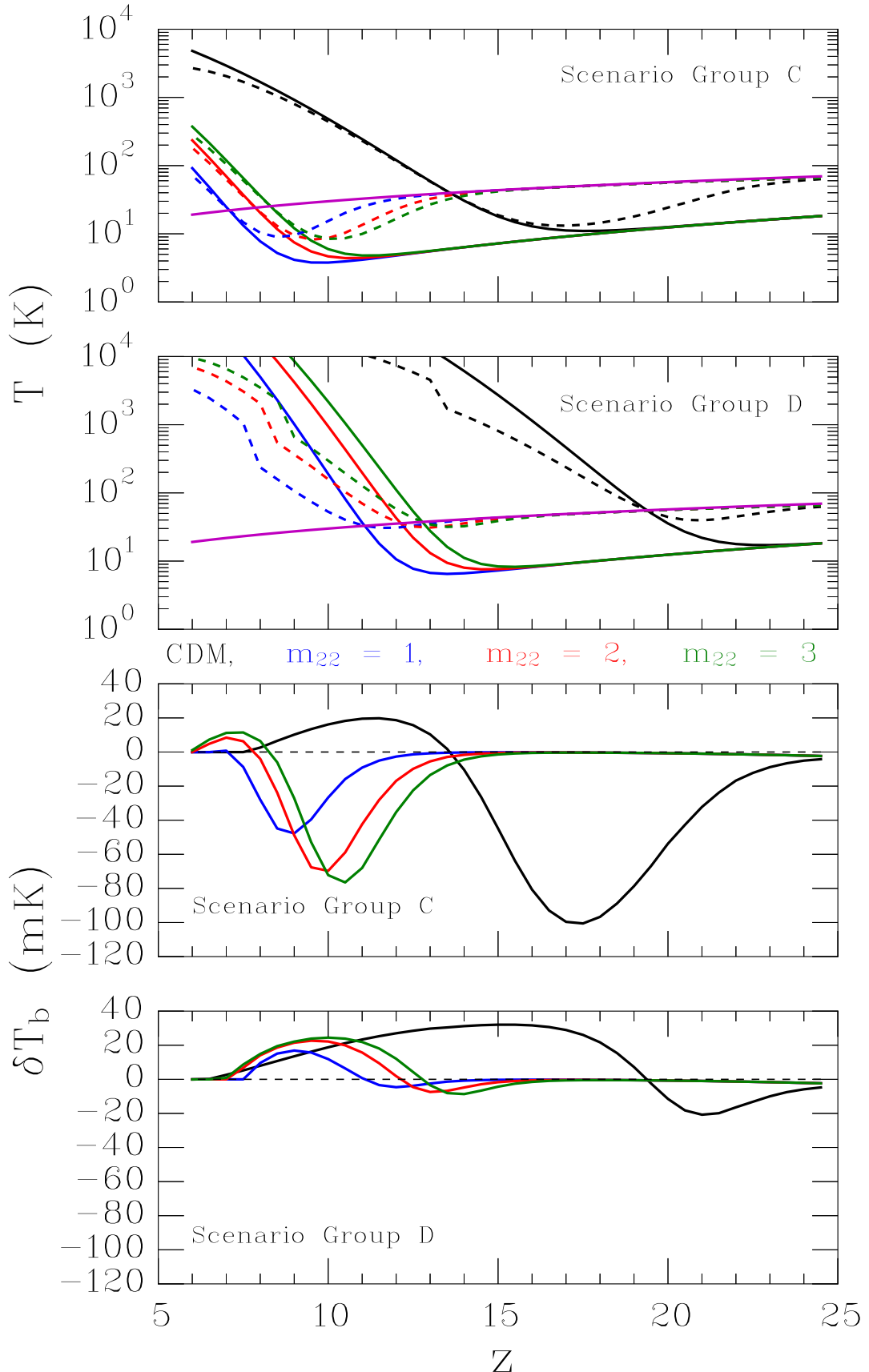


FIGURE 4.16. **Top two plots:** T_K (all the solid lines except the magenta-colored), T_S (dashed) and T_γ (solid magenta). **Lower two plots:** δT_b .

4.3 Scenario Groups C & D

Given fewer Lyman- α photons per stellar baryon (see $\mathcal{N}_{\alpha,*}$ in Table IV) for $m_{\text{FDM},22} = 1$ in scenario groups C and D compared to A and B,¹ we expect:

$$\text{Lower } \mathcal{N}_{\alpha,*} \rightarrow \text{Lower } x_\alpha \rightarrow \text{Delayed } T_S - T_K \text{ coupling} \rightarrow \text{Smaller dip in } \delta T_b.$$

Such a delay in coupling is barely visible at all when comparing scenario group C in Figure 4.16 with scenario group A in Figure 4.2 (looking only at $m_{\text{FDM},22} = 1$). However, the resulting smaller dip in δT_b is visible: The dips are $\delta T_{b,\min} \simeq -48$ mK and $\delta T_{b,\min} \simeq -61$ mK for scenario groups C and A respectively.

The smaller dip in scenario group C compared to scenario group A will come about because δT_b will interpolate between T_γ and T_K at a rate controlled by x_α . The evolution of T_γ and T_K are the same for both groups A and C (since f_X is unchanged) while x_α is smaller for group A. This will delay significant $T_S - T_K$ coupling to a time when X-ray heating has boosted the IGM temperature closer to the CMB temperature. Since $\delta T_b \propto 1 - T_\gamma/T_S$, this automatically gives rise to a lower dip in the 21 cm signal as observed. A comparison between scenario groups D and B reveals $\delta T_{b,\min} \simeq -5$ mK and $\delta T_{b,\min} \simeq -6$ mK for scenario groups D and B respectively, in accordance with expectations.

The 21 cm power spectrum (at $k = 0.1$ Mpc $^{-1}$) as well as the evolution of $\beta_\alpha \delta T_b$ and $\beta_T \delta T_b$ are plotted in Figure 4.17. The 21 cm power spectrum for scenario groups C and D evolves in a fashion very similar to scenario groups A and B (figures 4.4 and 4.11 respectively). *This indicates that the evolution and amplitude of the 21 cm power spectrum are insensitive to plausible variations in $\mathcal{N}_{\alpha,*}$, $\mathcal{N}_{LyL,*}$ and α_s .* Further evidence of this comes from plots of $|\delta T_b| \Delta_{21\text{cm}}$ on smaller and larger scales in Figure 4.18. A comparison with figures 4.6 (scenario group A) and 4.13 (scenario group B) reveals no significant deviations on scales $k = 0.5$ Mpc $^{-1}$ and $k = 0.05$ Mpc $^{-1}$. The scale dependence of $|\delta T_b| \Delta_{21\text{cm}}$ at $z = 15.5$, as seen in Figure 4.19, is also very similar to what is seen in figures 4.7 (scenario group A) and 4.14 (scenario group B). Numerically, scenario group C predicts

$$|\delta T_b| \Delta_{21\text{cm}} (k = 0.5 \text{ Mpc}^{-1}) \Big|_{z=15.5}^C \simeq \begin{cases} 25 \text{ mK} & \text{for CDM} \\ 0.053 \text{ mK} & \text{for } m_{\text{FDM},22} = 1 \\ 0.066 \text{ mK} & \text{for } m_{\text{FDM},22} = 2 \\ 0.099 \text{ mK} & \text{for } m_{\text{FDM},22} = 3 \end{cases}, \quad (4.12)$$

$$|\delta T_b| \Delta_{21\text{cm}} (k = 0.1 \text{ Mpc}^{-1}) \Big|_{z=15.5}^C \simeq \begin{cases} 11 \text{ mK} & \text{for CDM} \\ 0.027 \text{ mK} & \text{for } m_{\text{FDM},22} = 1 \\ 0.062 \text{ mK} & \text{for } m_{\text{FDM},22} = 2 \\ 0.14 \text{ mK} & \text{for } m_{\text{FDM},22} = 3 \end{cases}, \quad (4.13)$$

¹ $\mathcal{N}_{\alpha,*}$ is a bit smaller for $m_{\text{FDM},22} = 2$ as well compared to scenario groups A and B, but only by a factor of $6199/6520 \simeq 0.95$. For $m_{\text{FDM},22} = 1$, the reduction factor is $4274/6520 \simeq 0.66$.

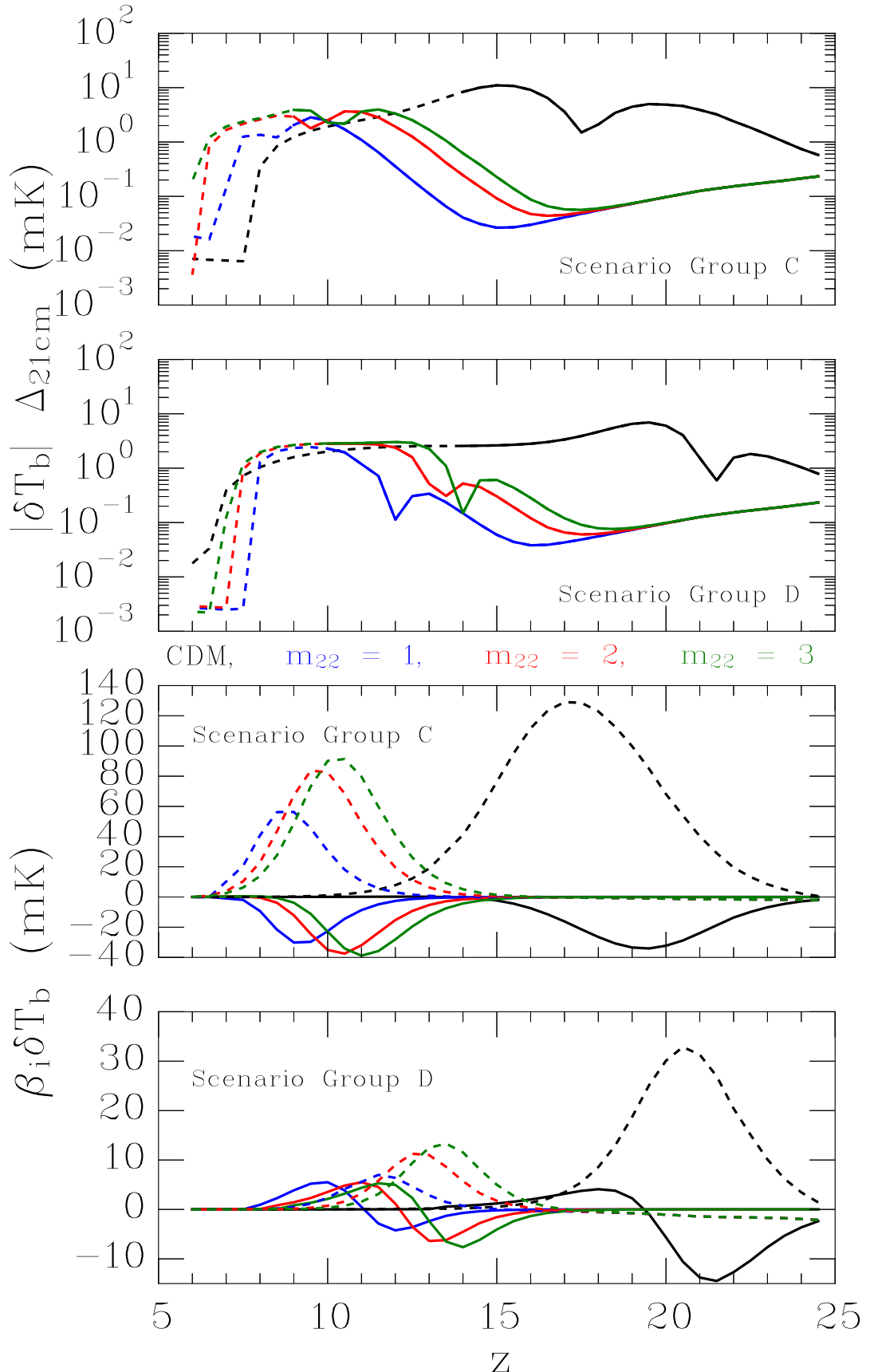


FIGURE 4.17. **Top two plots:** 21 cm power spectrum at $k = 0.1 \text{ Mpc}^{-1}$ (dashed for $x_i \gtrsim 0.05$). **Lower two plots:** $\beta_\alpha \delta T_b$ (solid) and $\beta_T \delta T_b$ (dashed).

4.3 Scenario Groups C & D

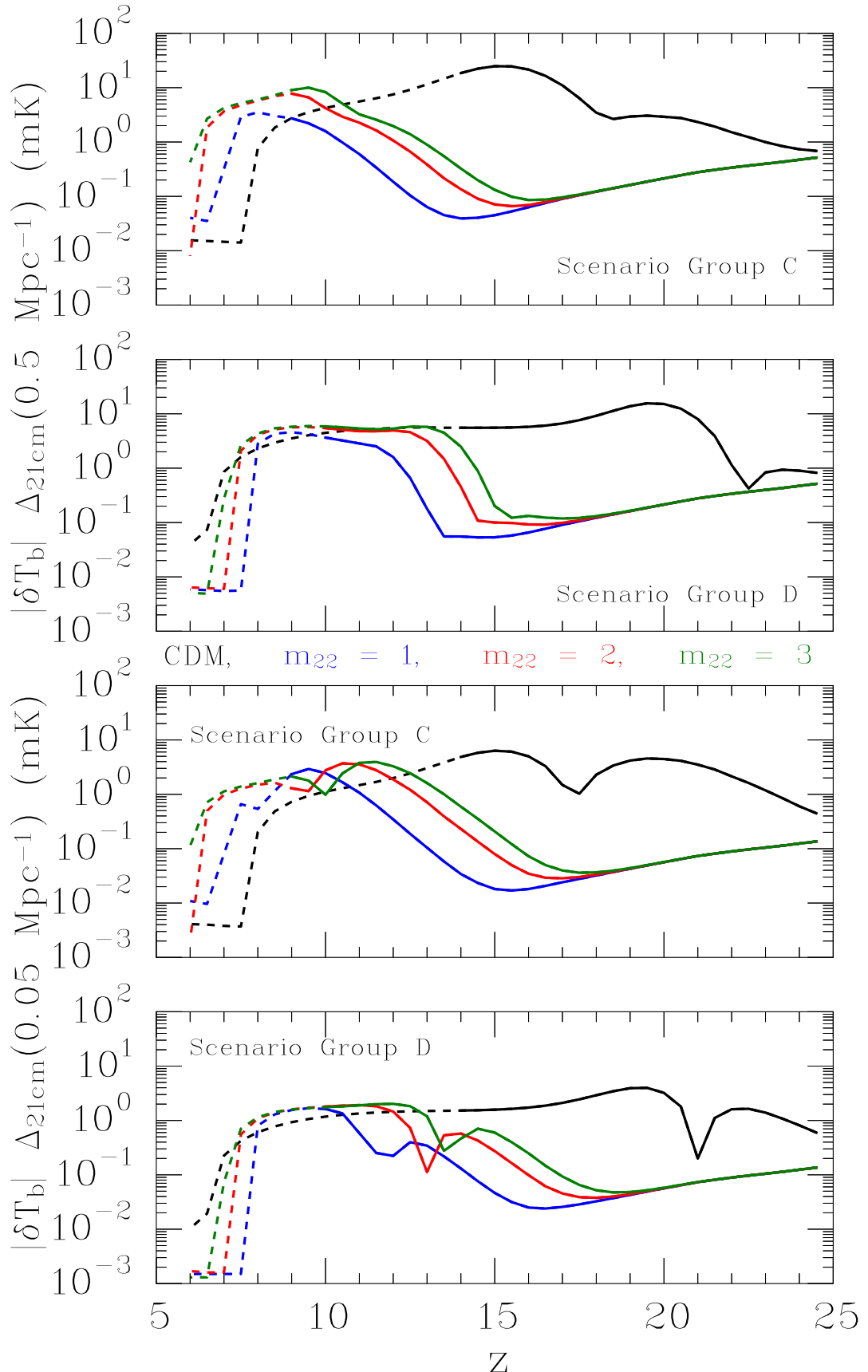


FIGURE 4.18. **Top two plots:** 21 cm power spectrum at $k = 0.5 \text{ Mpc}^{-1}$ (dashed for $x_i \gtrsim 0.05$). **Lower two plots:** 21 cm power spectrum at $k = 0.05 \text{ Mpc}^{-1}$ (dashed for $x_i \gtrsim 0.05$).

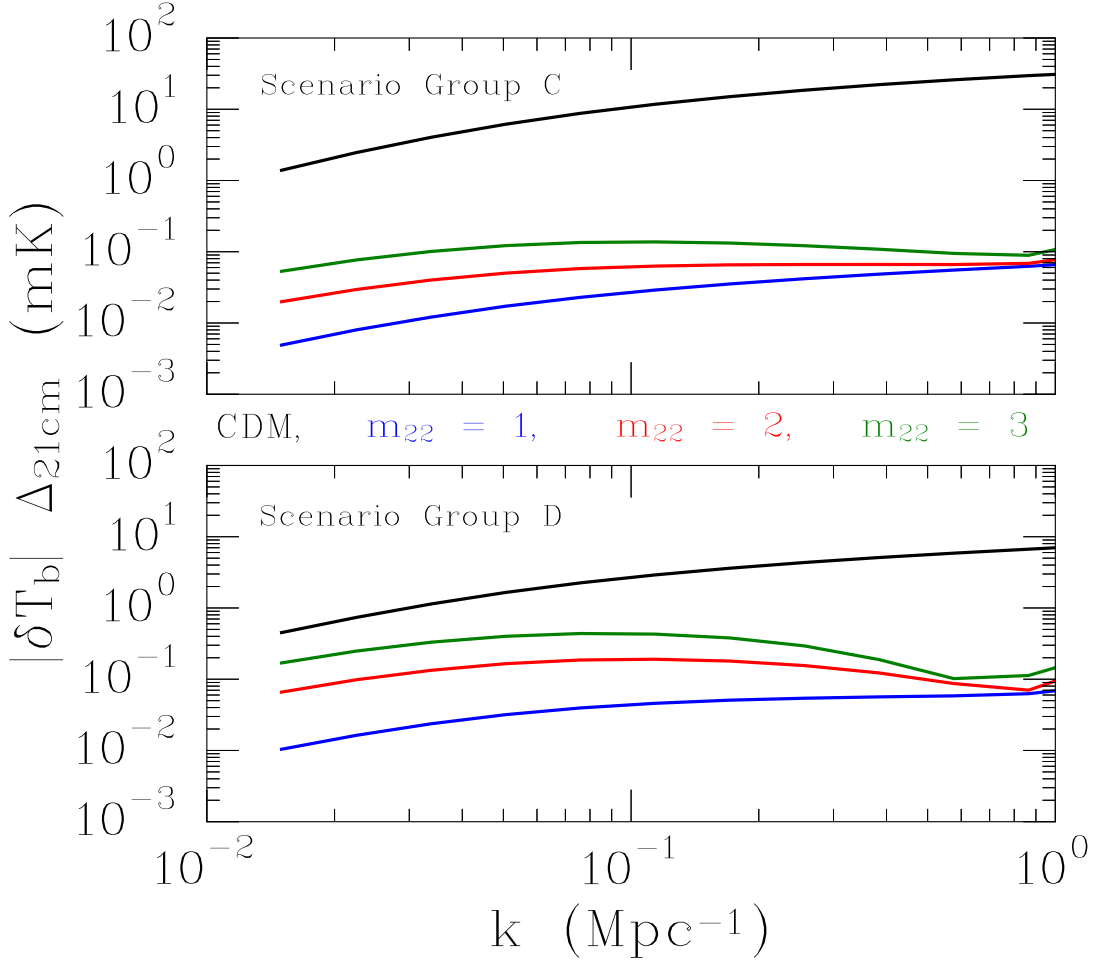


FIGURE 4.19. **Top two plots:** 21 cm power spectrum at $k = 0.5 \text{ Mpc}^{-1}$ (dashed for $x_i \gtrsim 0.05$). **Lower two plots:** 21 cm power spectrum at $k = 0.05 \text{ Mpc}^{-1}$ (dashed for $x_i \gtrsim 0.05$).

$$|\delta T_b| \Delta_{21\text{cm}}(k = 0.05 \text{ Mpc}^{-1}) \Big|_{z=15.5}^{\text{C}} \simeq \begin{cases} 6.1 \text{ mK} & \text{for CDM} \\ 0.017 \text{ mK} & \text{for } m_{\text{FDM},22} = 1 \\ 0.050 \text{ mK} & \text{for } m_{\text{FDM},22} = 2 \\ 0.12 \text{ mK} & \text{for } m_{\text{FDM},22} = 3 \end{cases}. \quad (4.14)$$

And the corresponding predictions from scenario group D are

$$|\delta T_b| \Delta_{21\text{cm}}(k = 0.5 \text{ Mpc}^{-1}) \Big|_{z=15.5}^{\text{D}} \simeq \begin{cases} 5.6 \text{ mK} & \text{for CDM} \\ 0.058 \text{ mK} & \text{for } m_{\text{FDM},22} = 1 \\ 0.098 \text{ mK} & \text{for } m_{\text{FDM},22} = 2 \\ 0.12 \text{ mK} & \text{for } m_{\text{FDM},22} = 3 \end{cases}, \quad (4.15)$$

$$|\delta T_b| \Delta_{21\text{cm}} (k = 0.1 \text{ Mpc}^{-1}) \Big|_{z=15.5}^D \simeq \begin{cases} 2.7 \text{ mK} & \text{for CDM} \\ 0.044 \text{ mK} & \text{for } m_{\text{FDM},22} = 1 \\ 0.19 \text{ mK} & \text{for } m_{\text{FDM},22} = 2 \\ 0.44 \text{ mK} & \text{for } m_{\text{FDM},22} = 3 \end{cases}, \quad (4.16)$$

$$|\delta T_b| \Delta_{21\text{cm}} (k = 0.05 \text{ Mpc}^{-1}) \Big|_{z=15.5}^D \simeq \begin{cases} 1.6 \text{ mK} & \text{for CDM} \\ 0.032 \text{ mK} & \text{for } m_{\text{FDM},22} = 1 \\ 0.16 \text{ mK} & \text{for } m_{\text{FDM},22} = 2 \\ 0.40 \text{ mK} & \text{for } m_{\text{FDM},22} = 3 \end{cases}. \quad (4.17)$$

The predicted amplitudes of the 21 cm power spectrum at $z = 15.5$ for all scenario groups are conveniently summarized in Table V in the next section for easier comparison.

4.4. Summary of Numerical Predictions

Table V.
Predicted amplitude of 21 cm power spectrum at $z = 15.5$

Scenario	Dark matter group	model	$ \delta T_b \Delta_{21\text{cm}} _{z=15.5}$ (mK)		
			$k = 0.5 \text{ Mpc}^{-1}$	$k = 0.1 \text{ Mpc}^{-1}$	$k = 0.05 \text{ Mpc}^{-1}$
A	CDM		25	11	6.1
A	$m_{\text{FDM},22} = 1$		0.053	0.029	0.019
A	$m_{\text{FDM},22} = 2$		0.067	0.064	0.052
A	$m_{\text{FDM},22} = 3$		0.099	0.14	0.12
B	CDM		5.6	2.7	1.6
B	$m_{\text{FDM},22} = 1$		0.059	0.050	0.037
B	$m_{\text{FDM},22} = 2$		0.10	0.20	0.17
B	$m_{\text{FDM},22} = 3$		0.12	0.44	0.40
C	CDM		25	11	6.1
C	$m_{\text{FDM},22} = 1$		0.053	0.027	0.017
C	$m_{\text{FDM},22} = 2$		0.066	0.062	0.050
C	$m_{\text{FDM},22} = 3$		0.099	0.14	0.12
D	CDM		5.6	2.7	1.6
D	$m_{\text{FDM},22} = 1$		0.058	0.044	0.032
D	$m_{\text{FDM},22} = 2$		0.098	0.19	0.16
D	$m_{\text{FDM},22} = 3$		0.12	0.44	0.40

5. Discussion & Conclusion

5.1. Discussion

5.1.1. Robustness of Results

As indicated in Table V, on the scales of interest all FDM scenarios in this thesis predict signals $|\delta T_b| \Delta_{21\text{cm}}|_{z=15.5} \lesssim 0.44 \text{ mK}$ — often an order of magnitude smaller than this upper limit. The CDM scenarios on the other hand all predict $|\delta T_b| \Delta_{21\text{cm}}|_{z=15.5} \gtrsim 1.6 \text{ mK}$, usually going upwards to $\sim 10 \text{ mK}$. How robust are these results? Can $|\delta T_b| \Delta_{21\text{cm}}|_{z=15.5}$ in FDM scenarios be pushed towards $1 - 10 \text{ mK}$, making FDM indistinguishable from CDM? It seems likely that further exploration of the plausible regions in parameter space will only reinforce the conclusion that FDM and CDM are distinguishable using 21 cm cosmology.

First off, the HMF for FDM used in this work (from [SCBH16]) will, if anything, *overestimate* the number of collapsed small halos as a simple comparison with the more accurate HMF in [DBN17] shows. More specifically, [DBN17] finds that there is an extremely sharp cut-off to the HMF near $\sim 10^9 M_\odot$ (for $m_{\text{FDM},22} = 1$) which is not seen in the HMF in [SCBH16] (see Eq. 3.5). The effect is not likely to be very big, mostly because for both HMF models there will be very few halos with masses $\sim 10^9 M_\odot$ in which Ly- α cooling is possible. The main takeaway, as noted in Chapter 3, is that more accurate modelling of the HMF for FDM would only make FDM *more distinguishable* from CDM.

Secondly, what about parameters like f_* and f_{esc} ? It seems unlikely that these parameters can be pushed up further for FDM. The chosen star formation efficiency of $f_* = 0.1 - 0.3$ is already fairly substantial. Feedback from supernovae (SNe) can limit the star formation efficiency by blowing out large quantities of gas from which stars would otherwise form [DS86, LF13]. This would likely prohibit larger star formation efficiencies, and picking smaller values of f_* would just further delay Lyman- α coupling and possibly making reionization by $z \sim 6$ impossible for FDM. So the results here should not be sensitive to plausible variations in f_* . The same holds for f_{esc} which is not expected to fall outside the range considered here [KC14]. Furthermore, f_{esc} has little impact on the 21 cm signal at very high redshifts. This follows because it effect the signal through $x_i \propto f_{\text{esc}}$, but $\delta T_b \propto 1 - x_i \simeq 1$ at $z = 15.5$.

Another assumption made in the FDM scenarios with $m_{\text{FDM},22} = 1, 2$ is that Pop III stars provide a significant, if not dominant, contribution to the ionization budget in *every* galaxy formed, regardless of redshift. However, in reality it may be the case that shortly after the first Pop III stars form in $\sim 10^{10} M_\odot$ they will

pollute the interstellar medium (ISM) with metals that induce a sharp transition in stellar formation physics. Cooling by molecular hydrogen forming in galaxies with $T_{\text{vir}} \gtrsim 10^4$ K can form stars in molecular clouds with temperatures $T \sim 10^2$ K [OH02]. With metals, cooling to even lower temperatures would be possible (as is typical in present-day galaxies), resulting in the formation of less massive Pop II stars.¹ The transition from Pop II stars to Pop III stars could happen fairly quickly for FDM. The reason for this is that the Pop III stars form in relatively massive halos compared to CDM (where Pop III stars could inhabit minihalos or atomically cooling halos with masses $\sim 10^8 M_\odot$, see Chapter 2). The more massive the halo, the harder it will be for supernovae to eject gas from the ISM and inhibit star formation (see e.g. [DS86, DW03] for simple models). Consequently, f_* should be greater for the first galaxies in FDM compared to CDM and result in a quicker metallicity increase.² So it might be the case that Pop III stars stop forming during, say, the EoR.

Would this impact the results here concerning the 21 cm power spectrum? First off, this seems to be unlikely for the simple reason that we have focused on a relatively high redshift of $z = 15.5$, roughly when the very first structures formed in the FDM scenarios. At such early times, metal enrichment would not have had time to make a transition to Pop II star formation. However, even if there was such a transition to Pop II star formation, the impact on the 21 cm power spectrum would mainly come from changes in the Lyman- α coupling (via changes in parameters like $\mathcal{N}_{\alpha,*}$). And this effect has already been explored in this thesis by varying $\mathcal{N}_{\alpha,*}$, $\mathcal{N}_{\text{LyL},*}$ and α_s from typical Pop II to Pop III values, yielding only small differences in the amplitude of the 21 cm power spectrum.

5.1.2. Observational Probes

The ultimate reason for considering the evolution of the 21 cm signal in different dark matter scenarios is to be able to use it to constrain the nature of dark matter. The key question, based on the results of this thesis, is then whether it is possible to differentiate a sub-mK signal (FDM) from a > 1 mK signal (CDM). In Figure 5.1 the approximate expected errors in the measured 21 cm power spectrum is shown at three redshifts as a function of scale. The redshift of most interest for us is the one at $z = 15.7$, close to $z = 15.5$ that has been the redshift of focus in this thesis. In the $z = 15.7$ plot it is seen that errors expected from radio arrays similar to SKA and MWA would be around $\sim 1 - 2$ mK and $\sim 3 - 10$ mK respectively for scales of $0.05 - 0.5 \text{ Mpc}^{-1}$.

¹All else being equal, the Jeans mass scales as $T^{3/2}$. The initial Jeans mass in molecular clouds is thought to be a major factor governing the characteristic masses of stars, as seen in the “knee” of the stellar initial mass function [BCB06].

²Indeed, [OH02] point out that the metallicity scales as $\sim f_*$ because a fraction of the stars formed will be supernovae ejecting metals into the ISM so that the fraction of mass in the form of metals in the galaxy scales with f_* .

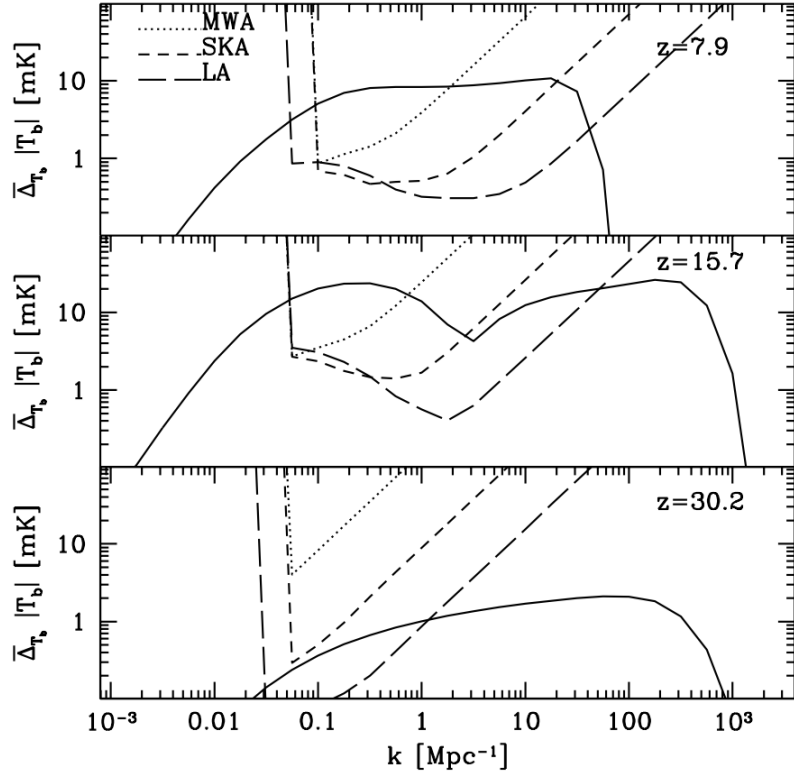


FIGURE 5.1. Figure from [PL08]. Here the expected errors in the measured 21 cm power spectrum are plotted for three representative 21 cm experiments: MWA (*Murchison Widefield Array*), SKA (*Square Kilometer Array*) and LA (*Lunar Array*). The first (preliminary) results with MWA have already been published [BHS⁺16] and SKA is being planned. LA refers to something more speculative being built on the Moon. It should be noted that the labels MWA, SKA and LA do not correspond exactly with the real, planned or imagined experiments. Thus, the errors should only be taken as ballpark figures. The predicted 21 cm power spectrum from a CDM simulation (solid line) is also shown.

The most conservative and plausible scenario group considered in this thesis was scenario group C. On all scales, this group yielded FDM signals $|\delta T_b| \Delta_{21\text{cm}}|_{z=15.5}^C \ll 1 \text{ mK}$ and CDM signals of $|\delta T_b| \Delta_{21\text{cm}}|_{z=15.5}^C = 6.1, 11, 25 \text{ mK}$ for scales of $k = 0.05, 0.1, 0.5 \text{ Mpc}^{-1}$ (see Table V). Thus, radio arrays like MWA and SKA would be expected to rule out $m_{\text{FDM},22} \leq 3$ for *any* signal detection at $z \sim 15 - 16$. Such a detection, especially if the amplitude of the signal is $\sim 10 \text{ mK}$ would instead provide some additional evidence for CDM-like structure formation.

Note, again, that for every scenario group we have $|\delta T_b| \Delta_{21\text{cm}}|_{z=15.5} \ll 1 \text{ mK}$ for FDM. *So the conclusion that a signal detection by arrays like MWA and SKA would rule out $m_{\text{FDM},22} \leq 3$ holds for every scenario group considered here.* It is a little more complicated for CDM. For scenario groups B and D, a signal detection for CDM is possible, but only seems plausible close to scales $\sim 0.5 \text{ Mpc}^{-1}$. Thus, a detectable signal from CDM at $z \sim 15 - 16$ should not be taken to be an inevitable

prediction of CDM, but it seems to be the most likely expectation.

While the PF model does not accurately model the 21 cm power spectrum for CDM at redshifts $z \sim 10$, it should provide a fairly good model of the 21 cm power spectrum for FDM at this redshift. From Figure 4.17 it is seen that the FDM scenarios produce signals of a few mK. So radio arrays like MWA and SKA could rule out $m_{\text{FDM},22} \leq 3$ by detecting a significantly stronger signal at $z \sim 10$. However, before much significance is drawn to this, some kind of comparison with CDM within the same model framework and at the same redshift would be needed, which is not provided here.

5.1.3. Future Work

To properly make predictions for what to expect of FDM compared to CDM at lower redshifts, better modelling of ionization fluctuations would be needed that are valid when HII regions occupy a significant portion of the IGM. With a model incorporating this, the possibility of distinguishing FDM from CDM at redshifts $z \lesssim 14$ could be explored. Such a follow-up project where ionization fluctuations are properly accounted for is planned by Dr. Raghunath Ghara, Prof. Garrelt Mellema and this author.

Future work could also consider better modelling of the HMF for FDM by trying to incorporate the results of [DBN17] that more accurately capture the physics that sets FDM apart from CDM. It would also be good to consider larger FDM particle masses to better understand at what point FDM becomes indistinguishable from CDM. Another potentially interesting improvement would be to model the star formation efficiency as a function of redshift and halo mass. A simple prescription based on energetic supernovae feedback with $f_* \propto M^{2/3}$ for low halo masses could suffice [DW03]. Such a model was considered for CDM in [BL05]. These changes could shrink the parameter space by promoting a previously free parameter (f_*) to a semi-fixed function.

5.2. Conclusion

In this thesis the question of whether 21 cm cosmology could distinguish the standard CDM paradigm from a more exotic dark matter model — fuzzy dark matter (FDM) — that suppresses small-scale structure formation has been explored. Four groups of scenarios were considered to probe parameter space and it was found that each scenario group predicted markedly different evolutions of the 21 cm signal during Cosmic Dawn and Reionization. All scenario groups converged on one robust result:

- FDM, for particle masses $m_{\text{FDM}} \leq 3 \times 10^{-22}$ eV, predicts extremely weak amplitudes ($\ll 1$ mK) in the 21 cm power spectrum at redshifts $z \sim 15 - 16$ during the first stages of Cosmic Dawn, whereas the natural, but not inevitable, expectation from CDM is the appearance of comparably strong

5.2 Conclusion

signals ($\gg 1$ mK) that could be detected by upcoming 21 cm experiments. Any detection of a signal at $z \sim 15 - 16$ would be evidence *against* FDM, and if this signal had an amplitude $\gg 1$ mK it would provide evidence *for* CDM-like structure formation.

The main reason for the weak signal predicted by FDM is the suppressed small-scale structure formation which results in a delayed Lyman- α coupling of the spin temperature to the kinetic temperature of the IGM.

The possibility of constraining fundamental dark matter physics with 21 cm cosmology opens up a new and exciting avenue of research. Most crucially, future work should include better modelling of ionization fluctuations so as to make it possible to make robust predictions for lower redshifts. This is planned for the near future by Dr. Raghunath Ghara, Prof. Garrelt Mellema and this author. Other areas of improvement include a more accurate modelling of the halo mass function for FDM, which should, if anything at all, make FDM *more* distinguishable from CDM.

Acknowledgments

I would first like to thank my supervisor Garrett Mellema for taking me on as a student. My enthusiasm for cosmology cannot be expressed in words, so to be able to do a project like this connecting various exciting sub-fields of cosmology has been a thrill. I appreciate his patience in explaining the various concepts concerning 21 cm cosmology which was completely new to me, as well as his willingness to discuss various issues and interesting subjects related to the project. I would also like to thank Raghunath Ghara for helping me so much with the code used for running the simulations. Without his help, the various problems I faced in running the program would make it implausible that the project would have finished before the heat death of the Universe. I also want to thank both Garrett and Raghu for giving me feedback on my thesis and spotting many of my glaringly obvious typos.

A. Appendix

A.1. Structure & Galaxy formation in Λ CDM

A.1.1. Deriving the differential equation for δ

We start with the Euler, continuity and Poisson equations,

$$\frac{\partial \mathbf{v}}{\partial t} + \frac{1}{a} (\mathbf{v} \cdot \nabla) \mathbf{v} = -\frac{\dot{a}}{a} \mathbf{v} - \frac{1}{a} \nabla \phi, \quad (\text{A.1})$$

$$\frac{\partial \rho}{\partial t} + 3\frac{\dot{a}}{a} \rho + \frac{1}{a} \nabla \cdot (\rho \mathbf{v}) = 0, \quad (\text{A.2})$$

$$\nabla^2 \phi = 4\pi G a^2 \bar{\rho} \delta. \quad (\text{A.3})$$

Next, write $\rho = \bar{\rho}(1 + \delta)$. Assuming that $\delta \ll 1$, the Universe will approximately follow the expansion of the Universe, so that the peculiar velocity \mathbf{v} will be small. To first order then, terms of order δ^2 , \mathbf{v}^2 or $\mathbf{v}\delta$ can be discarded. Using this and $\partial\bar{\rho}/\partial t + 3(\dot{a}/a) = 0$ reduces the Euler and continuity equations to

$$\frac{\partial \mathbf{v}}{\partial t} = -\frac{\dot{a}}{a} \mathbf{v} - \frac{1}{a} \nabla \phi, \quad (\text{A.4})$$

$$\frac{\partial \delta}{\partial t} = -\frac{1}{a} \nabla \cdot \mathbf{v}. \quad (\text{A.5})$$

Next, taking the divergence of the Euler equation and the time derivative of the continuity equation yields

$$\nabla \cdot \frac{\partial \mathbf{v}}{\partial t} = -\frac{\dot{a}}{a} \nabla \cdot \mathbf{v} - \frac{1}{a} \nabla^2 \phi, \quad (\text{A.6})$$

$$\frac{\partial^2 \delta}{\partial t^2} = \frac{\dot{a}}{a} \left(\frac{1}{a} \nabla \cdot \mathbf{v} \right) - \frac{1}{a} \nabla \cdot \frac{\partial \mathbf{v}}{\partial t}. \quad (\text{A.7})$$

Using Eq. A.5 and Eq. A.6 to replace $(1/a) \nabla \cdot \mathbf{v}$ and $\nabla \cdot \partial \mathbf{v} / \partial t$ respectively in Eq. A.7, as well as the Poisson equation for $\nabla^2 \phi$ then gives us

$$\frac{\partial^2 \delta}{\partial t^2} + 2\frac{\dot{a}}{a} \frac{\partial \delta}{\partial t} = 4\pi G \bar{\rho} \delta. \quad (\text{A.8})$$

To finally get it in the form written in Eq. 2.3, we can use $4\pi G \bar{\rho} = (3/2) \Omega_m (\dot{a}/a)^2$.

A.1.2. Approximate expressions for $\sigma(M)$ and the low-mass HMF

For a spectral index $n_s \simeq 1$, the power spectrum can be written as $P(\kappa) \propto \kappa T(\kappa)^2$ where $\kappa \equiv k/2k_{\text{eq}}$.¹ The transfer function is approximately,

$$T(\kappa) \simeq \begin{cases} 1 & \kappa \ll 1 \\ A\kappa^{-2} \log(\kappa) & \kappa \gg 1 \end{cases}, \quad (\text{A.9})$$

where A is a constant. The RMS density fluctuation within a dimensionless radius $r \sim 1/\kappa$, using a sharp- k window function, is then

$$\begin{aligned} \sigma^2 &\propto \text{const.} + \int_{\bar{\kappa}}^{\kappa} d\kappa' \kappa'^{-1} \log^2 \kappa' \\ &= \text{const.} + \int_{\log \bar{\kappa}}^{\log \kappa} d\log \kappa' \log^2 \kappa' \\ &\propto \text{const.} + \log^3 \kappa. \end{aligned} \quad (\text{A.10})$$

The constant in the first step comes from integrating the power spectrum in the regime when $T(k) \simeq A\kappa^{-2} \log(\kappa)$ and $T(k) \simeq 1$ are bad approximations. This constant can be found by comparison with accurate numerical results. Finally, using $\kappa = (8M/M_{\text{eq}})^{-1/3}$, the growth factor $\sim a$ and normalization yields

$$\begin{aligned} \sigma(M) &\simeq \sigma_8 \left\{ \frac{\mu - \log^3(8M/M_{\text{eq}})}{\mu - \log^3(8M_8/M_{\text{eq}})} \right\}^{1/2} a, \\ \mu &\simeq 20. \end{aligned} \quad (\text{A.11})$$

The numerical values for the horizon mass at matter-radiation equality M_{eq} and $M_8 \equiv M(R < 8 \text{ Mpc}/h)$ are²

¹The “2” comes from the crude approximation that a perturbation will not be causally connected (and so be said to evolve on a sub-horizon scale) if its radius is more than half the horizon radius.

²The former can be found using the horizon radius at $a = a_{\text{eq}}$; $R_H(a_{\text{eq}}) = 2(\sqrt{2}-1)cH_0^{-1}\Omega_{m,0}^{-1/2}a_{\text{eq}}^{1/2}$.

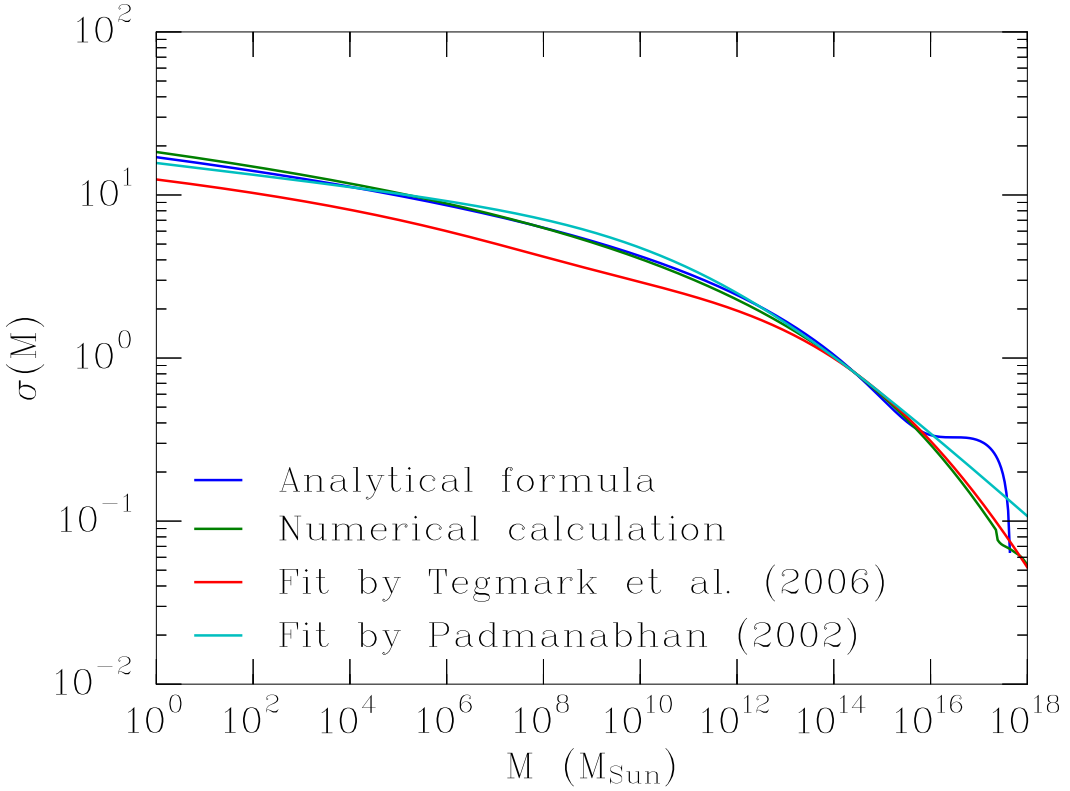


FIGURE A.I. A plot of $\sigma(M)$ at the present as predicted by the analytical approximation in Eq. A.11, a numerical calculation and the fits provided in [TARW06] (see their Eq. A13) and [Pad02] (p. 12). All calculations are for $\sigma_8 = 0.8149$ and $n_s = 1$. The numerical calculation made use of the transfer function in Eq. 29 of [EH98].

$$M_{\text{eq}} \simeq 2.4 \times 10^{17} \left(\frac{\Omega_{\text{m},0} h^2}{0.14} \right)^{-1/2} \left(\frac{1 + z_{\text{eq}}}{3400} \right)^{-3/2} M_\odot, \quad (\text{A.12})$$

$$M_8 \simeq 2.7 \times 10^{14} \left(\frac{\Omega_{\text{m},0} h^2}{0.14} \right) \left(\frac{h}{0.68} \right)^{-3} M_\odot.$$

A comparison between Eq. A.11, a numerical calculation and a fits by [TARW06] and [Pad02] is shown in Figure A.I. It is clear that Eq. A.11 provides a remarkably good — in fact the best — approximation below $\sim 10^{14} M_\odot$, above which the formula breaks down. Since this thesis mainly focuses on small-scale galaxy formation, larger scales are of little importance here. Beyond being more accurate than the fits in the relevant mass range, the analytical formula was derived, to some extent, from first principles whereas the fits were not. And even with this in mind, the analytical formula is also significantly simpler than the two fits — it is the only formula that is invertable.

The low-mass HMF can be deduced from Eq. 2.11. At low masses, the exponential

factor can be neglected so that

$$\frac{\partial n}{\partial M} \propto \frac{1}{M^2} \frac{1}{\sigma(M)} \left| \frac{\partial \log \sigma}{\partial \log M} \right|. \quad (\text{A.13})$$

Defining $\bar{M} \equiv 8M/M_{\text{eq}}$, $\gamma \equiv -\partial \log \{\partial n/\partial M\} / \partial \log M$ and $\eta \equiv |\partial \log \sigma / \partial \log M|$ then yields

$$\begin{aligned} \gamma &\simeq 2 - \eta - \frac{\partial \log \eta}{\partial \log M} \\ &= 2 - \frac{3}{2} \frac{\log^2 \bar{M}}{\mu - \log^3 \bar{M}} - \frac{2}{\log \bar{M}} - 3 \frac{\log^2 \bar{M}}{\mu - \log^3 \bar{M}} \\ &= 2 - \frac{2}{\log \bar{M}} - \frac{9}{2} \frac{\log^2 \bar{M}}{\mu - \log^3 \bar{M}}. \end{aligned} \quad (\text{A.14})$$

For very low masses $-\log^3 \bar{M} \gg \mu$ so that we get

$$\gamma \simeq 2 + \frac{5}{2} \frac{1}{\log \bar{M}}. \quad (\text{A.15})$$

The logarithmic factor changes slowly, but in the very large mass range $1 M_{\oplus} \lesssim M \lesssim 10^9 M_{\odot}$ we get $\gamma \simeq 1.9$.

A.1.3. Ly- α cooling and the minimum mass of galaxies

The Ly- α cooling rate (in $\text{erg s}^{-1} \text{cm}^{-3}$) is $4\pi j_{\text{Ly}\alpha} = n_2 A_{21} \times (3/8) \alpha^2 m_e c^2$ where n_2 is the number density of hydrogen atoms in the $n = 2$ state, A_{21} is the Einstein coefficient for spontaneous emission and $(3/8) \alpha^2 m_e c^2$ is the energy associated with the Lyman- α photon (where $\alpha \simeq 1/137$ is the fine-structure constant). The level population is set by the balance between collisional excitation and de-excitation as well spontaneous de-excitation: $\langle \sigma_{12} v \rangle n_e n_1 = (A_{21} + \langle \sigma_{21} v \rangle n_e) n_2$ where $\langle \sigma_{12} v \rangle$ and $\langle \sigma_{21} v \rangle$ is the collisional excitation and de-excitation rate respectively. Since the gas in a newly formed virialized halo is quite tenuous, we have $A_{21} \gg \langle \sigma_{21} v \rangle n_e$, and thus $n_2 \simeq \langle \sigma_{12} v \rangle n_e n_1 / A_{21}$. For the same reason $n_1 \simeq n_{\text{HI}}$, yielding,

$$4\pi j_{\text{Ly}\alpha} \simeq \frac{3}{8} \langle \sigma_{12} v \rangle n_e n_{\text{HI}} \alpha^2 m_e c^2. \quad (\text{A.16})$$

The cross section for collisional excitation on physical grounds should be of order $\sim \pi (\hbar/m_e v)^2$ where the quantity within the parenthesis is the (reduced) de Broglie wavelength of the impending electron and is therefore often parametrized as (see e.g. p. 324 in [Pad00]),

$$\sigma_{12} = \pi \left(\frac{\hbar}{m_e v} \right)^2 \frac{\Omega_{12}}{g_1}. \quad (\text{A.17})$$

Where Ω_{12} is known as the “collisional strength” and $g_1 = 2$ is the statistical weight of the ground state. The collisional excitation rate, averaged over a Maxwell-Boltzmann distribution for a gas of temperature T , is then

$$\langle \sigma_{12} v \rangle = \frac{\Omega_{12} \hbar^2}{(k_B T)^{1/2} m_e^{3/2}} \left(\frac{\pi}{2} \right)^{1/2} \exp \left(-\frac{3}{8} \frac{\alpha^2 m_e c^2}{k_B T} \right). \quad (\text{A.18})$$

The collisional strength varies only very slowly with temperature and is of order one in the relevant temperature range of interest (fig. 7 in [Dij17]). The time scale for a hydrogen gas to cool is then $t_{\text{cool}} = (3/2) n_H k_B T / 4\pi j_{\text{Ly}\alpha}$, yielding,

$$t_{\text{cool}} \simeq \frac{2}{\pi^{1/2} \Omega_{12}} \left(\frac{\alpha m_e^2 c}{\hbar^2} \right) \frac{\gamma^{-3/2} e^{(3/4)\gamma}}{x(1-x)n_H}. \quad (\text{A.19})$$

Where $\gamma \equiv (1/2) \alpha^2 m_e c^2 / k_B T = \text{Ryd}/k_B T$ and $x \equiv n_e / (n_e + n_{\text{HI}}) = n_{\text{HII}}/n_H$ is the ionization fraction. Eq. A.19 is written in a form that can be compared to Eq. 7 in [TR98]. In collisional ionization equilibrium the ionization fraction is $x \sim (1 + \alpha^3 \gamma^{7/6} e^\gamma)^{-1}$ (e.g. Eq. 8 in [TR98] and p. 408 in [Pad02]) yielding

$$t_{\text{cool}} \simeq \frac{2}{\pi^{1/2} \Omega_{12}} \left(\frac{m_e^2 c}{\hbar^2 \alpha^2 n_H} \right) \left\{ \gamma^{-8/3} e^{-\gamma/4} (1 + \alpha^3 \gamma^{7/6} e^\gamma)^2 \right\}. \quad (\text{A.20})$$

This cooling time is a sensitive function of temperature. Specifically, for temperatures below $T_{\min} \sim (1/2) \alpha^2 m_e c^2 / k_B \log(\alpha^{-2}) = 1.6 \times 10^4$ K the cooling time becomes exponentially long (so that $t_{\text{cool}} \gg t_{\text{ff}}$) [TR98]. With this in mind it is straightforward to determine the minimum mass of a galaxy. The mass of a newly formed halo in terms of the virial temperature is (ignoring numerical factors of order one),

$$M \sim \left(\frac{k_B T_{\text{vir}}}{G \mu m_p} \right)^{3/2} \rho_{\text{vir}}^{-1/2}. \quad (\text{A.21})$$

To find the minimum galactic mass we set $T_{\text{vir}} \sim T_{\min}$ and try to express the virial density in terms of cosmological parameters. Furthermore, we write $\rho_{\text{vir}} \sim 18\pi^2 \bar{\rho}_0 (1+z_{\text{col}})^3$. The redshift at collapse for a $\nu\sigma$ -halo can be estimated using Eq. 2.10. To first approximation, we can let $\sigma(M)$ vary as a power law of the mass: $\sigma(M) \simeq \sigma_0 (M/M_0)^{-\eta} a$. All of this yields,

$$M_{\text{Ly}\alpha, \min} \sim M_0^{\frac{3\eta}{2(3\eta/2-1)}} \left(\frac{\alpha^2 \beta c^2 \delta_{\text{crit}}}{2G\mu \log(\alpha^{-2}) \nu \sigma_0} \right)^{\frac{3}{2(1-3\eta/2)}} (18\pi^2 \bar{\rho}_0)^{\frac{1}{2(3\eta/2-1)}}, \quad (\text{A.22})$$

where $\beta \equiv m_e/m_p$.

A.2. Simple model of Cosmic Dawn

We can construct a simple model of the heating history of the IGM using Eq. 2.20 by assuming that the IGM temperature is determined only by adiabatic cooling

and X-ray heating, so that,

$$\dot{T}_K + 2\frac{\dot{a}}{a}T_K \simeq \frac{2}{3}f_{X,h}\frac{N_X}{k_B}h\nu_0 f_\star \frac{df_{coll}}{dt}. \quad (\text{A.23})$$

The formal solution is then,

$$T_K(a) \simeq T_{K,0} \left(\frac{a_0}{a} \right)^2 + \frac{2}{3} \frac{h\nu_0 N_X}{a^2 k_B} f_\star \int_{a_0}^a da' f_{X,h} a'^2 \frac{df_{coll}}{da'}. \quad (\text{A.24})$$

Since we are only interested in a rough reconstruction of the heating history here, and to make the problem more analytically tractable, we can use the simple Press-Schechter formula $f_{coll} \simeq \text{erfc} \left\{ \delta_{\text{crit}} (1+z) / \sqrt{2} \sigma [M_{\min}(z)] \right\}$ [PS74, Pee93, Fur06, LF13] instead of Eq. 2.18. In writing the collapse fraction as this I have assumed, as is reasonable in the early matter-dominated Universe, that density perturbations grow as $\propto a$. And M_{\min} is the minimum halo mass above which gas can cool, which (as discussed in the main text) is set by the requirement $T_{\text{vir}} \gtrsim 10^4$ K and depends on the redshift of collapse. Since the complementary error function is defined as $\text{erfc}(x) \equiv \frac{2}{\sqrt{\pi}} \int_x^\infty dt e^{-t^2}$ (e.g. [Boa05], p. 547), it follows that $\frac{d}{dx} \text{erfc}(x) = -\frac{2}{\sqrt{\pi}} e^{-x^2}$. Using this and writing the integral in terms of redshift instead of the scale factor then yields³

$$\begin{aligned} T_K(z) &\simeq T_{K,0} \left(\frac{1+z}{1+z_0} \right)^2 \\ &- \frac{4(1+z)^2}{3\sqrt{2\pi}} h\nu_0 \frac{N_X}{k_B} f_\star \delta_{\text{crit}} \int_z^{z_0} dz' \frac{f_{X,h} e^{-\delta_{\text{crit}}^2(1+z')^2/2\sigma^2(M_{\min})}}{(1+z')^2 \sigma(M_{\min})}. \end{aligned} \quad (\text{A.25})$$

The fraction of the X-ray radiation that goes into heating can be approximated as $f_{X,h} \sim (1+2\bar{x})/3$ ([FOB06], p. 209) where the global ionization fraction is roughly $\bar{x} \sim \min[1, \zeta f_{coll}/(1+n_{\text{rec}})]$ (where I choose $n_{\text{rec}} = 1.5$). The initial IGM temperature $T_{K,0}$ can be determined through $T_{K,0} \simeq T_{\gamma,0}(1+z_0)$ at $z_0 \sim 200$. This prediction of this simple model should be taken with caution since opacity changes during reionization is not accounted for. But it still paints a surprisingly good heating history of the IGM.

³I have used

$$\frac{dx}{dz} = \frac{d}{dz} \left(\frac{\delta_{\text{crit}} (1+z)}{\sqrt{2} \sigma [M_{\min}(z)]} \right) \simeq \frac{\delta_{\text{crit}}}{\sqrt{2} \sigma [M_{\min}(z)]}.$$

Where in the last step the derivative of $\sigma [M_{\min}(z)]$ has been ignored, since σ is a relatively weak function of the mass near M_{\min} and therefore redshift.

A.3. Jeans mass in FDM

The equations governing the FDM “fluid” were,

$$\begin{aligned} \frac{\partial \mathbf{v}}{\partial t} + \frac{1}{a} (\mathbf{v} \cdot \nabla) \mathbf{v} &= -\frac{\dot{a}}{a} \mathbf{v} - \frac{1}{a} \nabla \phi + \frac{\hbar^2}{2a^3 m_{\text{FDM}}^2} \nabla \left(\frac{\nabla^2 \sqrt{\rho}}{\sqrt{\rho}} \right), \\ \frac{\partial \rho}{\partial t} + 3 \frac{\dot{a}}{a} \rho + \frac{1}{a} \nabla \cdot (\rho \mathbf{v}) &= 0, \\ \nabla^2 \phi &= 4\pi G a^2 \bar{\rho} \delta. \end{aligned} \quad (\text{A.26})$$

Now consider a small density perturbation $\delta \ll 1$. To first order in δ and \mathbf{v} , the continuity equation becomes

$$\frac{\partial \delta}{\partial t} + \frac{1}{a} \nabla \cdot \mathbf{v} = 0. \quad (\text{A.27})$$

As for the Euler equation, the gradient in the pressure term can be expanded to first order as follows,

$$\begin{aligned} \nabla \left(\frac{\nabla^2 \sqrt{\rho}}{\sqrt{\rho}} \right) &= \nabla \left(\frac{\nabla^2 \sqrt{1+\delta}}{\sqrt{1+\delta}} \right) \\ &\simeq \nabla \left\{ \left(1 - \frac{1}{2} \delta \right) \frac{1}{2} \nabla^2 \delta \right\} \\ &\simeq \frac{1}{2} \nabla \nabla^2 \delta. \end{aligned} \quad (\text{A.28})$$

Thus, the Euler equation reduces to an equation in terms of δ instead of ρ ,

$$\frac{\partial \mathbf{v}}{\partial t} + \frac{1}{a} (\mathbf{v} \cdot \nabla) \mathbf{v} = -\frac{\dot{a}}{a} \mathbf{v} - \frac{1}{a} \nabla \phi + \frac{\hbar^2}{4a^3 m_{\text{FDM}}^2} \nabla \nabla^2 \delta. \quad (\text{A.29})$$

Like in Appendix A.1.1 we take the divergence of Eq. A.29 and the time derivative of Eq. A.27 and simplify in a similar fashion to get

$$\frac{\partial^2 \delta}{\partial t^2} + 2 \frac{\dot{a}}{a} \frac{\partial \delta}{\partial t} = 4\pi G \bar{\rho} \delta - \frac{\hbar^2}{4a^4 m_{\text{FDM}}^2} \nabla^2 \nabla^2 \delta. \quad (\text{A.30})$$

To derive the Jeans scale we make a Fourier transformation,

$$\delta = \frac{1}{(2\pi)^3} \int d^3 \mathbf{k} \delta_{\mathbf{k}} e^{-i\mathbf{k}\cdot\mathbf{x}}. \quad (\text{A.31})$$

With this, we get,

$$\begin{aligned} \nabla^2 \nabla^2 \delta &= \frac{1}{(2\pi)^3} \int d^3 \mathbf{k} \delta_{\mathbf{k}} \nabla^2 \nabla^2 e^{-i\mathbf{k}\cdot\mathbf{x}} \\ &= \frac{1}{(2\pi)^3} \int d^3 \mathbf{k} k^4 \delta_{\mathbf{k}} e^{-i\mathbf{k}\cdot\mathbf{x}}, \end{aligned} \quad (\text{A.32})$$

where $k \equiv |\mathbf{k}|$. Thus, using Eq. A.30 for $\delta_{\mathbf{k}}$ yields

$$\ddot{\delta}_{\mathbf{k}} + 2\frac{\dot{a}}{a}\dot{\delta}_{\mathbf{k}} = \left(4\pi G\bar{\rho} - \frac{\hbar^2 k^4}{4a^4 m_{\text{FDM}}^2}\right) \delta_{\mathbf{k}}. \quad (\text{A.33})$$

This equation has growing solutions only if the right-hand side is positive. And this condition is only fulfilled for wavenumbers smaller than the Jeans wavenumber $k_{\text{FDM,J}}$ where

$$\begin{aligned} k_{\text{J}} &= 2 \left(\frac{\pi G}{\hbar^2} \bar{\rho} m_{\text{FDM}}^2 \right)^{1/4} a \\ &= 2 \left(\frac{\pi G}{\hbar^2} \bar{\rho}_0 m_{\text{FDM}}^2 \right)^{1/4} a^{1/4} \\ &\simeq 36 m_{\text{FDM},22}^{1/2} \left(\frac{\Omega_{\text{m},0} h^2}{0.14} \right)^{1/4} \left(\frac{1+z}{13} \right)^{-1/4} \text{Mpc}^{-1}. \end{aligned} \quad (\text{A.34})$$

Here I have defined $m_{\text{FDM},22} \equiv m_{\text{FDM}}/10^{-22}$ eV. The corresponding Jeans mass $M_{\text{FDM,J}} = (4\pi/3)(\pi/k_{\text{FDM,J}})^3 \bar{\rho}_0$ is

$$\begin{aligned} M_{\text{FDM,J}} &= \frac{\pi^{13/4}}{6} \left(\frac{\hbar^2}{G m_{\text{FDM}}^2} \right)^{3/4} \bar{\rho}_0^{1/4} a^{-3/4} \\ &\simeq 1.0 \times 10^8 m_{\text{FDM},22}^{-3/2} \left(\frac{\Omega_{\text{m},0} h^2}{0.14} \right)^{1/4} \left(\frac{1+z}{13} \right)^{3/4} M_{\odot}. \end{aligned} \quad (\text{A.35})$$

These expressions agree with the literature (e.g. [HBG00, WC09, HOTW17]).

Bibliography

- [ABN02] T. Abel, G.L. Bryan, and M.L. Norman. The formation of the first star in the universe. *Science*, 295(5552): 93–98, 2002.
- [BCB06] I.A. Bonnell, C.J. Clarke, and M.R. Bate. The jeans mass and the origin of the knee in the imf. *Monthly Notices of the Royal Astronomical Society*, 368(3): 1296–1300, 2006.
- [BFPR84] G.R. Blumenthal, S.M. Faber, J.R. Primack, and M.J. Rees. Formation of galaxies and large-scale structure with cold dark matter. *Nature*, 311: 517–525, 1984.
- [BHS⁺16] A. P. Beardsley, B. J. Hazelton, I. S. Sullivan, P. Carroll, N. Barry, M. Rahimi, B. Pindor, C. M. Trott, J. Line, Daniel C. Jacobs, M. F. Morales, J. C. Pober, G. Bernardi, Judd D. Bowman, M. P. Busch, F. Briggs, R. J. Cappallo, B. E. Corey, A. de Oliveira-Costa, Joshua S. Dillon, D. Emrich, A. Ewall-Wice, L. Feng, B. M. Gaensler, R. Goeke, L. J. Greenhill, J. N. Hewitt, N. Hurley-Walker, M. Johnston-Hollitt, D. L. Kaplan, J. C. Kasper, H. S. Kim, E. Kratzenberg, E. Lenc, A. Loeb, C. J. Lonsdale, M. J. Lynch, B. McKinley, S. R. McWhirter, D. A. Mitchell, E. Morgan, A. R. Neben, Nithyanandan Thyagarajan, D. Oberoi, A. R. Offringa, S. M. Ord, S. Paul, T. Prabu, P. Procopio, J. Riding, A. E. E. Rogers, A. Roshi, N. Udaya Shankar, Shiv K. Sethi, K. S. Srivani, R. Subrahmanyan, M. Tegmark, S. J. Tingay, M. Watson, R. B. Wayth, R. L. Webster, A. R. Whitney, A. Williams, C. L. Williams, C. Wu, and J. S. B. Wyithe. First season mwa eor power spectrum results at redshift 7. *The Astrophysical Journal*, 833(1), 2016.
- [BL01] R. Barkana and A. Loeb. In the beginning: the first sources of light and the reionization of the universe. *Physics Reports*, 349(2): 125–238, 2001.
- [BL05] R. Barkana and A. Loeb. Detecting the earliest galaxies through two new sources of 21 centimeter fluctuations. *The Astrophysical Journal*, 626(1), 2005.
- [Boa05] M.L. Boas. *Mathematical Methods in the Physical Sciences*. Wiley, 2005.
- [BT88] J.D. Barrow and F.J. Tipler. Action principles in nature. *Nature*, 331: 31–34, 1988.
- [CAMD17] P.S. Corasaniti, S. Agarwal, D.J.E. Marsh, and S. Das. Constraints on dark matter scenarios from measurements of the galaxy luminosity function at high redshifts. *Physical Review D*, 95(8), 2017.

- [CSC17] S. Chen, H. Schive, and T. Chiueh. Jeans analysis for dwarf spheroidal galaxies in wave dark matter. *Monthly Notices of the Royal Astronomical Society*, 468(2): 1338–1348, 2017.
- [DBN17] X. Du, C. Behrens, and J.C. Niemeyer. Substructure of fuzzy dark matter haloes. *Monthly Notices of the Royal Astronomical Society*, 465(1): 941–951, 2017.
- [Dij17] M. Dijkstra. Saas-fee lecture notes: Physics of lyman alpha radiative transfer. 2017, <https://arxiv.org/abs/1704.03416>.
- [DMS05] J. Diemand, B. Moore, and J. Stadel. Earth-mass dark-matter haloes as the first structures in the early universe. *Nature*, 433: 389–391, 2005.
- [DS86] A. Dekel and J. Silk. The origin of dwarf galaxies, cold dark matter, and biased galaxy formation. *The Astrophysical Journal*, 303: 39–55, 04 1986.
- [DW03] A. Dekel and J. Woo. Feedback and the fundamental line of low-luminosity low-surface-brightness/dwarf galaxies. *Monthly Notices of the Royal Astronomical Society*, 344(4): 1131–1144, 2003.
- [EH98] D.J. Eisenstein and W. Hu. Baryonic features in the matter transfer function. *The Astrophysical Journal*, 496(2): 605–614, 1998.
- [Fie59] G.B. Field. The spin temperature of intergalactic neutral hydrogen. *The Astrophysical Journal*, 129: 536–550, 1959.
- [FOB06] S.R. Furlanetto, S.P. Oh, and F.H. Briggs. Cosmology at low frequencies: The 21 cm transition and the high-redshift universe. *Physics Reports*, 433(4-6): 181–301, 2006.
- [FSS⁺03] Xiaohui Fan, Michael A. Strauss, Donald P. Schneider, Robert H. Becker, Richard L. White, ZoltÁjn Haiman, Michael Gregg, Laura Pentericci, Eva K. Grebel, Vijay K. Narayanan, Yeong-Shang Loh, Gordon T. Richards, James E. Gunn, Robert H. Lupton, Gillian R. Knapp, Zeljko Ivezic, W. N. Brandt, Matthew Collinge, Lei Hao, Daniel Harbeck, Francisco Prada, Joop Schaye, Iskra Strateva, Nadia Zakamska, Scott Anderson, Jon Brinkmann, Neta A. Bahcall, Don Q. Lamb, Sadanori Okamura, Alex Szalay, and Donald G. York. A survey of $z > 5.7$ quasars in the sloan digital sky survey. ii. discovery of three additional quasars at $z > 6$. *The Astronomical Journal*, 125(4): 1649–1659, 2003.
- [Fur06] S.R. Furlanetto. The global 21-centimeter background from high redshifts. *Monthly Notices of the Royal Astronomical Society*, 371(2): 876–878, 2006.
- [GJKB08] T.H. Grief, J.L. Johnson, R.S. Klessen, and V. Bromm. The first galaxies: assembly, cooling and the onset of turbulence. *Monthly Notices of the Royal Astronomical Society*, 387(3): 1021–1036, 2008.

- [GP65] J.E. Gunn and B.A. Peterson. On the density of neutral hydrogen in intergalactic space. *The Astrophysical Journal*, 142: 1633–1641, 1965.
- [Gri04] D.J. Griffiths. *Introduction to Quantum Mechanics*. Pearson Prentice Hall, second edition, 2004.
- [Gri08] David Griffiths. *Introduction to Elementary Particles*. Wiley, 2008.
- [HBG00] W. Hu, R. Barkana, and A. Gruzinov. Fuzzy cold dark matter: The wave properties of ultralight particles. *Physical Review Letters*, 85(6): 1158–1161, 2000.
- [HOTW17] L. Hui, J.P. Ostriker, S. Tremaine, and E. Witten. Ultralight scalars as cosmological dark matter. *Physical Review D*, 95(4), 2017.
- [Hub29] E. Hubble. A relation between distance and radial velocity among extra-galactic nebulae. *Proceedings of the National Academy of Sciences of the United States of America*, 15(3): 168–173, 1929.
- [IVH⁺17] V. Irsic, M. Viel, M.G. Haehnelt, J.S. Bolton, and G.D. Becker. First constraints on fuzzy dark matter from lyman- α forest data and hydrodynamical simulations. *Physical Review Letters*, 119, 2017.
- [KC14] T. Kimm and R. Cen. Escape fraction during reionization: Effects due to supernova feedback and runaway ob stars. *The Astrophysical Journal*, 788(2), 2014.
- [Ken90] I.R. Kenyon. *General Relativity*. Oxford University Press, 1990.
- [KMIS14] K. Kadota, Y. Mao, K. Ichiki, and J. Silk. Cosmologically probing ultra-light particle dark matter using 21 cm signals. *Journal of Cosmology and Astroparticle Physics*, 2014, 2014.
- [KMS⁺17] T. Kobayashi, R. Murgia, A. De Simone, V. Irsic, and M. Viel. Lyman-alpha constraints on ultralight scalar dark matter: Implications for the early and late universe. 2017, <https://arxiv.org/abs/1708.00015>.
- [Kra99] H. Kragh. *Cosmology and Controversy: The Historical Development of Two Theories of the Universe*. Princeton University Press, 1999.
- [KWH96] N. Katz, D.H. Weinberg, and L. Hernquist. Cosmological simulations with treesph. *The Astrophysical Journal Supplement Series*, 105: 19–35, 1996.
- [LED⁺17] N. Leite, C. Evoli, M. D’Angelo, B. Ciardi, G. Sigl, and A. Ferrara. Do cosmic rays heat the early intergalactic medium? 2017, <https://arxiv.org/abs/1703.09337>.
- [LF13] A. Loeb and S.R. Furlanetto. *The First Galaxies in the Universe*. Princeton University Press, 2013.
- [Lid03] A. Liddle. *An Introduction to Modern Cosmology*. Wiley, 2:nd edition, 2003.
- [LL69] L.D. Landau and E.M. Lifshitz. *Mechanics (Volume 1 of Course of Theoretical Physics Series)*. Pergamon Press, second edition, 1969.

- [Loe10] A. Loeb. *How Did the First Stars and Galaxies Form?* Princeton University Press, 2010.
- [Mad00] P. Madau. The intergalactic medium. 2000, <http://xxx.lanl.gov/abs/astro-ph/0005106>.
- [ME03] J. Miralda-Escude. The dark age of the universe. *Science*, 300(5627): 1904–1909, 2003.
- [Mel17] G. Mellema. Private communication, May 2017.
- [MFS13] A. Mesinger, A. Ferrara, and D.S. Spiegel. Signatures of x-rays in the early universe. *Monthly Notices of the Royal Astronomical Society*, 431(1): 621–637, 2013.
- [MMR97] P. Madau, A. Meiksin, and M.J. Rees. 21 centimeter tomography of the intergalactic medium at high redshift. *The Astrophysical Journal*, 475(2): 429–444, 1997.
- [MPA⁺12] A.V. Maccio, S. Paduroiu, D. Anderhalden, A. Schneider, and B. Moore. Cores in warm dark matter haloes: a catch 22 problem. *Monthly Notices of the Royal Astronomical Society*, 424(2): 1105–1112, 2012.
- [MVR⁺17] P. Mocz, M. Vogelsberger, V. Robles, J. Zavala, M. Boylan-Kolchin, A. Fialkov, and L. Hernquist. Galaxy formation with becdm: I. turbulence and relaxation of idealised haloes. 2017, <https://arxiv.org/abs/1705.05845>.
- [NFW96] J.F. Navarro, C.S. Frenk, and S.D.M. White. The structure of cold dark matter halos. *The Astrophysical Journal*, 462: 563–575, 05 1996.
- [OH02] S.P. Oh and Z. Haiman. Second-generation objects in the universe: Radiative cooling and collapse of halos with virial temperatures above 10^4 k. *The Astrophysical Journal*, 569(2): 558–572, 2002.
- [Pad00] T. Padmanabhan. *Theoretical Astrophysics: Volume 1, Astrophysical Processes*. Cambridge University Press, 2000.
- [Pad02] T. Padmanabhan. *Theoretical Astrophysics: Volume 3, Galaxies and Cosmology*. Cambridge University Press, 2002.
- [Pad06] T. Padmanabhan. Advanced topics in cosmology: A pedagogical introduction. 2006, <https://arxiv.org/abs/astro-ph/0602117>.
- [PD17] A. Del Popolo and M. Le Delliou. Small scale problems of the λ cdm model: a short review. *Galaxies*, 5(1): 17, 2017.
- [Pea98] J.A. Peacock. *Cosmological Physics*. Cambridge University Press, 1998.
- [Pee82] P.J.E. Peebles. Large-scale background temperature and mass fluctuations due to scale-invariant primeval perturbations. *The Astrophysical Journal*, 263: L1–L5, 1982.
- [Pee93] P.J.E. Peebles. *Principles of Physical Cosmology*. Princeton University Press, 1993.

- [Pee17] P.J.E. Peebles. Growth of the nonbaryonic dark matter theory. *Nature Astronomy*, 1(id. 0057), 2017.
- [PF07] J.R. Pritchard and S.R. Furlanetto. 21-cm fluctuations from inhomogeneous x-ray heating before reionization. *Monthly Notices of the Royal Astronomical Society*, 376(4): 1680–1694, 2007.
- [PL08] J.R. Pritchard and A. Loeb. Evolution of the 21 cm signal throughout cosmic history. *Physical Review D*, 78(10), 2008.
- [PL12] J.R. Pritchard and A. Loeb. 21 cm cosmology in the 21st century. *Reports on Progress in Physics*, 75(8), 2012.
- [Pla16a] PlanckCollaboration. Planck 2015 results. xiii. cosmological parameters. *Astronomy & Astrophysics*, 594, 2016, <https://arxiv.org/abs/1502.01589>.
- [Pla16b] PlanckCollaboration. Planck intermediate results xlvi. planck constraints on reionization history. *Astronomy & Astrophysics*, 596, 2016.
- [PR03] P.J.E. Peebles and B. Ratra. The cosmological constant and dark energy. *Reviews of Modern Physics*, 75(2): 559–606, 2003.
- [PS74] W.H. Press and P. Schechter. Formation of galaxies and clusters of galaxies by self-similar gravitational condensation. *The Astrophysical Journal*, 187: 425–438, 1974.
- [PS16] E. Papastergis and F. Shankar. An assessment of the "too big to fail" problem for field dwarf galaxies in view of baryonic feedback effects. *Astronomy & Astrophysics*, 591(A58), 2016.
- [PYK⁺17] A.H. Patil, S. Yatawatta, L.V.E. Koopmans, A.G. de Bruyn, M. A. Brentjens, S. Zaroubi, K. M. B. Asad, M. Hatef, V. Jelic, M. Mevius, A. R. Offringa, V.N. Pandey, H. Vedantham, F. B. Abdalla, W. N. Brouw, E. Chapman, B. Ciardi, B. K. Gehlot, A. Ghosh, G. Harker, I. T. Iliev, K. Kakiichi, S. Majumdar, M. B. Silva, G. Mellema, J. Schaye, D. Vrbanec, and S. J. Wijnholds. Upper limits on the 21-cm epoch of reionization power spectrum from one night with lofar. 2017, <https://arxiv.org/abs/1702.08679>.
- [RB07] S. Rosswog and M. Brüggen. *Introduction to High-Energy Astrophysics*. Cambridge University Press, 2007.
- [RDIM17] H. Ross, K.L. Dixon, I.T. Iliev, and G. Mellema. Simulating the impact of x-ray heating during the cosmic dawn. *Monthly Notices of the Royal Astronomical Society*, 468(4): 3785–3797, 2017.
- [SCB14] H. Schive, T. Chiueh, and T. Broadhurst. Cosmic structure as the quantum interference of a coherent dark wave. *Nature Physics*, 10(7): 496–499, 2014.
- [SCBH16] H. Schive, T. Chiueh, T. Broadhurst, and K. Huand. Contrasting galaxy formation from quantum wave dark matter, ψ dm, with λ cdm, using planck and hubble data. *The Astrophysical Journal*, 818(1), 2016.

- [Sch15] J. Schwichtenberg. *Physics from Symmetry*. Springer, 2015.
- [Shu91] F.H. Shu. *The Physics of Astrophysics Volume I: Radiation*. University Science Books, 1991.
- [Sil77] J. Silk. On the fragmentation of cosmic gas clouds. i - the formation of galaxies and the first generation of stars. *The Astrophysical Journal*, 211: 638–648, 1977.
- [SLW⁺14] H. Schive, M. Liao, T. Woo, S. Wong, T. Chiueh, T. Broadhurst, and W-Y. Pauchy Hwang. Understanding the core-halo relation of quantum wave dark matter from 3d simulations. *Physical Review Letters*, 113(26), 2014.
- [SMD⁺16] A. Sarkar, R. Mondal, S. Das, S.K. Sethi, S. Bharadwaj, and D.J.E. Marsh. The effects of the small-scale dm power on the cosmological neutral hydrogen (hi) distribution at high redshifts. *Journal of Cosmology and Astroparticle Physics*, 2016, 2016.
- [SN10] J.J. Sakurai and J.J. Napolitano. *Modern Quantum Mechanics*. Pearson, 2:nd edition, 2010.
- [TARW06] M. Tegmark, A. Aguirre, M.J. Rees, and F. Wilczek. Dimensionless constants, cosmology, and other dark matters. *Physical Review D*, 73(2): id. 023505, 2006.
- [Teg05] M. Tegmark. What does inflation really predict? *Journal of Cosmology and Astroparticle Physics*, 2005, 04 2005.
- [TGSP⁺17] S. Trujillo-Gomez, A. Schneider, E. Papastergis, D.S. Reed, and G. Lake. Another baryon miracle? testing solutions to the "missing dwarfs" problem. 2017, <https://arxiv.org/abs/1610.09335>.
- [TR98] M. Tegmark and M.J. Rees. Why is the cosmic microwave background fluctuation level 10^{-5} ? *The Astrophysical Journal*, 499(2): 526–532, 1998.
- [TRM17] B. Tula, V.H. Robles, and T. Matos. Scalar field dark matter in clusters of galaxies. *Monthly Notices of the Royal Astronomical Society*, 468(3): 3135–3149, 2017.
- [TSR⁺97] M. Tegmark, J. Silk, M.J. Rees, A. Blanchard, T. Abel, and P. Francesco. How small were the first cosmological objects? *The Astrophysical Journal*, 474: 1–12, 1997.
- [WBG⁺15] D.H. Weinberg, J.S. Bullock, F. Governato, R.Kuzio de Naray, and A.H.G. Peter. Cold dark matter: Controversies on small scales. *Proceedings of the National Academy of Sciences*, 112(40): 12249–12255, 2015.
- [WC09] T. Woo and T. Chiueh. High-resolution simulation on structure formation with extremely light bosonic dark matter. *The Astrophysical Journal*, 697(1): 850–861, 2009.

Bibliography

- [Wou52] S.A. Wouthuysen. On the excitation mechanism of the 21-cm (radio-frequency) interstellar hydrogen emission line. *The Astronomical Journal*, 57: 31–32, 1952.
- [WR78] S.D.M. White and M.J. Rees. Core condensation in heavy halos - a two-stage theory for galaxy formation and clustering. *Monthly Notices of the Royal Astronomical Society*, 183: 341–358, 1978.
- [ZKL⁺17] J. Zhang, J. Kuo, H. Liu, Y. Sming Tsai, K. Cheung, and M. Chu. Is fuzzy dark matter in tension with lyman-alpha forest? 2017, <https://arxiv.org/abs/1708.04389>.
- [ZMM⁺16] Q. Zhu, F. Marinacci, M. Maji, Y. Li, V. Springel, and L. Hernquist. Baryonic impact on the dark matter distribution in milky way-sized galaxies and their satellites. *Monthly Notices of the Royal Astronomical Society*, 458(2): 1559–1580, 2016.

